A 3D Numerical Study of Thermofluid Characteristics of a Flat Plate Solar Collector using Nanofluid

by

Rehena Nasrin
Student No. **1010094001P**
Registration No. **100609015**, Session: October-2010

DOCTOR OF PHILOSOPHY
IN
MATHEMATICS

Department of Mathematics
BANGLADESH UNIVERSITY OF ENGINEERING AND TECHNOLOGY, DHAKA-1000
August - 2015

The report entitled **"A 3D NUMERICAL STUDY OF THERMOFLUID CHARACTERISTICS OF A FLAT PLATE SOLAR COLLECTOR USING NANOFLUID"**, submitted by Rehena Nasrin, Roll no: **1010094001P**, Registration No. **1010094001P**, Session October-2010 has been accepted as satisfactory in partial fulfillment of the requirement for the degree of Doctor of Philosophy in Mathematics on 23 August 2015.

Board of Examiners

1. ____________________________________

Dr. Md. Abdul Alim — **Chairman (Supervisor)**
Professor
Department of Mathematics
BUET, Dhaka-1000.

2. ____________________________________

Head — **Member (Ex-Officio)**
Department of Mathematics
BUET, Dhaka-1000.

3. ____________________________________

Dr. Md. Mustafa Kamal Chowdhury — **Member**
Professor
Department of Mathematics
BUET, Dhaka-1000.

4. ____________________________________

Dr. Md. Manirul Alam Sarker — **Member**
Professor
Department of Mathematics
BUET, Dhaka-1000.

5. ____________________________________

Dr. Sheikh Reaz Ahmed **Member**
Professor
Department of Mechanical Engineering
BUET, Dhaka-1000.

6. ____________________________________

Dr. Muhammad Anisuzzaman Talukder **Member**
Professor
Department of Electrical and Electronic Engineering
BUET, Dhaka-1000.

7. ____________________________________

Dr. Md. Anwar Hossain **Member**
Professor (External)
Department of Mathematics (Rtd)
University of Dhaka, Dhaka-1000
Present Address: 35/4 Lake Circus, Opposite of Square Hospital
Panthapoth, Dhaka.

Certificate of Research

This is to certify that the work presented in this thesis is carried out by the author under the supervision of **Dr. Md. Abdul Alim**, Professor, Department of Mathematics, Bangladesh University of Engineering & Technology, Dhaka-1000.

-------------------------------------- ------------------------------

Dr. Md. Abdul Alim **Rehena Nasrin**

Candidate's Declaration

It is hereby declared that this thesis or any part of it has not been submitted elsewhere for the award of any degree or diploma.

____

Rehena Nasrin

This work is dedicated

to

my Mother

Acknowledgement

I would like to affirm the continual mercy, help and blessing showered by the Almighty without which it would have been impossible to accomplish the arduous job I was assigned to. I owe a deep depth to my supervisor, **Dr. Md. Abdul Alim**, Professor, Department of Mathematics, Bangladesh University of Engineering and Technology who restlessly supported me through the Ph.D. process. I would like to thank him for his invaluable contribution. His knowledge about the Ph.D. process is beyond par. His contribution to this thesis, however, does not only encompass his role as an academic supervisor, but include his ongoing friendship, care and support on a personal level without which this journey may have never been completed.

My special thanks to **Dr. S. Reaz Ahmed**, Professor, Department of Mechanical Engineering, BUET, whose support and suggestions was imperative in the whole stages of the Ph.D. process. I am very much obliged to him for his outstanding recommendation and counsel in the thesis of being successful to reach the objectives of this dissertation. His stimulating and enthusiastic encouragement and guidance in regards to fluid dynamics in general and my Ph.D. topic in particular have challenged and greatly contributed to my thinking on dissertation.

I wish to express my heartiest gratitude and indebtness to **Dr. Muhammad Anisuzzaman Talukder**, Professor, Department of Electrical & Electronic Engineering, BUET for giving me valuable ideas, suggestions and opinions which helped me to complete the work smoothly.

I would like to take the opportunity to thank **Dr. Md. Mustafa Kamal Chowdhury**, Professor (Rtd.), Department of Mathematics, BUET for their comments and constructive criticism which helped me for better understanding the issues of this thesis.

I am indebted to the external member of the Board of Examiners, **Dr. Md. Anwar Hossain**, Professor (Rtd.), Department of Mathematics, University of Dhaka, for his valuable suggestions in upgrading the quality of the work.

I also owe a favor to **Dr. Md. Manirul Alam Sarker**, Professor and Head, Department of Mathematics, BUET, for his support in allowing me to use the departmental facilities in various stages of my work. I also thank the staffs of the Department of Mathematics, BUET for being so helpful.

I am grateful to all my colleagues for their encouragement and psychological support that proved to be a tremendous boost in all affairs especially in my research work.

I am thankful to **Dr. Md. Zahurul Haq,** Professor and Head, Department of Mechanical Engineering, for giving me permission to use the Computational Lab of the Dept. of ME, BUET. I would also like to thank **Dr. Md. Ali**, **Dr. Noor Al Kuddus**, **Dr. Sumon Saha** and **M. Jane Alam Khan**, faculty member, Department of Mechanical Engineering, BUET, who have assisted me in computational procedure at the time of working in the Computational Lab of the Dept. of ME, BUET.

I owe my gratitude to **Dr. Ali Javed Chamkha,** Professor of Mechanical Engineering, Public Authority for Applied Education & Training, Kuwait, **Dr. Md. Hasanuzzaman**, Senior Lecturer, UM Power Energy Dedicated Advanced Centre, University of Malaya, **Dr. Omid Mahian**, Mechanical Engineering, Ferdousi University of Mashad, Iran and **Syed Mithun Ali** (on leave), Assistant Professor, Department of IPE, BUET who have helped me by providing relevant journals, necessary informations and valuable suggestions.

My deep love and appreciation goes to my family members for creating a delightful atmosphere as well as relieving me from family duties in order to complete the courses, research studies and final production of the thesis work. These past several years have not been an easy ride for me, both academically and personally. I truly thank my family members for keeping faith in my quirkiness and intellect as well as sticking by my side, even when I was irritable and depressed.

Abstract

Solar collector generation is growing quickly around the world to lessen some of the negative environmental impacts of the heating sector. The variability of these renewable sources of heat possesses technical and economical challenges when integrated on a large scale. One of the potential solutions to deal with the variations of renewable energy sources, energy storage is being widely regarded. An elaborate theoretical study on thermofluid characteristics of a nanofluid filled flat plate solar collector (FPSC) has been presented in this thesis. The relevant governing equations have been solved by using finite element method.

In this thesis numerical analysis has been performed for better understanding of the heat transfer phenomena of the flat plate solar collector using water as well as water/copper nanofluid. Both 2D and 3D models of the flat plate solar collector (FPSC) have been taken into account. Heat transfer and flow characteristics have been presented for various pertinent parameters. Then comparison in various forms has been shown to check whether 3D study is necessary or not. Two correlations for heat transfer rate and thermal efficiency have been developed from obtained 3D results. Higher heat transfer rate of 3%, mean output temperature of 1.6K and collector efficiency of 5% have been obtained in 3D analysis than that of 2D analysis. Not more than 2% solid volume fraction of water/copper nanofluid has found to be advantageous. Suitable mass flow rate has obtained 0.0248Kg/s from this numerical study. More heat transfer rate of 17% and thermal efficiency of 8% has found for using 2% concentrated water/copper nanofluid than base fluid in 3D simulation.

Water based nanofluid having double nanoparticles (copper and silver) has also been used as heat transfer medium instead of nanofluid having single nanoparticle (copper or silver) in 3D study to observe whether thermal efficiency of FPSC increases or not. Also a quadratic form of thermal efficiency has been derived using the results obtained from current 3D numerical study and compared with a survey report for a good FPSC available in the literature.

A published experimental study has been modeled and solved numerically. Obtained numerical results have been compared with experimental values and percentage of error has been calculated. Then a linear correlation has been developed between collector efficiency and temperature difference (input and ambient) and correlation coefficient has been calculated from the numerical data.

Contents

Nomenclature

A	aperature area of solar collector (m^2)
A_e	area base on the perimeter of collector (m^2)
$\overline{A}$	area of 2D cross section of riser pipe (m^2)
C	constant defined in subsection 3.2.4
C_p	specific heat at constant pressure ($Jkg^{-1}K^{-1}$)
f	friction factor
h	convective heat transfer coefficient ($Wm^{-2}K^{-1}$)
h_a	convective heat transfer coefficient between glass and ambient air ($Wm^{-2}K^{-1}$)
H	height of the collector (m)
I	solar irradiation (Wm^{-2})
k	thermal conductivity of fluid ($Wm^{-1}K^{-1}$)
k_b	back insulation conductivity ($Wm^{-1}K^{-1}$)
k_e	edge insulation conductivity ($Wm^{-1}K^{-1}$)
L	length of the solar collector (m)
N	number of glass
Nu	average Nusselt number
p	pressure ($kgms^{-2}$)
Pr	Prandtl number
q	heat flux (Wm^{-2})
Re	Reynolds number
T	fluid temperature (K)
u, v, w	velocity components along x, y, z direction (ms^{-1})
U_l	overall heat transfer coefficient ($Wm^{-2}K^{-1}$)
V	magnitude of velocity (ms^{-1})
$\overline{V}$	volume of riser pipe (m^3)
x_b	back insulation thickness (m)
x_e	edge insulation thickness (m)

x, y, z	Cartesian coordinates (m)
X, Y, Z	dimensionless Cartesian coordinates
W	collector width (m)

Greek symbols

α	thermal diffusivity ($m^2 s^{-1}$)
β	tilt angle (^{0})
λ	transmitivity
ε	emissivity
η	thermal efficiency
ϕ	nanoparticles volume fraction
θ	dimensionless fluid temperature
μ	dynamic viscosity of the fluid ($m^2 s^{-1}$)
v	kinematic viscosity of the fluid ($m^2 s^{-1}$)
ρ	density of the fluid (kgm^{-3})
κ	absorption coefficient

Subscripts

a	absorber
amb	ambient
av	average
b	back
c	cover
col	collector
e	edge
f	fluid
in	input
loss	lost
nf	nanofluid
out	output
recv	received

s	solid particle
t	top
usfl	useful
1	Cu nanoparticle
2	Ag nanoparticle

Abbreviation

CBC	convective boundary conditions
CFD	computational fluid dynamics
DASC	direct absorption solar collector
FEM	finite element method
FPSC	flat plate solar collector
2D	two dimensional
3D	three dimensional

List of Tables

List of Figures

Chapter 1: Introduction

1.1 Introduction

Because of the desirable environmental and safety aspects it is widely believed that solar energy should be utilized instead of other alternative energy forms, even when the costs involved are slightly higher. The flat-plate solar collector is commonly used today for the collection of low temperature solar thermal energy. Solar collectors are key elements in many applications, such as building heating systems, solar drying devices etc. Solar energy has the greatest potential of all the sources of renewable energy especially when other sources in the country have depleted. The sun is a sphere of intensely hot gaseous matter with a diameter of 1.39×10^9 m. The sun has an effective blackbody temperature of 5800 K. The solar energy strikes our planet a mere 8 min and 20 s after leaving the giant furnace. Only a tiny fraction, 1.7 kW to 1014 kW, of the total radiation emitted is intercepted by the earth. However, even with this small fraction it is estimated that 30 min of solar radiation falling on earth is equal to the world energy demand for one year. This technology is friendly to our environment.

Quite often researchers encounter fluid flow and heat transfer in solar collectors at different orientations. These classical problems have some analytical and huge numerical solutions. But things used in practical purpose are much more complicated in design and prediction of their performance using results from simple geometry cause huge error. For this complexity, in recent years, attention has been given to study thermal characteristics of complex geometrical form of solar collector. Mathematical models used to predict flow and thermal behavior mainly involve a set of coupled non-linear partial differential equations whose analytical solution is impossible except some special cases.

1.1.1 Solar collector

Solar collectors can be classified broadly into two types:

- **Non-concentrating solar collector:**

When no optical concentration is done, the device in which the collection is achieved is called a flat plate collector. The absorber and collector area in flat plate solar collectors is numerically the same. FPSC is simple in design, has no moving parts and requires less maintenance. It was first introduced in 1950. It can be used for a variety of applications in which temperatures ranging from 30^0C to about 90^0C. It can collect both beam and diffused solar radiations. It is also effective on cloudy days where there is no direct radiation. A heat-conducting fluid, usually water, glycol, or air, passes through pipes attached to the absorber plate. The main use of this technology is in residential buildings where the demand for hot water has a large impact on energy bills. This generally means a situation with a large family, or a situation in which the hot water demand is excessive due to frequent laundry washing. Figure 1.1 shows the non-concentrating solar collector [1].

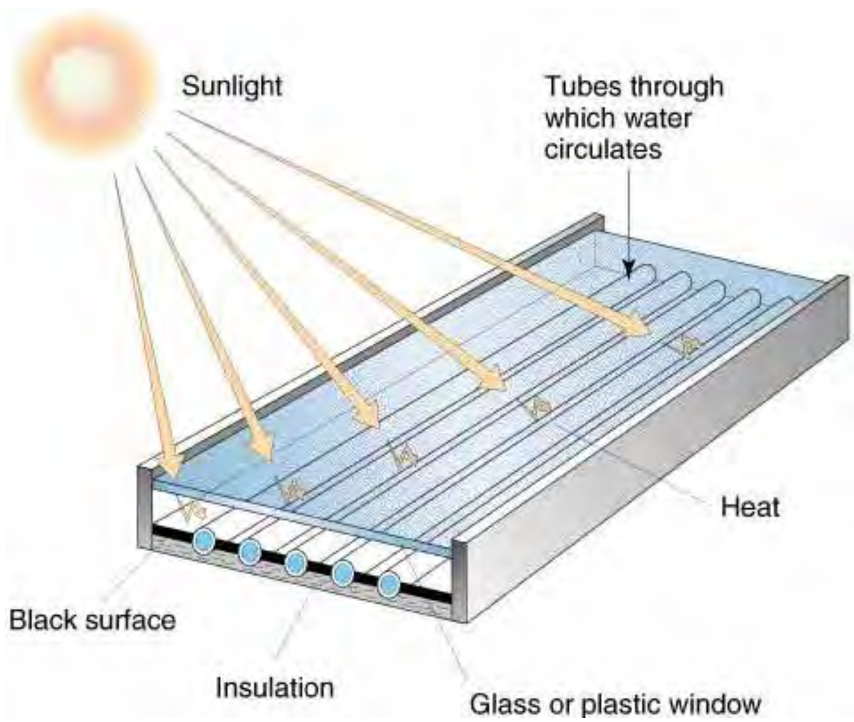

Figure 1.1: Non-concentrating solar collector

Non-concentrating solar collectors are mainly two types:

❖ **Glazed solar collector:**

Glazed flat-plate collectors can operate efficiently at a wider temperature range than unglazed collectors. Flat-plate collectors are often used to complement traditional water boilers, pre-heating water to reduce fuel demand. They can also be effective for space heating. Using a heat exchange system, they can reliably produce hot air for large buildings during daylight hours. Figure 1.2 shows glazed solar collector [2].

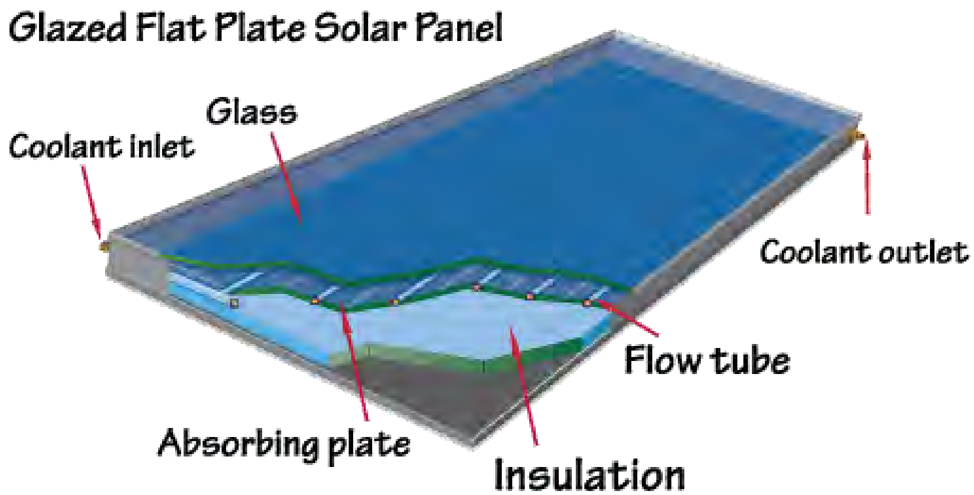

Figure 1.2: Glazed solar collector

- **Unglazed solar collector:**

An unglazed solar collector is one of the simplest forms of solar thermal technology.

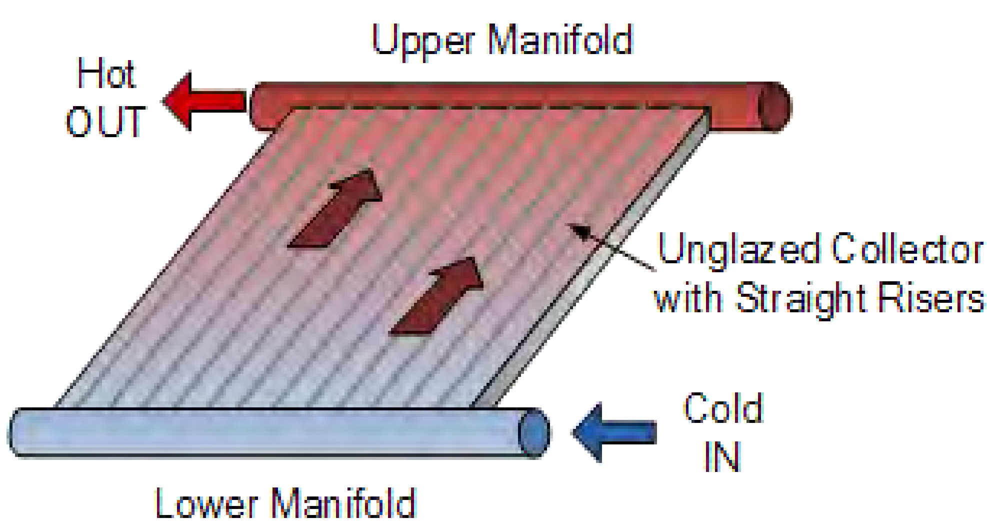

Figure 1.3: Unglazed solar collector

A heat-conducting material, usually a dark metal or plastic, absorbs sunlight and transfers the energy to a fluid passing through or behind the heat-conducting surface. The process is similar to how a garden hose, laying out in the open, will absorb the sun‟s energy and heat the water inside the hose. It [3] is displayed in the figure 1.3

- **Concentrating solar collector:**

For this type of collector large areas of mirrors or lenses focus the sunlight into a smaller absorber. By using reflectors to concentrate sunlight on the absorber of a solar collector, the size of the absorber can be dramatically reduced, which reduces heat losses and increases efficiency at high temperatures. The reflectors can cost substantially less per unit area than collectors. Figure 1.4 shows the concentrating solar collector [4].

Figure 1.4: Concentrating solar collector

1.1.2 Earth-Sun distance

The earth has a diameter of 12.7×10^3 km, which is approximately 110 times less than the sun‟s diameter. The earth‟s orbit‟s eccentricity is very small, about 0.0167, which causes the elliptical path to be nearly circular. The average earth–sun distance of 14.9×10^7 km is defined as the Astronomical Unit (AU), which is used for calculating distances within the solar system.

1.1.3 Solar irradiation

Irradiance of sunlight is the power per unit area on the Earth's surface. Sunlight is a portion of the electromagnetic radiation given off by the sun, particularly infrared, visible, and ultraviolet light. On the Earth, sunlight is filtered through the Earth's atmosphere and is obvious as daylight when the sun is above the horizon. When the direct solar radiation is not blocked by clouds, it is experienced as sunshine, a combination of bright light and radiant heat. Figure 1.5 shows different form of solar radiation [5]. There are three types of radiation:

Direct or beam radiation: Radiation that is not reflected or scattered and reaches the earth"s surface directly in line from the sun is called direct or beam radiation.

Diffuse radiation: The scattered radiation which reaches the ground is called diffused radiation.

Albedo: Part of radiation reflected from the ground is called Albedo.

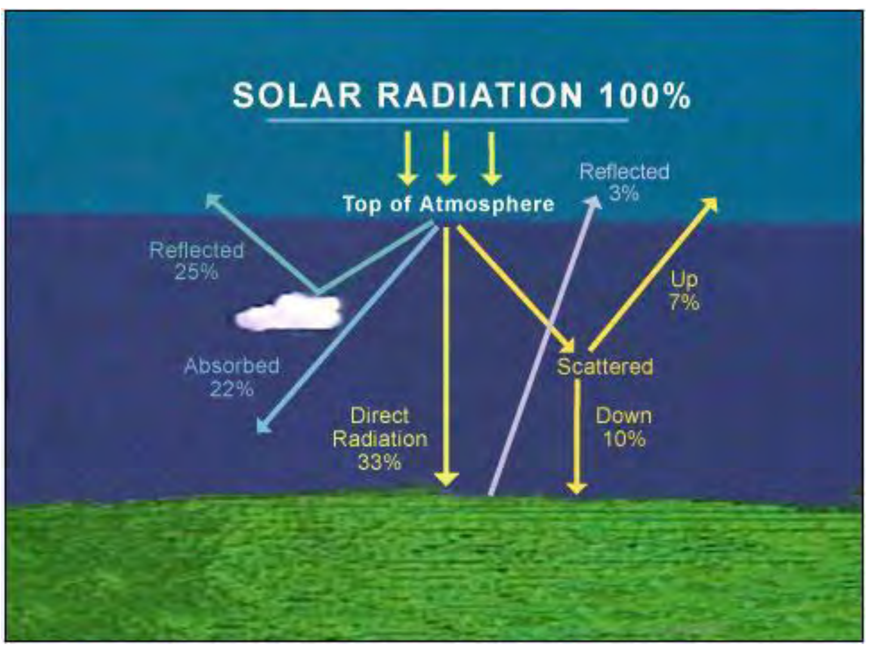

Figure 1.5: Various forms of solar irradiation

Global radiation is the sum of these three kinds of radiation. Solar radiation is received at the earth's surface in an attenuation form because it is subjected to the mechanism of absorption and scattering as it passes through the earth's atmosphere. Incoming radiation from the sun is the shortwave radiation. It has more energy, whereas the reflection from the earth is the long wave radiation. It has less energy.

1.1.4 Radiative heat flux

Solar radiation is radiant energy emitted by the sun. It is particularly electromagnetic energy. In the case of electromagnetic radiation-such as light-in free space, the phase speed is the speed of light, about 3×10^8 m/s. The wavelength of visible light ranges from deep red, roughly 700 nm, to violet, roughly 400 nm. Figure 1.6 displays wavelength of sunlight [6]. Heat transfer due to emission of electromagnetic waves is known as thermal radiation. The heat transfer rate per unit area as thermal radiation is called radiative heat flux.

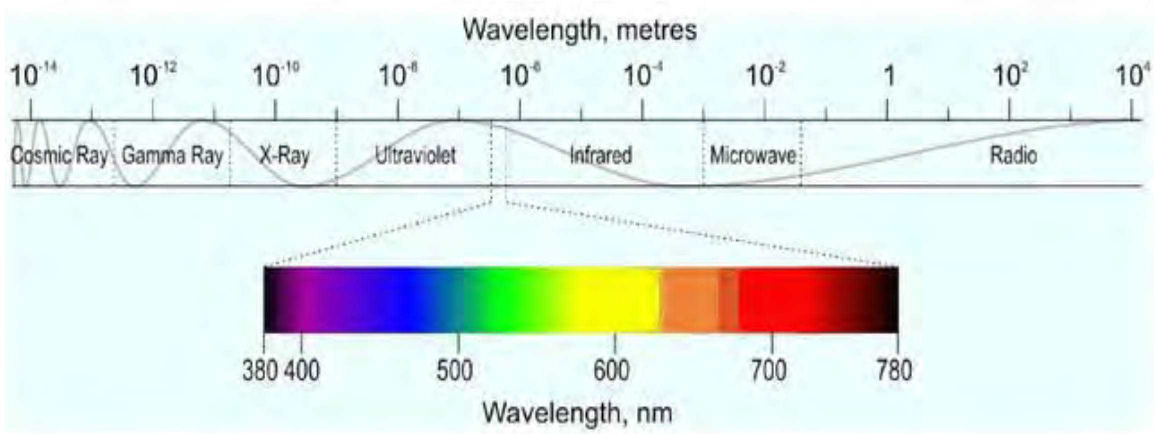

Figure 1.6: Wavelength of sunlight

1.1.5 Nanofluids

The fluids with solid-sized nanoparticles suspended in them are called “nanofluids”. In other words, nanofluid is a fluid containing nanometer-sized particles, called nanoparticles. Nanofluids is the term coined by Choi (1998) to describe this new class of nanotechnology-based heat transfer fluids. They exhibit thermal properties superior to those of their host fluids Das (2008). Nanoparticle is defined as the smallest unit that can still behave as a whole entity in terms of properties and transport. Suspensions of nanoparticles (i.e., particles with diameters < 100 nm) in liquids, termed nanofluids, show remarkable thermal and optical property changes from the base liquid at low particle loadings. To determine the effectiveness of nanofluids in solar applications, their ability to convert light energy to thermal energy must be known. That is, their absorption of the solar spectrum must be established. The efficiency of these collectors is limited by the absorption properties of the working fluid, which is very poor for typical fluids used in solar collectors. Nanoparticles also offer the potential of improving the radiative properties of liquids, leading to an increase in the efficiency of absorption solar collectors. The nanoparticles are typically made of metals, oxides, carbides, or carbon nanotubes. Common base fluids include water, ethylene glycol and oil. Nanofluids have novel properties that make them potentially useful in many applications in heat transfer including microelectronics, solar collector, fuel cells, pharmaceutical processes, hybrid-powered engines, engine cooling/vehicle thermal management, domestic refrigerator, chiller, heat exchanger, nuclear reactor, grinding, machining, space, defense and ships, and boiler flue gas temperature reduction etc.

1.1.6 Thermal conductivity

In physics, thermal conductivity is the intensive property of fluid that indicates its ability to conduct heat. The fluids that have been traditionally used for heat transfer applications have a rather low thermal conductivity, taking into account the rising demands of modern technology. Thus, there is a need to develop new types of fluids that will be more effective in terms of heat exchange performance. In order to achieve this, it has been recently proposed to disperse small amounts of nanometer-sized solids in the fluid. The resulting “nanofluid” is a multiphase material that is macroscopically uniform. If it is focused on maximizing the heat transfer coefficient, it is clear that the thermal conductivity of the fluid is the dominant parameter.

1.1.7 Viscosity

The viscosity of a fluid is a measure of its resistance to gradual deformation by shear stress or tensile stress. For liquids, it corresponds to the informal notion of "thickness".

Viscosity is due to friction between neighboring parcels of the fluid that are moving at different velocities. It is the measure of the internal friction of a fluid. This friction becomes apparent when a layer of fluid is made to move in relation to another layer. But the viscosity of nanofluid depends on many parameters such as base fluids, particle volume fraction, particle size, particle shape, temperature, shear rate, pH value, surfactants, dispersion techniques, particle size distribution and particle aggregation. The viscosity models available in the literature are generally applied to measure the viscosity of nanofluids.

1.1.8 Heat transfer mode

Heat transfer describes the exchange of thermal energy, between physical systems depending on the temperature and pressure, by dissipating heat. Figure 1.7 expresses general heat transfer procedure [7]. The fundamental modes of heat transfer are conduction or diffusion, convection (free and forced) and radiation. All these three kinds of heat transfer are accounted in the present study of FPSC. Thermal equilibrium is reached when all involved bodies and the surroundings reach the same temperature. Thermal expansion is the tendency of matter to change in volume in response to a change in temperature. In FPSC all these three kinds of heat transfer play important role.

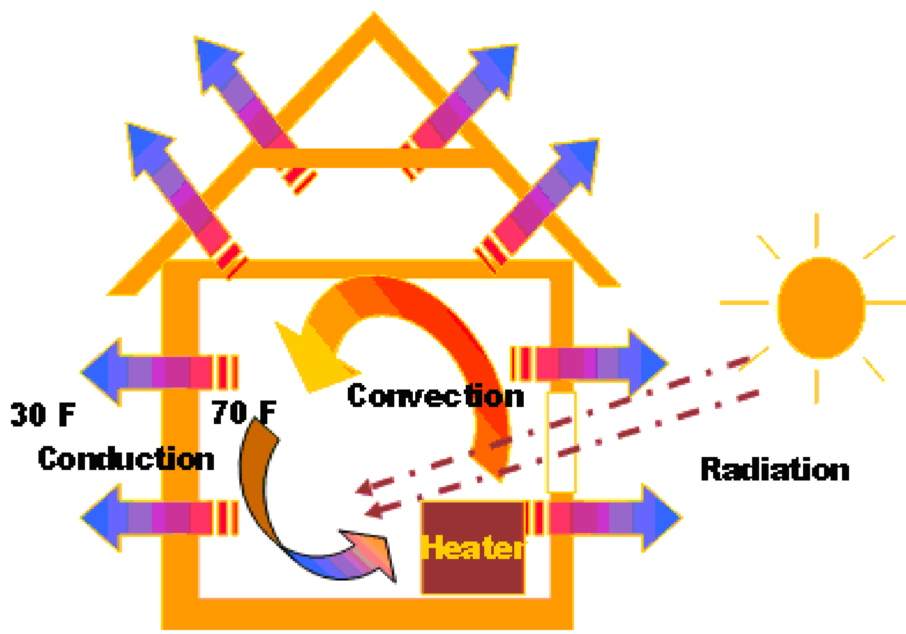

Figure 1.7: Heat transfer system

1.2 Literature Review

Heat transfer problem with fluid flow are of importance in many processes and have, therefore, received a considerable amount attention in recent years. In forced convection, only inertia force is required and it arises in many technological processes. Few researchers investigated the effects of forced convective flows in solar collectors by using analytical, experimental and numerical methods. Some important works are presented below.

The one-dimensional analysis offers a desired accuracy required in a routine analysis even though a two-dimensional temperature distribution exists over the absorber plate of the collector Rao (1977). Heat transfer enhancement in solar devices is one of the key issues of energy saving and compact designs Kreith and Kreider (1978), Sukhatme (1991) and Parker *et al.* (1993). General thermal analysis of parallel-flow flat-plate solar collector absorbers was analyzed by Lund (1986). Nag *et al.* (1989) investigated parametric study of parallel flow flat plate solar collector using finite element method. The investigators have used two dimensional conduction equations in their analysis with different boundary conditions for glazed and unglazed solar collectors Soltau (1992), Molineaux *et al.* (1994), Tripanagnostopoulos *et al.* (2000), Orel *et al.* (2002), Wazwaz (2002), Konttinen (2003), Modest (2003), Xiaowu and Hua (2005).

Forced convective temperature distribution through different shapes solar collector with wavy absorber plate is analyzed by Piao *et al.* (1994), Gao (1996), Gao *et al.* (2000), Joudi *et al.* (2004), Ho and Chen (2006), Hussain (2006), Varol and Oztop (2007). Two dimensional parallel flow flat-plate solar collector was investigated by Kazeminejad (2002). He analyzed temperature distribution over the absorber plate of a parallel flow flat-plate solar collector with steady-state conduction equations and heat generation. Survey report was also conducted on various types of solar collectors by Kalogirou (2004). Lambert *et al.* (2006) investigated enhanced heat transfer using oscillatory flows in solar collectors. They proposed the use of oscillatory laminar flows to enhance the transfer of heat from solar collectors. Their idea was to explore the possibility of transferring the heat collected from a solar device to a storage tank by means of a zeromean oscillating fluid contained in a tube.

Heat transfer in a directly irradiated solar receiver/reactor for solid gas-reactions was conducted by Klein *et al.* (2007). Struckmann (2008) analyzed a flat-plate solar collector. Efforts had been made to combine a number of the most important factors into a single equation and thus formulate a mathematical model which will describe the thermal performance of the collector in a computationally efficient manner. Álvarez *et al.* (2010) studied finite element modelling of a solar collector. A mathematical model of a serpentine flat-plate solar collector using finite elements was presented. The numerical simulations focused on the thermal and hydrodynamic behavior of the collector. Saleh (2012) investigated modeling of flat-plate solar collector operation in transient states. His proposed model simulated the complete solar collector system including the flat-plate and the storage tank.

Amrutkar *et al.* (2012) studied solar flat plate collector analysis. The objective of their study was to evaluate the performance of FPSC with different geometric absorber configuration. It was expected that with the same collector space higher thermal efficiency or higher water temperature could be obtained. Dara *et al.* (2013) conducted evaluation of a passive flat-plate solar collector. Their research investigated the variations of top loss heat transfer coefficient with absorber plate emittance and air gap spacing between the absorber plate and the cover plate. Iordanou (2009) investigated flat-plate solar collectors for water heating with improved heat Transfer for application in climatic conditions of the mediterranean region. The aim of his research project was to improve the thermal performance of passive flat plate solar collectors using a novel cost effective enhanced heat transfer technique. Conduction convection radiation processes of a solar collector using FEA was performed by Moningi (2008). Radiation dominated the other two processes.

To determine the effectiveness of nanofluids in solar applications, their ability to convert light energy to thermal energy must be known. That is, their absorption of the solar spectrum must be established. Natarajan & Sathish (2008) performed role of nanofluids in solar water heater. The aim of this paper was to analyze and compare the heat transfer properties of the nanofluids with the conventional fluids. Tyagi *et al.* (2009) investigated predicted efficiency of a low-temperature nanofluid-based direct absorption solar collector (DASC). It was observed that the presence of nanoparticles increased the absorption of incident radiation by more than nine times over that of pure water. According to their results, under similar operating conditions, the efficiency of a DASC using nanofluid as the working fluid is found to be up to 10% higher than that of a flat-plate collector. Selected nanofluids might improve the efficiency of direct absorption solar thermal collectors Otanicar *et al.* (2009, 2010) and Robert (2011). Taylor *et al.* (2011) analyzed nanofluid optical property characterization: towards efficient direct absorption solar collectors. Polvongsri and Kiatsiriroat (2011) studied enhancement of flat-plate solar collector thermal performance with silver nanofluid. They reported that with higher thermal conductivity of the working fluid the solar collector performance could be enhanced compared with that of water. Mahian *et al.* (2013) conducted a review of the applications of nanofluids in solar energy. The effects of nanofluids on the performance of solar collectors and solar water heaters from the efficiency, economic and environmental considerations viewpoints, and the challenges of using nanofluids in solar energy devices were discussed in their article.

Experimental studies were performed based on solar collectors by Kolb *et al.* (1999), Xuesheng *et al.* (2005). Azad (2009) analyzed interconnected heat pipe solar collector. Performance of a prototype of the heat pipe solar collector was experimentally examined and the results were compared with those obtained through theoretical analysis. Martín *et al.* (2011) performed experimental heat transfer research in enhanced flat-plate solar collectors. To test the enhanced solar collector and compare with a standard one, an experimental side-by-side solar collector test bed was designed and constructed. Karuppa *et al.* (2012) investigated a new solar flat plate collector. Experiments had been carried out to test the performance of both the water heaters under water circulation with a small pump and the results were compared. Zambolin (2011) theoretically and experimentally studied solar thermal collector systems and components. Testing of thermal efficiency and optimization of these solar thermal collectors were addressed and discussed in their work. Sandhu (2013) experimentally studied temperature field in flat-plate collector and heat transfer enhancement with the use of insert devices. Various new configurations of the conventional insert devices were tested over a wide range of Reynolds number (200-8000). Chabane *et al.* (2013) experimentally studied thermal performance optimization of a flat plate solar air heater. Optimum values of air mass flow rates were suggested maximizing the performance of the solar collector.

For more accurate analysis at low mass flow rates, a three-dimensional temperature distribution must be considered. Three dimensional numerical simulations are carried on solar collectors using various techniques. 3D model of the collector involving the water pipe, absorber plate, the glass top and the air gap in-between the absorber plate and the glass top is modeled to provide for conduction, convection and radiation. Karanth *et al.* (2011) numerically simulated a solar flat plate collector using Discrete Transfer Radiation Model (DTRM) – a CFD approach. Dynamics (CFD) by employing conjugate heat transfer showed that the heat transfer simulation due to solar irradiation to the fluid medium, increased with an increase in the mass flow rate. Manjunath *et al.* (2012) studied comparatively solar dimple plate collector with flat plate collector to augment the thermal performance. Their result described that the average exit water temperature showed a marked improvement of about 5.5^0C for a dimple solar collector as compared to that of a flat plate solar collector. CFD analysis of solar flat plate collector was conducted by Ingle *et al.* (2013). His work attempted to present numerical simulation of solar collector developed exclusively for grape drying. CFD analysis of triangular absorber tube of a solar flat plate collector was performed by Basavanna and Shashishekar (2013) where the numerical results obtained using the experimentally measured temperatures are compared to the temperatures determined by the CFD model. 3D conjugate heat transfers through unglazed, glazed water-filled and gas-filled solar flat plate collectors with and without finned tubes were investigated by Manjunath *et al.* (2011), Vestlund (2012), Ekramian *et al.* (2014) and Tagliafico *et al.* (2014).

Nasrin and Alim (2012a-e, 2013a-f, 2014a-d, 2015a-b, accepted), **Nasrin** *et al.* (2013a-d, 2014a-c, 2015) and Parvin *et al.* (2014) studied free and forced convective heat and mass transfer with entropy generation of nanofluid having single as well as double nanoparticles considering different geometry namely complicated cavity, direct absorption solar collector, prism shaped solar collector, solar collector having wavy absorber, flat plate solar collector etc. They analyzed nanofluid flow with double nanoparticles using necessary modification of established nanoparticles effective properties. They showed how to enhance thermal performance of different types of solar collectors in their analyses.

1.3 Motivation

Solar energy, radiant light and heat from the sun, has been harnessed by humen since ancient times using a range of ever-evolving technologies.

In the light of above discussions, it is seen that there has been a good number of works in the field of heat transfer system through a flat plate solar collector. Among them 1D, 2D and 3D analytical, numerical and experimental studies toke place. Some 2D numerical analyses have been done using base fluid as well as various nanofluids. Researchers considered only riser pipe domain or only air gap domain on 2D analyses. None considered whole geometry of FPSC. Actual phenomena of solar collector haven‟t been modeled properly on 2D.

Up until now, no work has been done using water based nanofluid having multiple nanoparticles in 2D heat transfer model through a flat plate solar collector even though nanofluid is extensively used.

Some experimental works has also been done based on solar collectors in various countries. But in Bangladesh there is no scope to run research based experiments.

A very few researchers conducted 3D numerical modeling on FPSC because of difficulties. They used air and water as heat transfer medium. But no 3D numerical studies have been conducted using nanofluids on this device.

That‟s why there is a large scope to work on 3D numerical investigation of heat transfer through a flat plate solar collector using nanofluids. A 3D numerical model represents a practical geometry as a prototype of actual view whereas a 2D numerical model can‟t do that perfectly. Accurate and reliable 3D numerical studies are essential to determine the variation of collector efficiency, heat transfer characteristics with economic and environmental considerations due to using different nanofluids in forced convective mode, which forms the basis of the motivation behind selecting the present work.

1.4 Objectives of the Present Study

The overall goal of this study is to numerically simulate 2D as well as 3D models of heat transfer by nanofluids through a flat plate solar collector as stated in previous section. The investigation is to be carried out at different governing parameters such as solar irradiation, Reynolds number, Prandtl number and solid volume fraction of nanoparticles. In addition, the effects of these parameters on overall temperature distribution are examined. Results are presented in terms of isothermal lines, streamlines, iso-surface plot, slice plot, arrow plot, contour plot and boundary plot. Average Nusselt number, mean bulk temperature, mean subdomain velocity, temperature at the middle of the riser pipe, mean outlet temperature and collector efficiency for different values of the governing parameters are depicted. However, the specific aims of the study are as follows:

- To use 2D and 3D mathematical models regarding the heat transfer mechanism through a flat plate solar collector.
- To solve the model using finite element method.
- To carry out the numerical result validation by reproducing the previous published works.
- To examine the effects of solar irradiation, Reynolds number, Prandtl number, solid volume fraction on heat transfer characteristics through FPSC.
- To show the importance of 3D numerical study for FPSC.
- To develop correlations among the obtained results in 3D modeling.

- To compare thermal efficiency using various nanofluids.
- To solve an experimental work numerically and compare numerical result with experimental one.

1.5 Scope of the Thesis

A brief description of the present numerical investigation of heat transfer and thermal efficiency through a flat plate solar collector have been presented in this thesis through six chapters as stated below:

Chapter 1 contains introduction with the aim and objectives of the present work. This chapter also includes a literature review of the past studies on heat transfer through different types of solar collector which are relevant to the present work. Different aspects of the previous studies have been mentioned categorically. Present study and motivation behind it has also been incorporated in this chapter.

Chapter 2 presents a detailed description for the structural design of flat plate solar collector. Physical model of a FPSC is described for a family member of two in the aspect of Bangladesh. Schematic diagram is drawn and mathematical formulation is given for numerical computation in this chapter.

In Chapter 3, the 2D numerical study regarding the heat transfer and fluid flow characteristics through the FPSC taking heat transfer medium as water and water based nanofluid is performed. Effects of solar irradiation, Reynolds number, Prandtl number and solid volume fraction of nanoparticles are conducted. Results are shown in isothermal lines, streamlines, surface plot, boundary plot, arrow plot to better understand the heat transfer mechanism through FPSC.

Chapter 4 numerically describes the heat transfer and collector efficiency phenomena through a FPSC in 3D model. Numerical outcomes are displayed in terms of iso-surfaces, slice plot, streamlines, surface plot. Thermal efficiency and heat transfer coefficients are compared using various nanofluids through FPSC. New correlations are developed among present results. Comparison is shown from obtained results between 2D and 3D numerical studies. Clarification is given for the importance of 3D analysis in

FPSC. In addition comparison is shown results between present study and survey/project report available in the literature. A quadratic form of thermal efficiency is also derived from present 3D numerical analysis.

Chapter 5 presents 3D numerical study of an experimental analysis. A comparison is shown between numerical and experimental results. Also percentage of error is calculated. A correlation is developed from this numerical result and correlation coefficient is also calculated.

Chapter 6 mentions some important factors on which attention should be given to use FPSC. Also concluding remarks of the whole work and the recommendations for the future work have been presented systematically.

Finally in Appendix, optimization technique of thermal performance of a FPSC in Dhaka city is mentioned.

Chapter 2: Flat Plate Solar Collector

2.1. Introduction

Solar energy is one of the best sources of renewable energy with minimal environmental impact. The forced convection in solar collector continues to be a very active area of research during the past few decades. Commercial applications of solar collectors include laundromats, space heating, car washes, military laundry facilities and eating establishments. Solar water heating systems are most likely to be cost effective for facilities with water heating systems that are expensive to operate, or with operations such as laundries or kitchens that require large quantities of hot water. Unglazed liquid collectors are commonly used to heat water for swimming pools while glazed collectors are used for household‟s purposes. While solar collectors are most cost-effective in sunny, temperate areas, they can be cost effective virtually anywhere in the country so should be considered.

2.2 Flat Plate Solar Collector

Solar radiations fall over the absorber plate which absorbs the solar radiations and convert it into heat. This heat is then conducted from the absorber plate to the tubes carrying the fluids. After conduction the heat is convected to the working fluid. Due to the involvement of three resistances between solar radiations and working fluid the losses are more. As the fluid flows through the pipes, its temperature increases. This is the energy to be utilized for productive activities (e.g., power generation). The amount of the energy taken by the working fluid corresponds to a fraction of the useful energy collected after the heat losses. Figure 2.1 shows the typical components of a classic flat plate collector [8]. A flat plate collector generally consists of the following components:

- **Glazing:** One or more sheets of glass or other radiation-transmitting material is known as glazing. In selecting glass for covers, the mechanical strength must be adequate to resist breakage from maximum expected wind and snow loads and normally expected impacts. The mechanical strength is proportional to the square of the thickness of glass.

- **Air gap:** The gap between the cover and the absorber is filled up by air. This air gap domain plays a role of insulation for FPSC. Some amount of heat is trapped in this domain under the glass cover.
- **Absorber plate:** Flat, corrugated or grooved plates to which tubes, passages are attached. The absorber plate material should have high thermal conductivity, adequate tensile and compressive strength and good corrosion resistance. Coating is also an important factor in absorption of incident radiation. Black of all other colors tend to absorb more light and increases the temperature of the absorber plate.
- **Tubes or Passages:** Tube is used to conduct or direct the heat transfer fluid from the inlet to the outlet. Tube material should have good internal corrosion resistance and low thermal capacity when in direct contact with heat transfer liquids.
- **Insulation:** To minimize the heat losses from the back and sides of the collector insulation is used. The desired characteristics of an insulating material are: low thermal conductivity, stability at high temperature, no degassing, self-supporting feature without tendency to settle, ease of application and no contribution in corrosion.
- **Container or Casing:** The role of casing is to surround the above mentioned components and keep them free from dust, moisture etc.

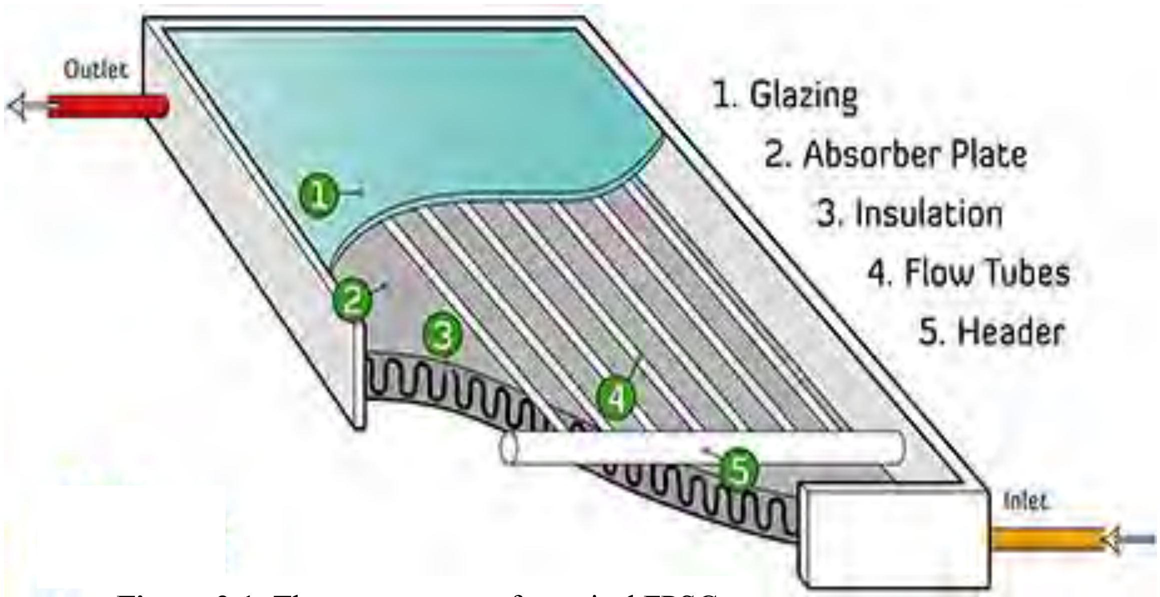

Figure 2.1: The components of a typical FPSC

2.2.1 Standard dimension of FPSC

The standard dimension of a FPSC for water system is given in Table 2.1 and is taken from Sunmaxx Solar hot water solution [9].

Table 2.1: The standard dimension of a FPSC

Parts of FPSC	Size and property
Gross surface area	2.61 m²
Absorber surface area	2.364 m²
Aperture area	2.41 m²
Format (*L* x *W* x *H*)	2151 x 1215 x 110 mm
Glass cover	Highly transparent, anti-reflection, thickness 2-5 mm, transmission 96%
Air gap	5-20 mm
Absorber	Laser-welded single surface absorber with selective vacuum coating; absorption 95%; emmision 5%; thickness 0.2-1 mm
Inner diameter of pipe	7-13mm
Pipe thickness	0.5-1 mm
Fluid capacity	1 liter
Fluid velocity	0.1-1 m/s
Insulation	40-50 mm

2.2.2 Size and cost of collector

About 2 m^2 collector area is needed for 2 family members. For every additional person 0.7 m^2 is added. Any other sizes are possible as per customer requirements. The size of insulated storage tank increases with the size of collector-typically 1.5 gallons per square foot of collector. 66-gallon system is for 1 to 3 people; 80-gallon system works is for 3 to 4 people and 120-gallon system is for 4 to 6 people [10]. Annual utility costs for solar water heaters are about 50% to 85% lower than those for electric water heaters.

2.2.3 Storage tank

Hot water storage tank is a water tank that is used for storing hot water for space heating or domestic use. A heavily insulated tank can retain heat for days. Water is convenient heat storage medium, because it has a high specific heat capacity. Compared with other substances it can store more heat per unit of volume. Water is non-toxic and almost free. Water heaters for washing, bathing, or laundry have thermostat controls to regulate the temperature, in the range 40^0C to 60^0C, and are connected to the domestic cold water supply. Where the water supply has a high content of dissolved minerals such as limestone, heating the water causes the minerals to precipitate in the tank; a water tank may develop leaks due to corrosion after only a few years. Dissolved oxygen in the water can also accelerate corrosion of the tank and its fittings. A hot water storage tank is wrapped in heat insulation to reduce heat loss and energy consumption. Conventionally used storage tank [11] is shown in the figure 2.2.

Figure 2.2: Conventionally used storage tanks

2.2.4 Riser and header

Riser and header is the pipe network through which heat transfer fluid pass through. The material selection is same as absorber with high thermal conductivity and low heat capacity and also light-weight for flexible construction. The headers and risers can be assembled in different manner for heating purposes and efficient heat transfer.

Absorber plate lies in different position of the risers such as above the risers, below the risers and at the middle of the risers. Figure 2.3 (A-C) describes riser and header setting of a FPSC [12].

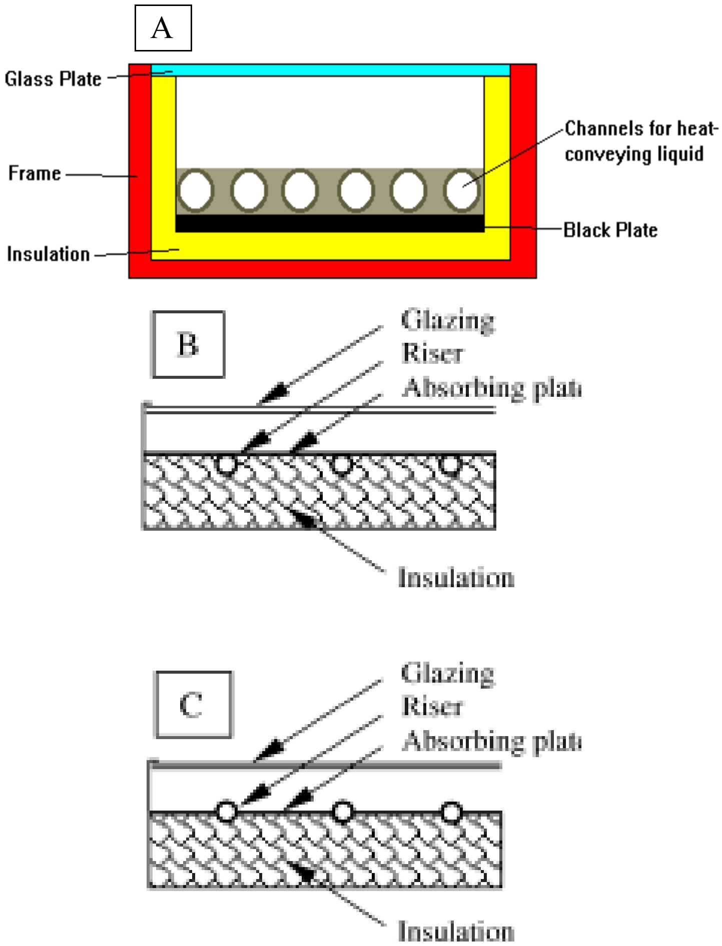

Figure 2.3: Riser and header setting in FPSC (A) above riser, (B) below riser and (C) middle of riser

2.2.5 Various types of bonding

The riser tubes must be bonded to the flat plate with a good thermal contact to facilitate transfer of the heat from absorber to riser. There is a great variety in riser pipe and absorber bonding of successful solar collector-absorber plate {[13] and Kalogirou (2004)}for liquid heating as shown in figure 2.4 (A-D). Trapezium shaped, rectangular shaped, vertical shaped and semi-circular shaped bonding conductance are shown below. The tube-in-strip type of construction is the best from the thermal point of view, since the tubes are integral with the flat plate.

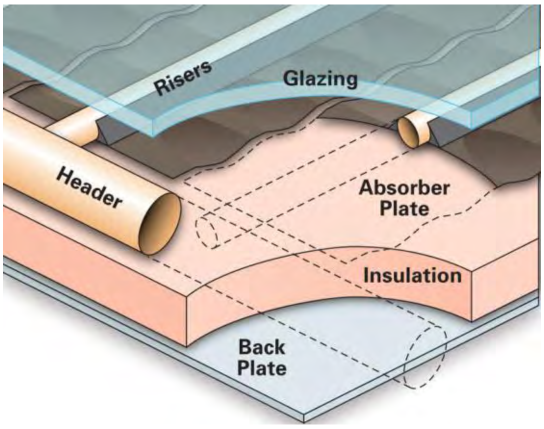

(A) Trapezium bonding

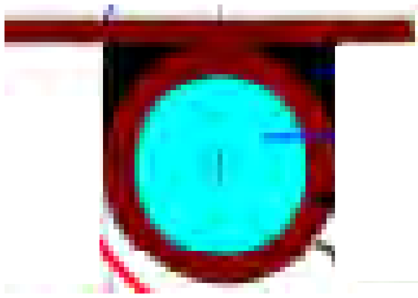

(B) Rectangular bonding

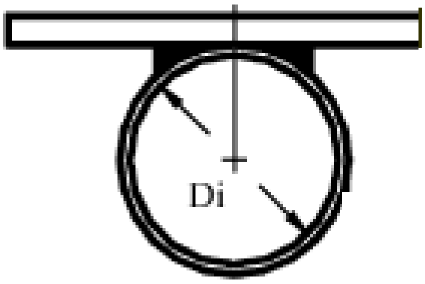

(C) Vertical bonding

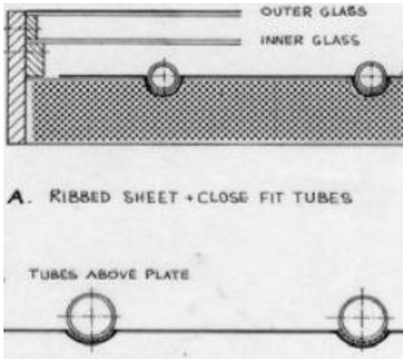

(D) Semi-circular bonding

Figure 2.4: Various types of bonding in FPSC (A) trapezium, (B) rectangular, (C) vertical and (D) semi-circular

2.2.6 Various types of riser pipe

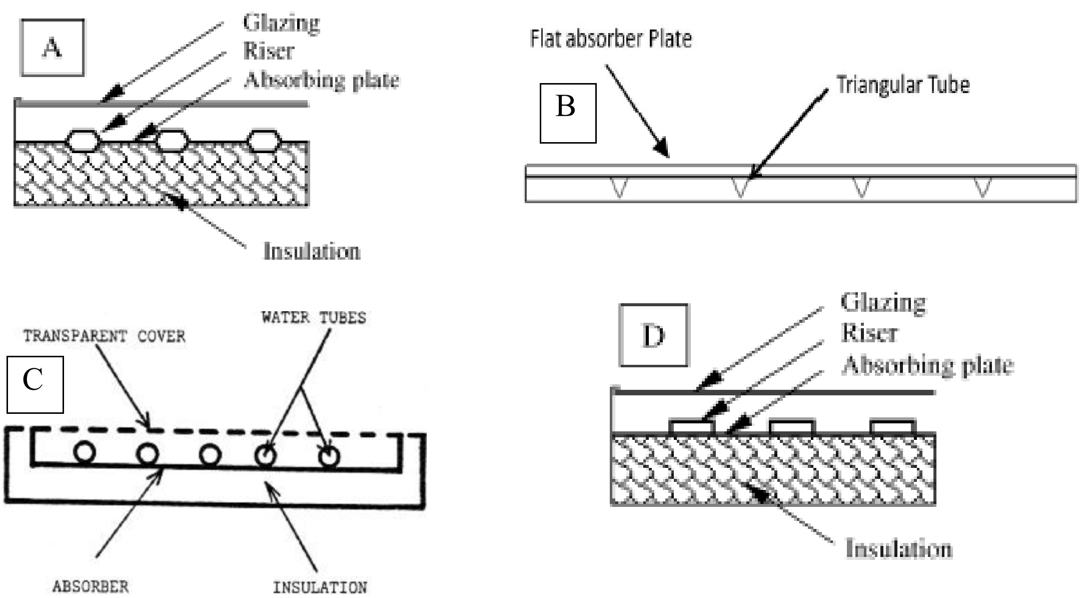

Figure 2.5: Various shapes of riser pipe (A) hexagonal, (B) triangular, (C) circular and (D) rectangular

Various shapes of riser pipe in FPSC for water heating system are shown in the figure 2.5(A)-(D) according to Kalogirou (2004). Different shapes of risers are: hexagonal, triangular, circular and rectangular. Among them the circular shape is commonly used.

2.2.7 Heat loss

According to Strukmann (2008) the figure 2.6 shows heat flow through a typical FPSC. Heat losses in different ways from a FPSC. The glass cover reflects a small part of the sunlight, which does not reach the absorber at all. Some amount of heat is lost by convection and radiation process from the collector. Also heat is lost from edge and backside of collector. Type of heat losses with percentages for a FPSC is given in Table 2.2. To minimize heat loss attention should be paid on following things:

1. The fin (absorber sheet) should be thick to minimize the temperature difference required to transfer heat to its base (tube).
2. Tubes should not be spaced too far apart; otherwise, a higher temperature difference between the tip of the fin (midway between the tubes) and the base will result.
3. The tube should be brazed or welded to the absorber sheet to minimize thermal contact resistance.
4. The tube and absorber sheet should be of similar material to prevent galvanic corrosion between them.

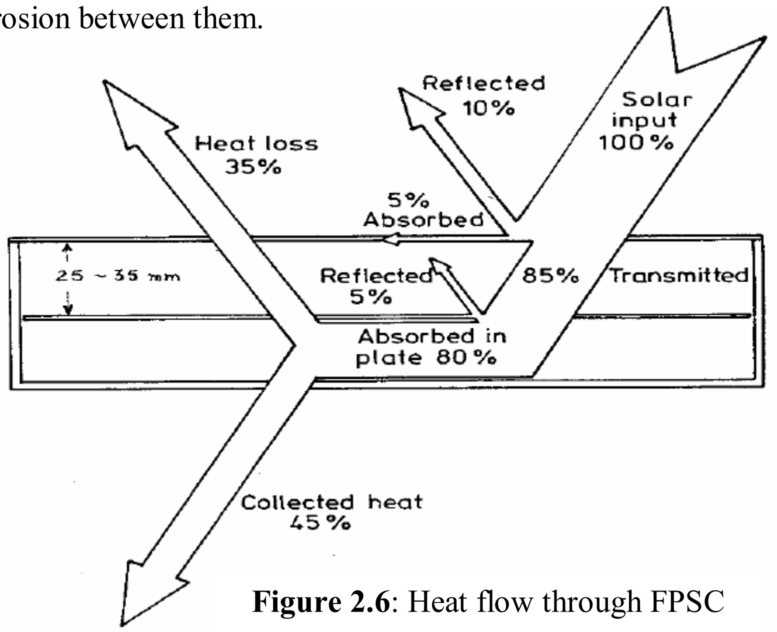

Figure 2.6: Heat flow through FPSC

Table 2.2: Type of heat losses through FPSC

Type of heat loss	Percentage
Edge	1-3%
Back	5-10%
Radiation	5-7%
Convection	15-25%

2.2.8 Area of FPSC

In the figure 2.7 the reference areas in the most common solar flat-plate collector is reported [14]. Three kinds of area are defined for a solar thermal collector:

- The absorber area is the area of the absorber element
- The aperture area is the area of the cover surface where the solar radiation enters the collector and
- The gross area is the total area occupied from a collector module.

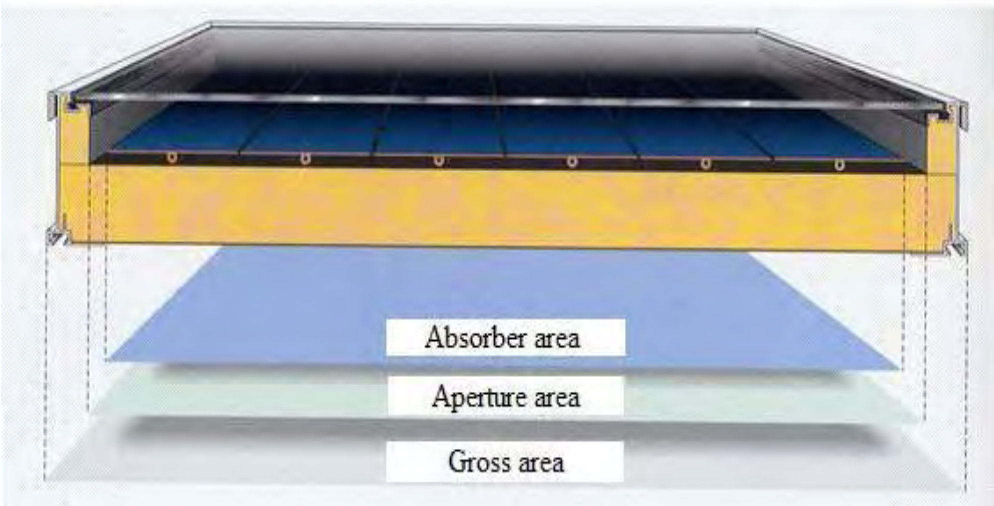

Figure 2.7: Reference areas for a FPSC

2.2.9 Temperature distribution

According to Ekramian *et al.* (2014) the temperature of absorber plate has a symmetry form on each riser pipe as the following figure 2.8. Because of symmetry of temperature distribution on riser pipes one riser pipe is considered for numerical simulation or theoretical calculation. Mass flow rate (m) and useful energy (q) will be calculated from total amount divided by number of riser pipes (N).

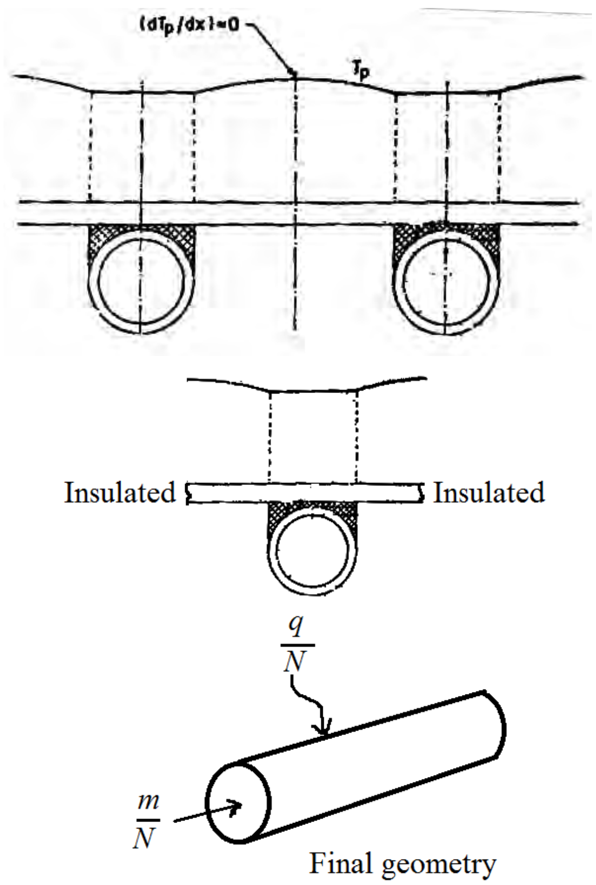

Figure 2.8: Temperature distribution of FPSC

2.3 Physical Model

Actual view of a traditional flat plate solar collector is shown in figure 2.9. This drawing is made using Solidworks software. This FPSC is considered for a family of two persons in Bangladesh. Some calculation is needed to draw this picture considering a family of two persons:

Mean demand of water per person per day in Bangladesh is V = 40 liter

Assumed temperature rise of water (T_{out} - T_{in}) = 30^0C

Heating load for a family of 2 persons per day $Q_{usfl} = mC_p\,(T_{out} - T_{in})$ = 2*40*4179*30 KJ/day = 10032 KJ/day

Let mean efficiency of collector η = 45%

Mean solar irradiation in Bangladesh I = 18000 KJ/m^2/day

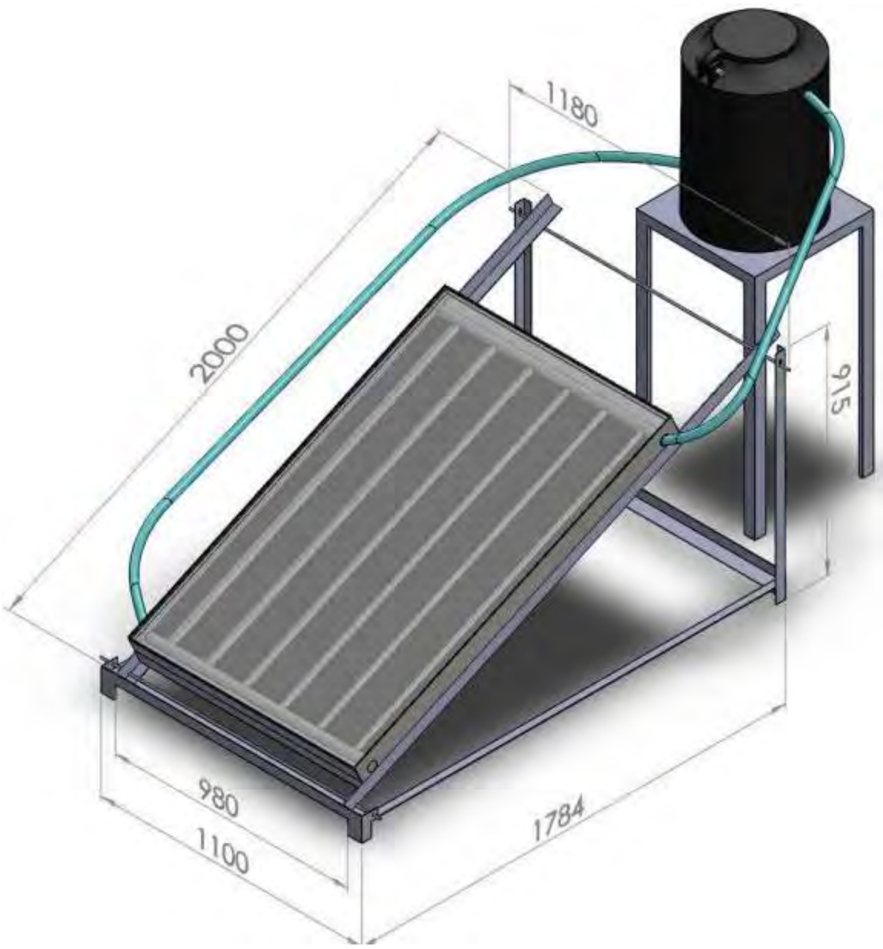

Figure 2.9: Traditional FPSC with storage tank

Thus collector area $A = Q_{usfl} / \eta I$ = 10032 / (0.45*18000) m^2 = 1.24 m^2

Let absorber plate length L = 1.32 m and width W = 0.94 m

Mass flow rate = 1.2 L/min per m^2 of collector = (1.2*1.24)/60 Kg/s = 0.0248 Kg/s

Recommended value of riser inner diameter = 0.01m and outer diameter = 0.0105m

Recommended value of header inner diameter = 0.038m, thickness = 0.002m

Let collector heat transfer coefficient U_l = 8 W/m^{2}K

Copper plate thermal conductivity k_a = 380 W/mK and thickness δ_a = 0.0005m

The collector efficiency factor represents the temperature distribution along the absorber plate (fins) between the tubes. The standard fin efficiency for straight fins with rectangular profiles is considered in the figure 2.10 according to Kalogirou (2004).

Let the parameter $m' = \sqrt{U_l / (k_a \delta_a)} = 10.26\text{m}^{-1}$ and the standard fin efficiency is

$$F = \frac{\tanh\left(m'\frac{w-D}{2}\right)}{\left(m'\frac{w-D}{2}\right)} = 0.8$$

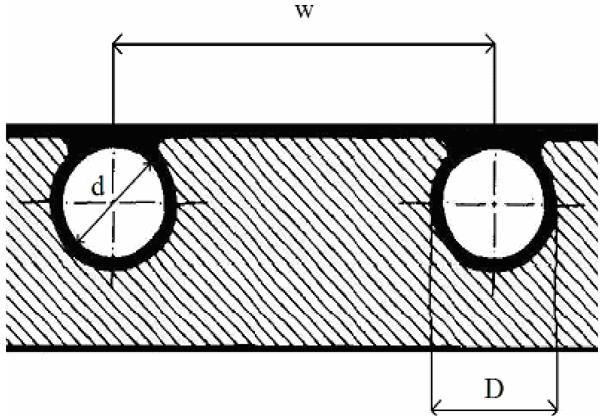

Figure 2.10: Fin and tube setting of a FPSC

Thus distance between the centres of two consecutive tubes:

w = fin efficiency / parameter = 0.8 / m' = 0.8 / 10.26 = 0.077m and

2w = 0.075*2 = 0.154m.

No. of riser = width / (2w + riser outer diameter) = 0.94m / (0.154+0.0105)m ≈ 6

2.4 Schematic Diagram

A schematic diagram of the system and its mesh are shown in figure. 2.11 (i)-(ii). The numerical computation is carried on taking single riser pipe of FPSC. FPSC with single riser pipe gives the average heat transfer and fluid flow phenomena. cover is at the top of the FPSC. It is highly transparent and anti-reflected (called the glazing). The glass top surface is exposed to solar irradiation. It is made up of borosilicate which has thermal conductivity of 1.14 W/mK and refractive index of 1.47, specific heat of 750 J/kgK and coefficient of sunlight transmission of 95%. The wavelength of visible light is roughly 700 nm. Thickness of glass cover is 0.005m. There is an air gap of 0.005m between glass cover and absorber plate. Air density = 1.269 Kg/m^3, specific heat = 287.058 J/kgK and thermal conductivity = 0.0243 W/mK. All these properties of air domain represent air of temperature at 298K. A dark colored copper absorber plate is under the air gap. Length, width and thickness of the absorber plate are 1m, 0.15m and 0.0005m respectively. Coefficients of heat absorption and emmision of copper absorber plate are 95% and 5% respectively. The riser pipe has inner diameter 0.01 m and thickness 0.0005m. The riser tube is also made in copper metal. A trapezium shaped bonding conductance of copper metal is attached to the absorber and riser pipe.

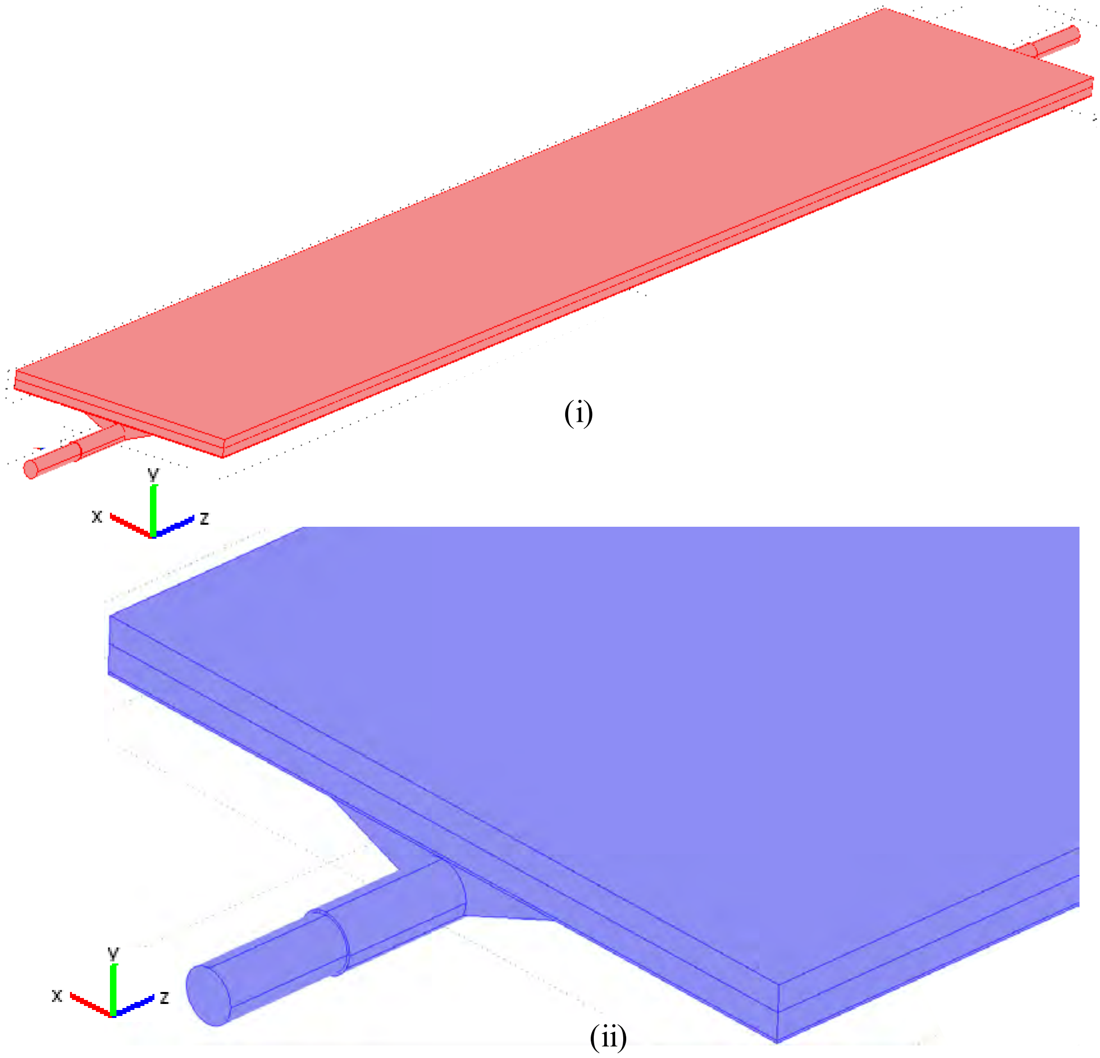

Figure 2.11: Schematic diagram of a FPSC (i) full view and (ii) close view

2.4.1 Computational domain

A trapezium shaped bonding conductance is located from middle one-third part of width of the absorber plate. It covers the three-fourth part of the riser pipe. It is as long as the absorber plate and tube. The absorber plate is modeled to provide for conduction, convection and radiation in the analysis. Figure 2.12 (i)-(ii) shows schematic diagram of the flat plate solar collector both in 3D view and 2D view.

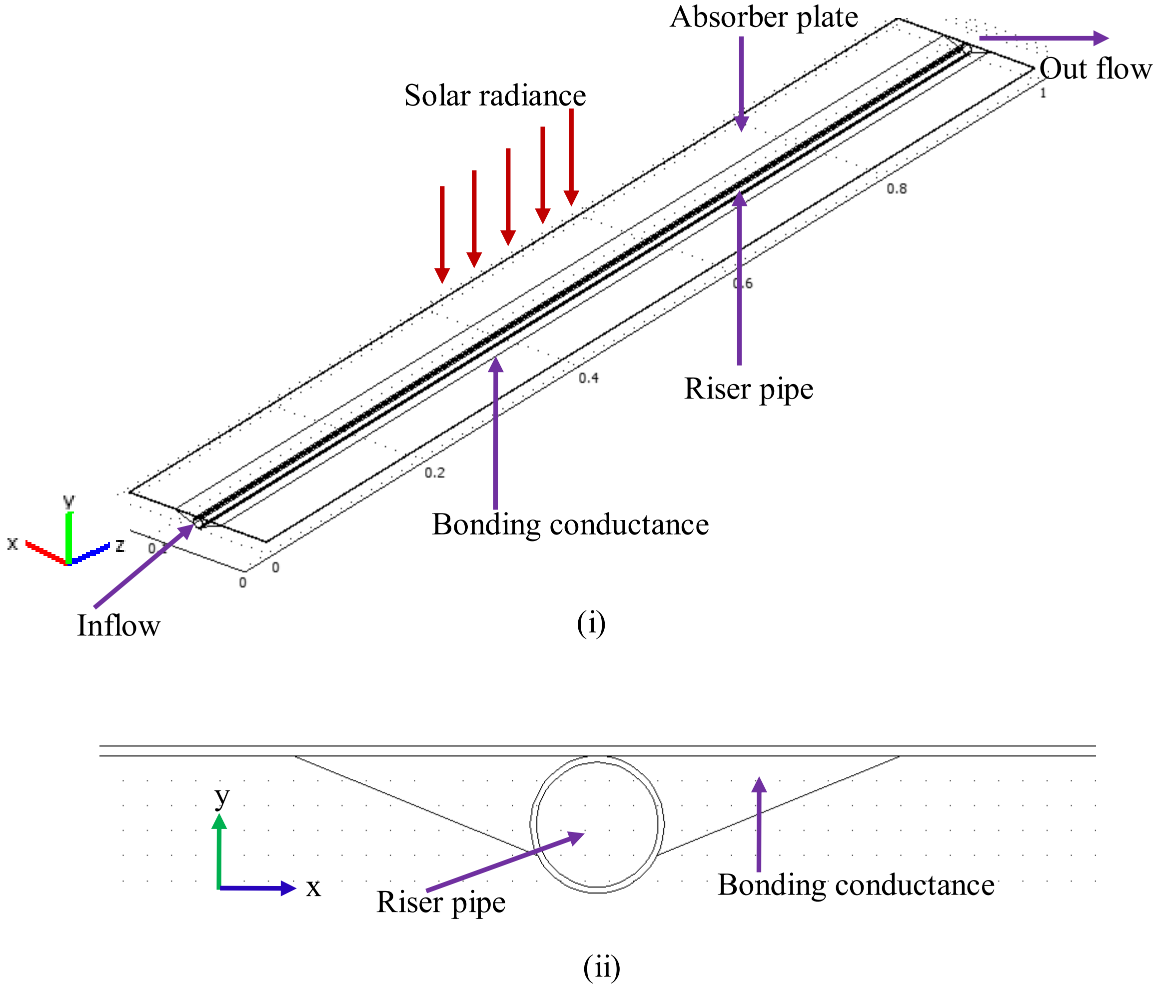

Figure 2.12: Computational domain of the FPSC (i) 3D and (ii) 2D views

2.5 Mathematical Formulation

Figure 2.13 (i)-(ii) {Strukmann (2008) and [15]} shows a typical liquid flat plate solar collector and cross sectional view. Figure 2.14 shows the process occurs at a flat plate solar collector [16]. Thus it is necessary to define step by step the heat flow equations in order to find the governing equations of the collector system. It is necessary to measure thermal performance of a flat plate solar collector, i.e. the useful energy gain or the collector efficiency.

Let I be the intensity of solar radiation, incident on the aperture plane of the solar collector having a collector surface area of A, then the amount of solar radiation received by the collector according to Strukmann (2008) is:

$$Q_i = I.A \tag{2.1}$$

(i)

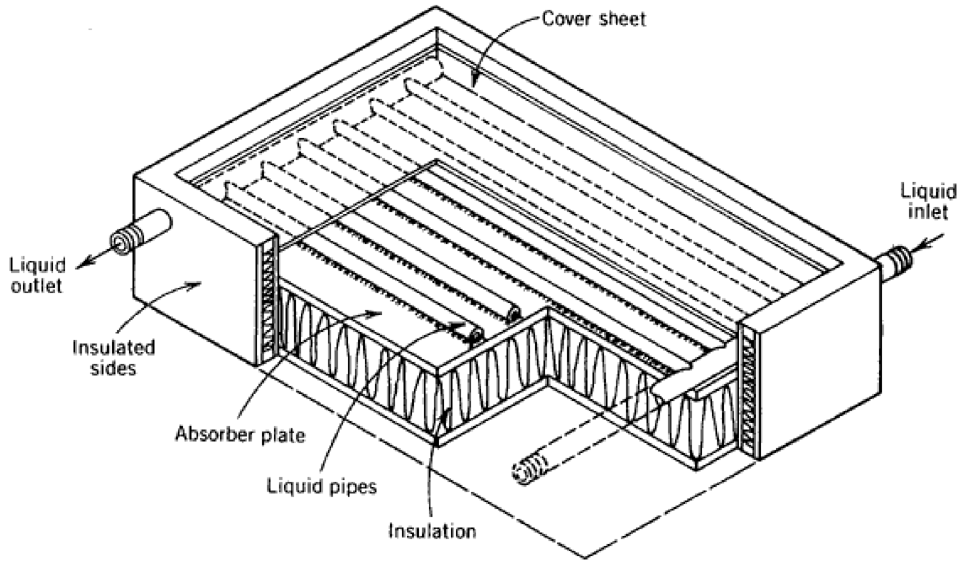

(ii)

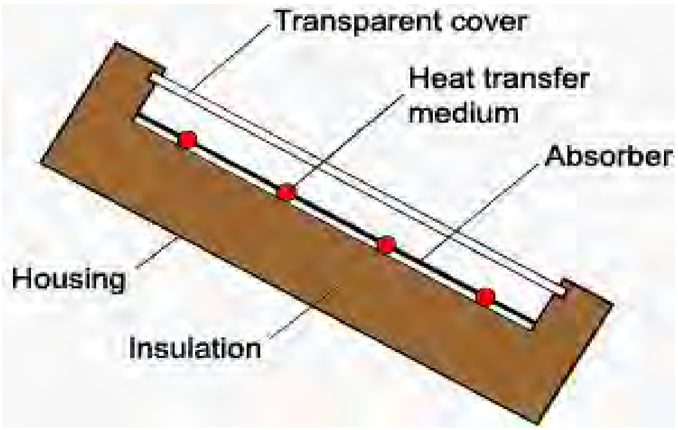

Figure 2.13: A typical liquid FPSC (i) full view and (ii) cross-sectional view

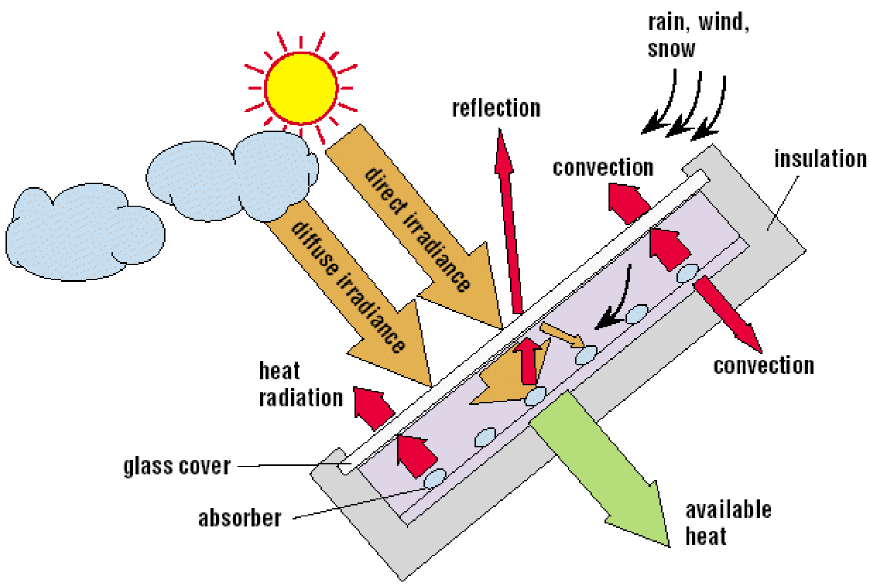

Figure 2.14: Process of heat transfer at a FPSC

A part of this radiation is reflected back to the sky, another component is absorbed by the glazing and the rest is transmitted through the glazing and reaches the absorber plate as short wave radiation.

The conversion factor indicates the percentage of the solar rays penetrating the transparent cover of the collector (transmission) and the percentage being absorbed. Basically, it is the product of the rate of transmission of the cover (λ) and the absorption rate of the absorber (κ). Thus,

$$Q_{recv} = I(\lambda\kappa)A \tag{2.2}$$

As the collector absorbs heat its temperature is getting higher than that of the surrounding and heat is lost to the atmosphere by convection and radiation. The rate of heat loss (Q_{loss}) depends on the collector overall heat transfer coefficient (h) and the collector temperature (T_{col}).

$$Q_{loss} = U_l A(T_{col} - T_{amb}) \tag{2.3}$$

Thus, the rate of useful energy extracted by the collector (Q_{usfl}), expressed as a rate of extraction under steady state conditions, is proportional to the rate of useful energy absorbed by the collector, less the amount lost by the collector to its surroundings. This is expressed as follows:

$$Q_{usfl} = Q_{recv} - Q_{loss} = I(\lambda\kappa)A - U_l A(T_{col} - T_{amb}) \tag{2.4}$$

where T_{col} and T_{amb} be collector average temperature and ambient temperature outside the absorber respectively. It is also known that the rate of extraction of heat from the collector may be measured by means of the amount of heat carried away in the fluid passed through it, that is:

$$Q_{usfl} = mC_p(T_{out} - T_{in}) \tag{2.5}$$

where m be the mass flow rate of the fluid flowing through the collector, C_p be the specific heat at constant pressure, T_{in} and T_{out} be inlet and outlet fluid temperatures, respectively.

Equation (2.4) may be inconvenient because of the difficulty in defining the collector average temperature. It is convenient to define a quantity that relates the actual useful energy gain of a collector to the useful gain if the whole collector surface is at the fluid inlet temperature. This quantity is known as "the collector heat removal factor (F_R)" and is expressed as:

$$F_R == \frac{mC_p\left(T_{out}-T_{in}\right)}{A\left[I\left(\tau\kappa\right)-U_l\left(T_{in}-T_{amb}\right)\right]} \tag{2.6}$$

The maximum possible useful energy gain in a solar collector occurs when the whole collector is at the inlet fluid temperature. The actual useful energy gain (Q_{usfl}), is found by multiplying the collector heat removal factor (F_R) by the maximum possible useful energy gain. This allows the rewriting of equation (2.4):

$$Q_{usfl} = F_R A\left[I\left(\tau\kappa\right)-U_l\left(T_{in}-T_{amb}\right)\right] \tag{2.7}$$

Equation (2.7) is a widely used relationship for measuring collector energy gain and is generally known as the "**Hottel-Whillier-Bliss equation**".

The heat flux (q) per unit area of the absorber surface is now denoted as

$$\frac{Q_{usfl}}{A} = q = I\tau\kappa - U_l\left(T_{in}-T_{amb}\right) \tag{2.8}$$

The incident radiation is considered to be the incoming solar radiation. For the study of the principal behavior of the nanofluid based FPSC, atmospheric absorption is neglected in this calculation. Once the intensity distributions are evaluated, the energy balance on the solar collector is performed and the temperature profile within it is obtained. In order to carry out these steps, some assumptions are made:

The working fluid in the collector is water-based nanofluid containing Cu nanoparticles. The nanoparticles are generally spherical shaped and diameter is taken as 10 nm. The nanofluid is considered as single phase flow and surfactant analysis is neglected. In the present problem, it can be considered that the flow is considered to be laminar and there is no viscous dissipation. The nanofluid is assumed incompressible. It is taken that water and nanoparticles are in thermal equilibrium and no slip occurs between them. The density of the nanofluid is approximated by the Boussinesq model. Only steady state case is considered.

Chapter 3: Two Dimensional Analysis

3.1 Introduction

The basic principle of solar thermal collection is that when solar radiation is incident on a surface (such as that of a black-body), part of this radiation is absorbed, thus increasing the temperature of the surface. As the temperature of the body increases, the surface loses heat at an increasing rate to the surroundings. Steady-state is reached when the rate of the solar heat gain is balanced by the rate of heat loss to the ambient surroundings.

In this chapter, the structure of a FPSC is described elaborately. Then 3D as well as 2D drawing of a FPSC are displayed. At first, the 2D numerical study is accounted to show the heat transfer by nanofluid through the riser pipe of a FPSC. Numerical code validation is shown also. Numerical solutions are obtained over a wide range of solar irradiation (I), Reynolds number (Re), Prandtl number (Pr) and solid volume fraction (ϕ). The numerical results are presented graphically in terms of isothermal lines, streamlines, surface plot, boundary plot and arrow plot. Finally the average Nusselt number (Nu) at the top of riser pipe, mean bulk temperature (T_{av}), subdomain mean velocity (V_{av}), mid-height temperature (T), mean output temperature (T_{out}) and percentage of collector efficiency (η) of water/Cu nanofluid as well as base fluid through FPSC are calculated.

3.2 Two Dimensional Modeling

At first, the 2D numerical analysis for fluid flow and heat transfer mechanism through a FPSC is considered due to simplicity of computation. Figure 2.12 (ii) represents 2D computational domain for the present study. That figure is the transverse cross section of 3D figure 2.12(i). But there is a problem to analyze fluid inflow and fluid outflow. Also output temperature of fluid and collector efficiency can‟t be calculated, because the 2D view doesn‟t have any fluid flow passage. That‟s why a longitudinal cross section of figure 2.12(i) is taken as the 2D geometry of a FPSC and is shown in figure 3.1.

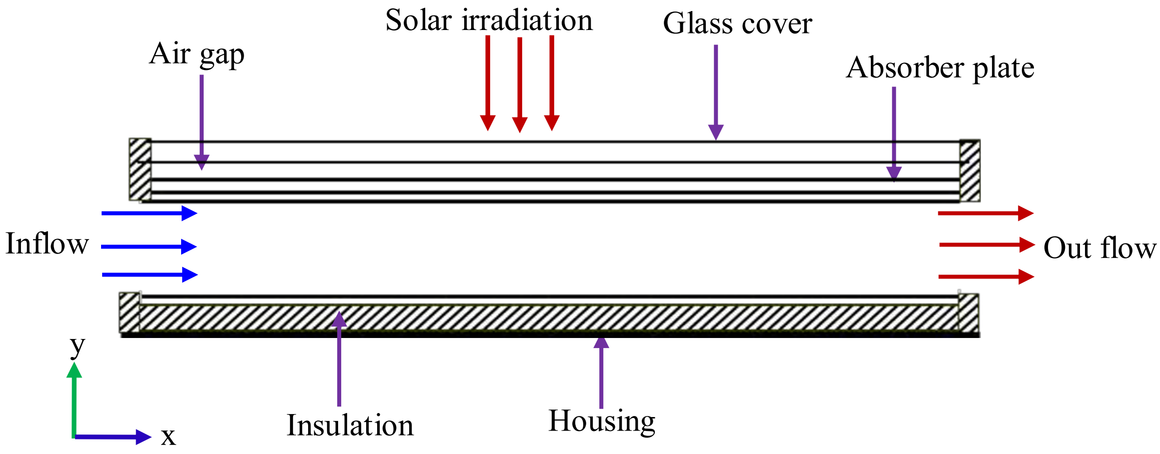

Figure 3.1: Longitudinal cross-section of a FPSC

The governing partial differential equations are as follows:

Continuity equation:

$$\frac{\partial u}{\partial x}+\frac{\partial v}{\partial y}=0 \tag{3.1}$$

x-momentum equation:

$$\rho_{nf}\left(u\frac{\partial u}{\partial x}+v\frac{\partial u}{\partial y}\right)=-\frac{\partial p}{\partial x}+\mu_{nf}\left(\frac{\partial^2 u}{\partial x^2}+\frac{\partial^2 u}{\partial y^2}\right)$$

$$\Rightarrow\left\{(1-\phi)\rho_f+\phi\rho_s\right\}\left(u\frac{\partial u}{\partial x}+v\frac{\partial u}{\partial y}\right)=-\frac{\partial p}{\partial x}+\frac{\mu_f}{(1-\phi)^{2.5}}\left(\frac{\partial^2 u}{\partial x^2}+\frac{\partial^2 u}{\partial y^2}\right) \tag{3.2}$$

$$\Rightarrow\left\{(1-\phi)+\phi\frac{\rho_s}{\rho_f}\right\}\left(u\frac{\partial u}{\partial x}+v\frac{\partial u}{\partial y}\right)=-\frac{1}{\rho_f}\frac{\partial p}{\partial x}+\frac{1}{(1-\phi)^{2.5}}\frac{1}{Re}u_{in}L\left(\frac{\partial^2 u}{\partial x^2}+\frac{\partial^2 u}{\partial y^2}\right)$$

y-momentum equation:

$$\rho_{nf}\left(u\frac{\partial v}{\partial x}+v\frac{\partial v}{\partial y}\right)=-\frac{\partial p}{\partial y}+\mu_{nf}\left(\frac{\partial^2 v}{\partial x^2}+\frac{\partial^2 v}{\partial y^2}\right)$$

$$\Rightarrow\left\{(1-\phi)\rho_f+\phi\rho_s\right\}\left(u\frac{\partial v}{\partial x}+v\frac{\partial v}{\partial y}\right)=-\frac{\partial p}{\partial y}+\frac{\mu_f}{(1-\phi)^{2.5}}\left(\frac{\partial^2 v}{\partial x^2}+\frac{\partial^2 v}{\partial y^2}\right) \tag{3.3}$$

$$\Rightarrow\left\{(1-\phi)+\phi\frac{\rho_s}{\rho_f}\right\}\left(u\frac{\partial v}{\partial x}+v\frac{\partial v}{\partial y}\right)=-\frac{1}{\rho_f}\frac{\partial p}{\partial y}+\frac{1}{(1-\phi)^{2.5}}\frac{1}{Re}u_{in}L\left(\frac{\partial^2 v}{\partial x^2}+\frac{\partial^2 v}{\partial y^2}\right)$$

Energy equation for nanofluid:

$$
\begin{aligned}
&\left(\rho C_p\right)_{nf}\left(u\frac{\partial T}{\partial x}+v\frac{\partial T}{\partial y}\right)=k_{nf}\left(\frac{\partial^2 T}{\partial x^2}+\frac{\partial^2 T}{\partial y^2}\right)\\
&\Rightarrow\left(u\frac{\partial T}{\partial x}+v\frac{\partial T}{\partial y}\right)=\frac{k_{nf}}{\left(\rho C_p\right)_{nf}}\left(\frac{\partial^2 T}{\partial x^2}+\frac{\partial^2 T}{\partial y^2}\right)\\
&\Rightarrow\left(u\frac{\partial T}{\partial x}+v\frac{\partial T}{\partial y}\right)=\alpha_{nf}\left(\frac{\partial^2 T}{\partial x^2}+\frac{\partial^2 T}{\partial y^2}\right)\\
&\Rightarrow\left(u\frac{\partial T}{\partial x}+v\frac{\partial T}{\partial y}\right)=\frac{\alpha_{nf}}{\alpha_f}\frac{1}{Re\,Pr}u_{in}L\left(\frac{\partial^2 T}{\partial x^2}+\frac{\partial^2 T}{\partial y^2}\right)
\end{aligned}
\tag{3.4}
$$

Energy equation for absorber:

$$\left(\frac{\partial^2 T_a}{\partial x^2}+\frac{\partial^2 T_a}{\partial y^2}\right)=0 \tag{3.5}$$

where $\alpha_{nf}=k_{nf}/\left(\rho C_p\right)_{nf}$ be the thermal diffusivity, (3.6)

$\rho_{nf}=(1-\phi)\rho_f+\phi\,\rho_s$ be the density, (3.7)

$\left(\rho C_p\right)_{nf}=(1-\phi)\left(\rho C_p\right)_f+\phi\left(\rho C_p\right)_s$ be the heat capacitance, (3.8)

$\mu_{nf}=\dfrac{\mu_f}{(1-\phi)^{2.5}}$ be the viscosity of Brinkman model (1952), (3.9)

$k_{nf}=k_f\dfrac{k_s+2k_f-2\phi\left(k_f-k_s\right)}{k_s+2k_f+\phi\left(k_f-k_s\right)}$ be the thermal conductivity of Maxwell Garnett (MG) model (1904), (3.10)

$Pr=\dfrac{\nu_f}{\alpha_f}$ be the Prandtl number and $Re=\dfrac{u_{in}L}{\nu_f}$ be the Reynolds number.

The boundary conditions of the riser pipe are:

at all solid boundaries: $u=v=0$

at the solid-fluid interface: $k_{nf}\left(\dfrac{\partial T}{\partial y}\right)_{nf}=k_{solid}\left(\dfrac{\partial T_a}{\partial y}\right)_{solid}$

at the inlet boundary: $T=T_{in}$, $u=u_{in}$

at the outlet boundary: convective boundary condition $p=0$

at the top surface of absorber: heat flux $-k_a\dfrac{\partial T_a}{\partial y}=q=I\tau\kappa-U_l\left(T_{in}-T_{amb}\right)$

at outer surface of riser pipe: $\frac{\partial T}{\partial y} = 0$

3.2.1 Average Nusselt number

The average Nusselt number (Nu) is expected to depend on a number of factors such as thermal conductivity, heat capacitance, viscosity, flow structure of nanofluids and volume fraction, dimensions and fractal distributions of nanoparticles.

Equation of local Nusselt number for flow through the absorber tube of solar collector can be written as

$$\overline{Nu} = \frac{U_l L}{k_f} = \frac{Q}{\Delta T}\left(\frac{L}{k_f}\right) = \frac{Q}{\left(qL/k_f\right)}\left(\frac{L}{k_f}\right)$$

where L is the length of riser pipe, ΔT is the difference between riser pipe surface temperature and ambient temperature, Q is the energy received or lost by the absorber pipe surface. For a flat plate solar collector constant heat flux is assigned at the absorber top surface. For water based nanofluid flow this equation becomes

$$\overline{Nu} = \frac{-k_{nf}\left(\frac{\partial T}{\partial y}\right)}{\left(qL/k_f\right)}\left(\frac{L}{k_f}\right) = -\left(\frac{k_{nf}}{k_f}\right)\left(\frac{k_f}{q}\right)\left(\frac{\partial T}{\partial y}\right)$$

The non-dimensional form of local heat transfer rate at the riser pipe solid surface is

$$\overline{Nu} = -\frac{k_{nf}}{k_f}\frac{\partial \theta}{\partial Y}$$

The above equations are non-dimensionalized by using the following dimensionless quantities

$$X = \frac{x}{L},\ Y = \frac{y}{L},\ \theta = \frac{\left(T - T_{in}\right)k_f}{qL}$$

By integrating the local Nusselt number over the riser pipe, the average heat transfer rate of the collector can be written as $Nu = \frac{1}{L}\int_0^L \overline{Nu}\, dX$ (3.11)

3.2.2 Mean bulk temperature and velocity

The mean bulk temperature and average sub domain velocity of the fluid inside the collector may be written as

$$T_{av} = \frac{\iint_{\overline{A}} T d\overline{A}}{\iint_{\overline{A}} d\overline{A}} = \frac{\iint_{\overline{A}} T d\overline{A}}{HL} \text{ and } \mathrm{V}_{av} = \frac{\iint_{\overline{A}} \mathrm{V} d\overline{A}}{\iint_{\overline{A}} d\overline{A}} = \frac{\iint_{\overline{A}} \mathrm{V} d\overline{A}}{HL} \tag{3.12}$$

where $\overline{A}$, L, H and V are the area, length and height of the of absorber tube, magnitude of subdomain velocity respectively.

3.2.3 Collector efficiency

A measure of a flat plate collector performance is the collector efficiency (η) defined as the ratio of the useful energy gain (Q_{usfl}) to the incident solar energy over a particular time period:

$$\eta = \frac{\int Q_{\text{usfl}}\, dt}{A\int I\, dt}$$

The instantaneous thermal efficiency of the collector is:

$$\eta = \frac{\text{useful gain}}{\text{available energy}} = \frac{Q_{\text{usfl}}}{AI} = \frac{F_R A\left[I(\tau\kappa) - U_l\left(T_{in} - T_{amb}\right)\right]}{AI} = F_R(\tau\kappa) - F_R U_l \frac{\left(T_{in} - T_{amb}\right)}{I} \tag{3.13}$$

where $F_R == \dfrac{mC_p\left(T_{out} - T_{in}\right)}{A\left[I(\tau\kappa) - U_l\left(T_{in} - T_{amb}\right)\right]}$.

3.2.4 Overall heat transfer coefficient

The overall heat transfer loss from the collector is the summation of three separate components, the top loss coefficient, the bottom loss coefficient and the edge loss coefficient. The empirical relations for these coefficients are mentioned by Duffie and Beckman (1991) and Al-Ajlan *et al.* (2003) as follows:

$$U_l = U_t + U_b + U_e \tag{3.14}$$

where U_t is the heat loss coefficient from the top, U_b is the heat loss coefficient from the bottom, and U_e is the heat loss coefficient from the edges of collector.
These can be calculated from the following relations:

$$U_t = \left\{ \frac{N}{\frac{C}{T_a}\left[\frac{T_a - T_{amb}}{N+f}\right]^c} + \frac{1}{h_{amb}} \right\}^{-1} + \frac{\sigma\left(T_a + T_{amb}\right)\left(T_a^2 + T_{amb}^2\right)}{\frac{1}{\left(\varepsilon_a + 0.00591 N h_{amb}\right)} + \frac{2N + f - 1 + 0.13\varepsilon_a}{\varepsilon_c} - N},$$

$$U_b = \frac{k_b}{x_b}, \qquad U_e = \frac{U_e A_e}{A} = \frac{k_e}{x_e}\left[\frac{2(L+W)H}{LW}\right],$$

$C = 520 * \left(1 - 0.000051\beta^2\right)$ and

$$f = \left(1 + 0.089 h_a - 0.1166 h_{amb}\varepsilon_a\right) * \left(1 + 0.07866N\right)$$

3.2.5 Thermo-physical properties

The thermo-physical properties of the water and nanoparticles are taken from **Nasrin *et al.*** (2015) and given in Table 3.1.

Table 3.1: Thermo physical properties of fluid and nanoparticles

Physical Properties	Fluid phase (Water)	Ag	Cu
C_p(J/kgK)	4179	235	385
ρ (kg/m^3)	997.1	10500	8933
k (W/mK)	0.613	429	400
$\alpha\times10^7$ (m^2/s)	1.47	1738.6	1163.1
$\mu\times10^6$ (Ns/ m^2)	855	---	-----

3.3 Computational procedure

For computational procedure and graphical representation the softwares Comsol Multiphysics and Tecplot are used in this work. The Galerkin finite element method of Zienkiewicz (1991), Taylor and Hood (1973) and Dechaumphai (1999) is used to solve the governing equations along with CBC for the considered problem. Conservation equations are solved for the FEM to yield the velocity and temperature fields for the water flow in the absorber tube and the temperature field for the absorber plate. The equation of continuity has been used as a constraint due to mass conservation and this restriction may be used to find the pressure distribution. Then the velocity components (u, v) and temperatures (T, T_a) of governing equations (3.1-3.5) are expanded using a basis set. The Galerkin finite element technique yields the subsequent nonlinear residual equations. Gaussian quadrature technique is used to evaluate the integrals in these equations. The non-linear residual equations are solved using Newton–Raphson method to determine the coefficients of the expansions. The convergence of solutions is assumed when the relative error for each variable between consecutive iterations is recorded below the convergence criterion such that $\left|\psi^{n+1} - \psi^{n}\right| \leq 1.0\text{e}^{-6}$, where n is the number of iteration and Ψ is a function of any one of u, v, T and T_a.

3.3.1 Grid refinement test

The arrangement of discrete points throughout the domain is simply called a grid. The determination of a proper grid for the flow through a given geometric shape is important. The way that such a grid is determined is called grid generation. The grid generation is a significant consideration in CFD. Finite element method can be applied to unstructured grids. This is because the governing equations in this method are written in integral form and numerical integration can be carried out directly on the unstructured grid domain in which no coordinate transformation is required.

An extensive mesh testing procedure is conducted to guarantee a grid-independent solution for Pr = 5.8, ϕ = 2%, I = 215W/m^2 and Re = 480 through a riser pipe of a FPSC. In the present work, five different non-uniform grid systems are examined with the number of elements within the resolution field: 42,010, 99,832, 1,50,472, 1,68,040 and 1,92,548. The numerical scheme is carried out for highly precise key in the average Nusselt number for water-copper nanofluid (ϕ = 2%) as well as base fluid (ϕ = 0%) for the aforesaid elements to develop an understanding of the grid fineness as shown in Table 3.2. This element size is taken from extra fine meshing. Hence, considering the non-uniform grid system of 1,68,040 elements is preferred for the computation.

Table 3.2: Grid test at $Pr = 5.8$, $\phi = 2\%$, $I = 215\text{W/m}^2$ and $Re = 480$

Elements	42,010	99,832	1,40,472	**1,68,040**	1,92,548
***Nu* (Nanofluid)**	1.87872	1.99127	2.10934	**2.14351**	2.14378
***Nu* (Base fluid)**	1.59326	1.69225	1.81524	**1.84333**	1.84341
Time (s)	127.52	308.75	581.11	**897.23**	1295.31

3.3.2 Mesh generation

The discrete locations at which the variables are to be calculated are defined by a mesh which covers the geometric domain on which the problem is to be solved. It divides the solution domain into a finite number of sub-domains called finite elements. The computational domains with irregular geometries by a collection of finite elements make the method a valuable practical tool for the solution of boundary value problems arising in various fields of engineering. Figure 3.2 displays the finite element mesh of the present physical domain. The length and width of the computational domain are 1m and 0.0115m respectively. The meshing consists of triangular element with six nodes.

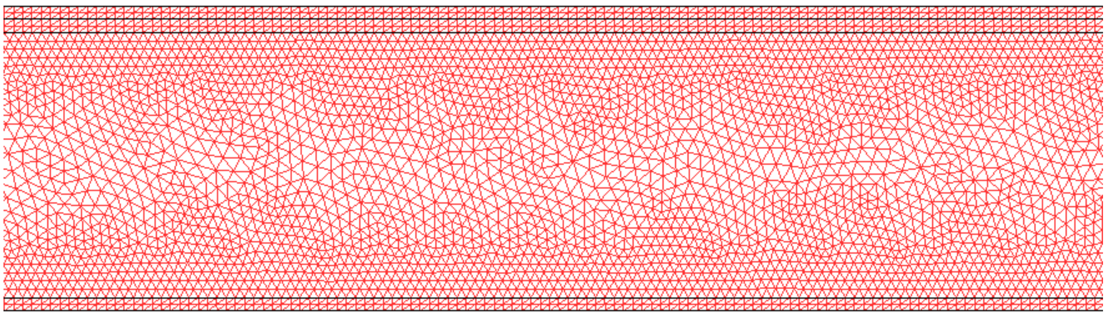

Figure 3.2: Mesh generation of the 2D domain

3.3.3 Numerical results validation

The result obtained from present numerical technique is verified against the existing result available in the literature:

The results for heat transfer -temperature difference profile using present numerical code with that of Gao *et al.* (2000) are compared at $Pr = 0.73$, $Gr = 10^4$, tilt angle $\phi =$

30^0, ratio of the channel height to the amplitude height of the wavelike absorber = 2, ratio of one-fourth of the wavelength to the amplitude height of the absorber = 1. They studied heat transfer augmentation inside a channel between the flat-plate cover and sine-wave absorber of a cross-corrugated solar air heater. Air is the heat transfer medium. Figure 3.3 depicts the result of numerical simulations of the effect of temperature difference (ΔT) on the natural convection heat transfer coefficient (h). The temperature difference between absorber plate and ambient fluid is known as (ΔT) As shown in figure. 3.3, ΔT – h profile of the numerical solutions (present code and Gao *et al.* (2000) are in good agreement.

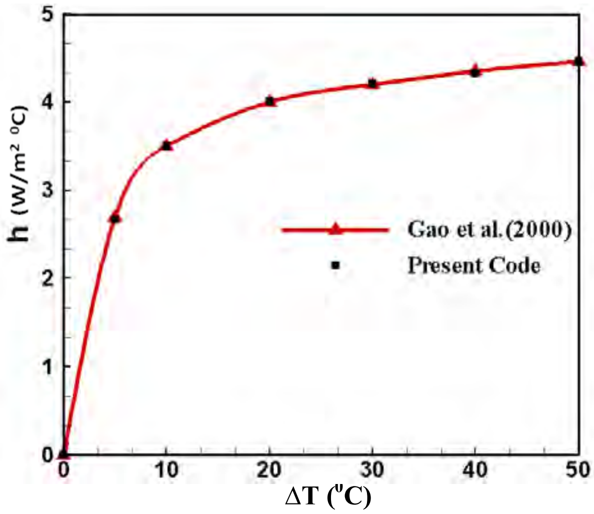

Figure 3.3: Result validation of heat transfer rate

Also, the current code results for streamlines and isotherms at Pr = 0.71, Ra = 10^6, ratio of average height of the channel to amplitude height of the wavy wall = 2, ratio of wavelength to amplitude height of wavy wall = 2, tilt angle ϕ = 40^0 with that of Varol and Oztop (2007) are compared and displayed by the figure 3.4. They studied Buoyancy induced heat transfer and fluid flow inside a tilted wavy solar collector. Figure 3.4 represents good matching of results.

In addition, figure 3.5 shows the results for collector efficiency against (Tfi - Ta) / I_T for 2% concentrated water/silver nanofluid using present code and Polvongsri (2011). Tfi, Ta, I_T are input fluid temperature, ambient temperature of fluid and solar radiation respectively. He studied enhancement of flat-plate solar collector thermal performance with silver nano-fluid. FPSC has area of 0.15 x 1.0 m^2. The nanoparticle size is 20 nm. The values of ($F_r\lambda\alpha$) and (F_rU_l) are chosen as 0.684 and 7.178 W/m^2K

respectively. The flow rate of working fluid is 1.2 liter/min-m^2 and the inlet temperature is varied from 35^0C – 65^0C. Solar irradiation is 18 MJ/m^2-day. Very good agreement is depicted by the figure 3.5.

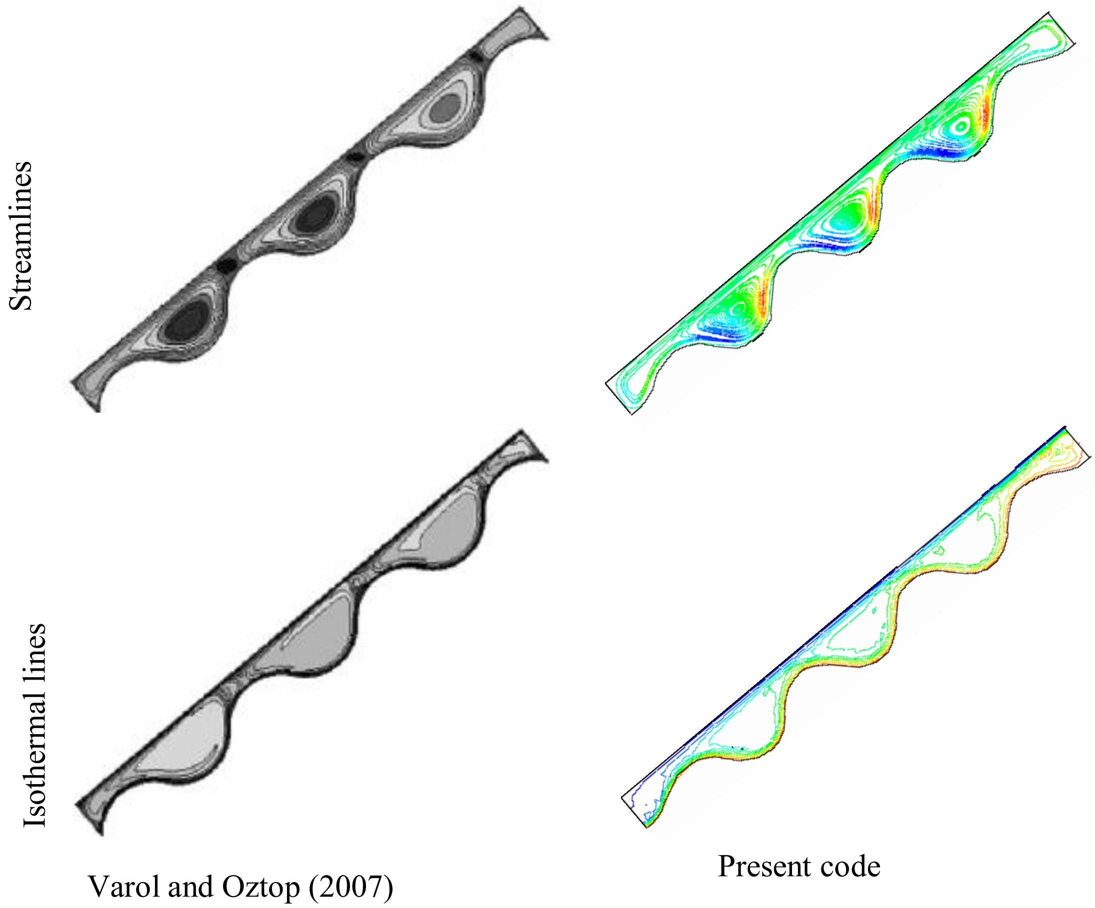

Figure 3.4: Result validation of isothermal lines and streamlines plots

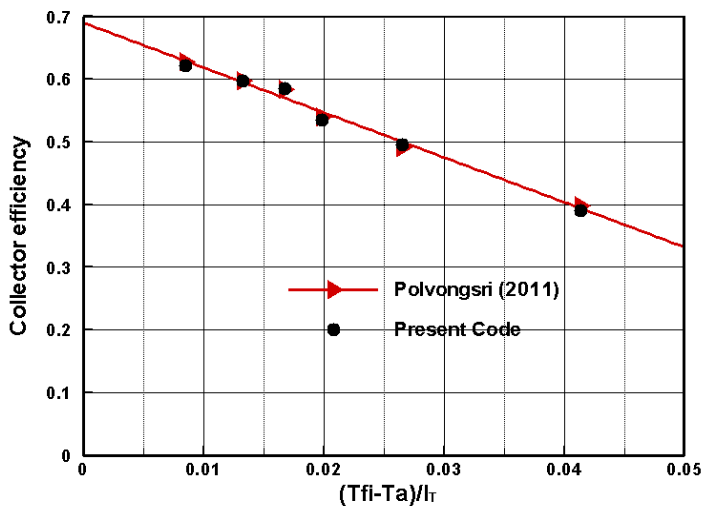

Figure 3.5: Result validation of thermal efficiency

3.4 Result and Discussions

Finite element simulation is applied to perform the analysis of laminar forced convection temperature and fluid flow through a riser pipe of a flat plate solar collector filled with water/copper nanofluid. Effects of the solar irradiation (I), Reynolds number (Re), Prandtl number (Pr) and solid volume fraction (ϕ) on heat transfer and collector efficiency have been studied. The ranges of I, Re, Pr and ϕ, for this investigation vary from 200 W/m^2 to 240 W/m^2, 400 to 500, 4.6 to 6.6 and 0% to 3% respectively. The mass flow rate per unit area (m) is 0.0248 Kg/s, overall heat transfer coefficient (U_l) is 8 W/m^{2}K, aperature area of the collector (A) is 1.8 m^2, number of glass (N) is 1 and nanoparticle size is 10 nm. The outcomes for the different cases are presented in the following sections. The results in this section are published in **Nasrin** and Alim (2014) in the journal of Solar Energy.

3.4.1 Effect of solar irradiation

The effect of solar irradiation (I) on the isothermal lines is presented in figure 3.6 for 2% concentrated water-Cu nanofluid while Pr = 5.8, Re = 480 are kept fixed. Blue and red colors indicate the lowest and highest temperature respectively. This figure shows that rising solar irradiation accelerates thermal current activities through solar collector. Isotherms are almost similar to the active part of riser pipe.

Increasing solar irradiation, the temperature lines at the exit port of the riser pipe become more flatten whereas initially they are bended due to spectral absorption coefficient is dominated across the FPSC. With rising values of I from 200 W/m^2 to 240 W/m^2, the temperature distributions become distorted resulting in an increase in the overall heat transfer. This result can be attributed to the dominance of the absorption coefficient. It is worth noting that as the solar irradiation increases, the thickness of the thermal boundary layer near the output surface expands which indicates a steep temperature gradients and hence, an increase in the overall heat transfer from the hot walls to the fluid through the fluid passing region.

Figure 3.7(i)-(vi) expresses the Nu - I, T_{av} - I, V_{av} - I, temperature at the middle of riser pipe for the effect of I, T_{out} - I and η - I profiles for copper/water nanofluid as well as clear water.

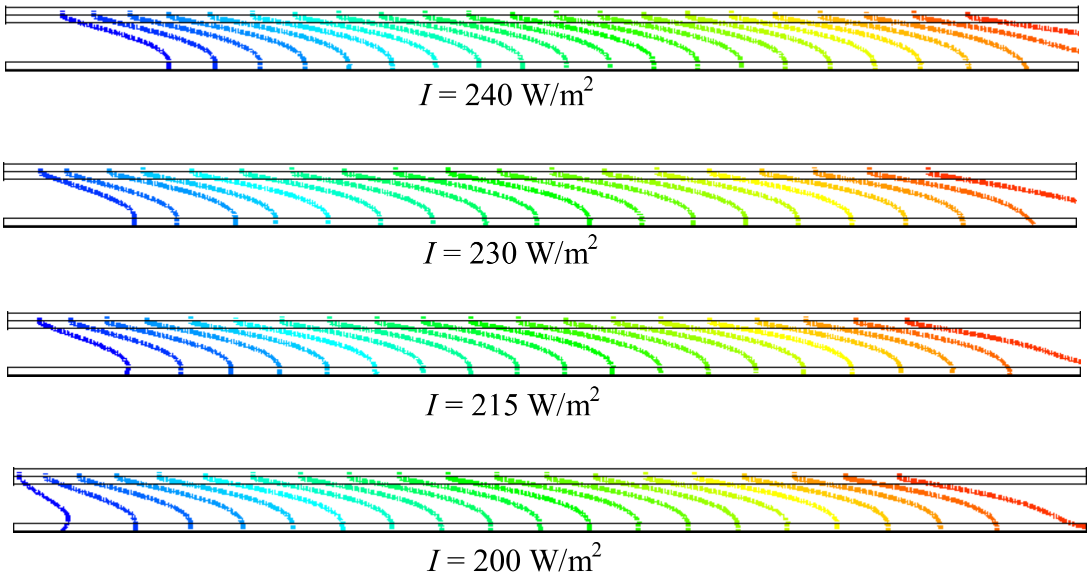

Figure 3.6: Effect of I on isothermal lines

The average Nusselt number increases with rising solar irradiation for both type fluids. The rate of heat transfer enhances 13% and 9% using 2% concentrated water-copper nanofluid and water respectively for rising solar irradiation (I) from 200 W/m^2 to 240 W/m^2.

It is seen from Fig. 3.7(ii) that T_{av} rises sequentially for growing I. It is well known that higher values of solar irradiation (I) indicate higher temperature of fluids. Due to escalating values of I the absorber as well as the riser pipe becomes more heated. As a result fluids can take more heat from hot walls and become hotter. Here base fluid has lower mean bulk temperature than the water-Cu nanofluid.

Magnitude of mean subdomain velocity (V_{av}) grows up for the variation of solar irradiation. Base fluid has higher velocity than nanofluid. It is obvious that density of fluid with solid nanoparticle is higher than clear water. Temperature of 2% concentrated water/Cu nanofluid at the middle of the riser pipe is shown in figure 3.7(iv). From this figure it is observed that the temperature of nanofluid increases gradually when it passes through the riser pipe. The entering cold fluid tries to take heat from the heated riser pipe.

From the figure 3.7(v) it is observed that the mean output temperature of fluids increases for the increasing values of I. The output temperature of nanofluid becomes

312K, 314K, 315K, 316K for nanofluid and 309K, 310K, 311K, 312K for base fluid for I = 200W/m^2, 215 W/m^2, 230 W/m^2 and 240 W/m^2 respectively.

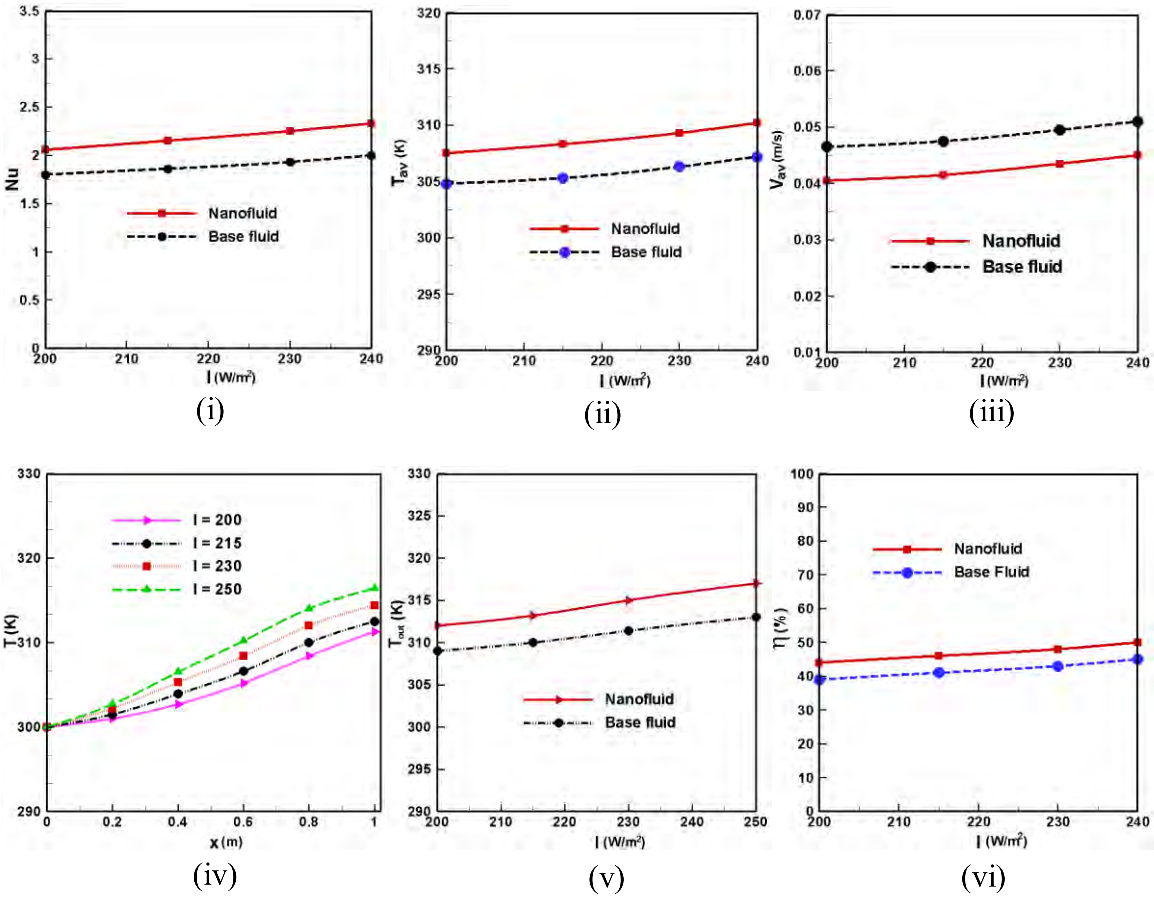

Figure 3.7: Effect of I on (i) mean Nusselt number, (ii) mean bulk temperature, (iii) mean velocity, (iv) mid-height temperature, (v) mean output temperature and (vi) collector efficiency

By introducing greater solar irradiation the collector efficiency increases. More solar irradiance is able to augment heat transfer system through the riser pipe of a flat plate solar collector. In this scheme 2% solid concentrated water/copper nanofluid performs better than clear water (ϕ = 0%). Thermal efficiency enhances from 44%-50% for nanofluid and 39%-45% for water.

3.4.2 Effect of Reynolds number

In the temperature distribution of figure 3.8 the isothermal lines of 2% concentrated water/Cu nanofluid for different values of Reynolds number (Re) is depicted at I = 215 W/m^2 and Pr = 5.8. Values of Re are chosen as 400, 440, 480 and 500. This figure shows that at low value of Re (= 400), the temperature of the fluid rapidly reaches to the temperature of hot riser pipe wall due to low velocity. With increasing Reynolds number, increment of temperature of fluid is happened slowly, as a result the isotherms are more compressed at the top surface of the riser pipe near the exit boundary. The thermal boundary layer thickness enhances for the greater values of inertia force. At *Re* = 500 it is observed that low tempered (green color) fluid also passes through the outlet due to high velocity of fluid. It doesn‟t become hotter.

The rate of heat transfer, average bulk temperature, mean sub-domain velocity, mean output temperature and thermal efficiency for two types of fluids and mid-height temperature for water/copper nanofluid are plotted against the Reynolds number in figure 3.9(i)-(vi). The rate of heat transfer for water-copper nanofluid (ϕ = 2%) is found to be higher than the clear water (ϕ = 0%) due to higher thermal conductivity of solid nanoparticles. Heat transfer rate enhances by 15% and 10% for nanofluid and base fluid respectively with the variation of Reynolds number from 400 to 480. After that at *Re* = 500 heat transfer rate decreases slightly due to higher inertia force. So, higher velocity of fluid doesn‟t give better performance of heat transfer.

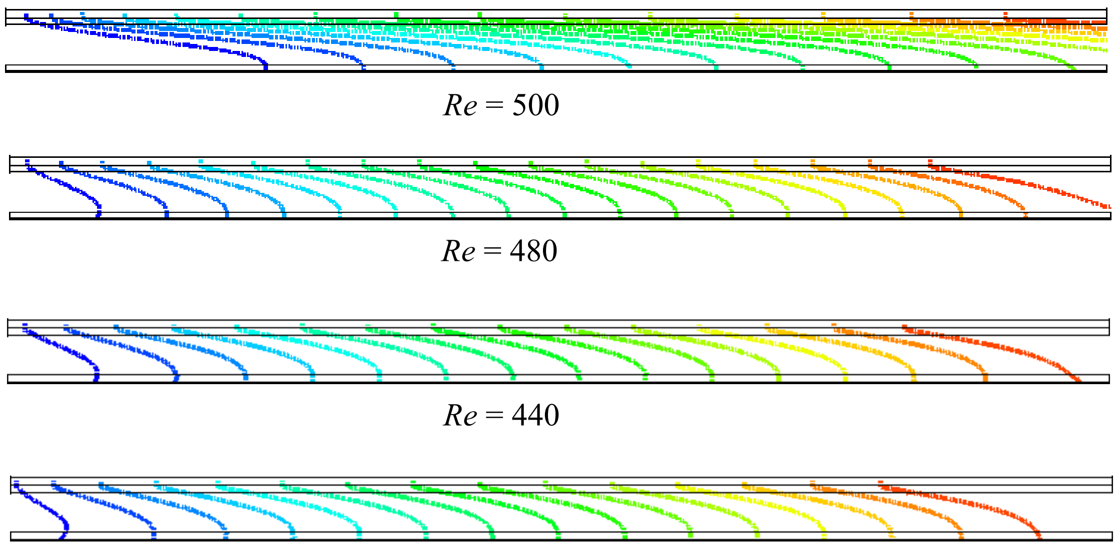

Re = 500

Re = 480

Re = 440

Re = 400

Figure 3.8: Effect of *Re* on isothermal lines

Average bulk temperature (T_{av}) has noteworthy changes with different values of Reynolds number. It rises consecutively for growing *Re* from 400 to 480. After that mean temperature devalues faintly. Increasing fluid velocity up to a certain level enhances temperature inside the domain due to particle friction. The Cu/water nanofluid has higher temperature than clear water.

From the figure 3.9(iii) it is seen that increasing Reynolds numbers raise the fluid velocity successively. Greater inertia force has capable to enhance the fluid velocity through the riser pipe. Nanofluid has lower velocity than base fluid.

Temperature of Cu-water nanofluid at the middle of the riser pipe is shown in figure 3.9(iv). Initially temperature of nanofluid is 300K. Its temperature rises when it passes through the riser pipe for each value of Reynolds number. Maximum temperature is obtained for Reynolds number is 480.

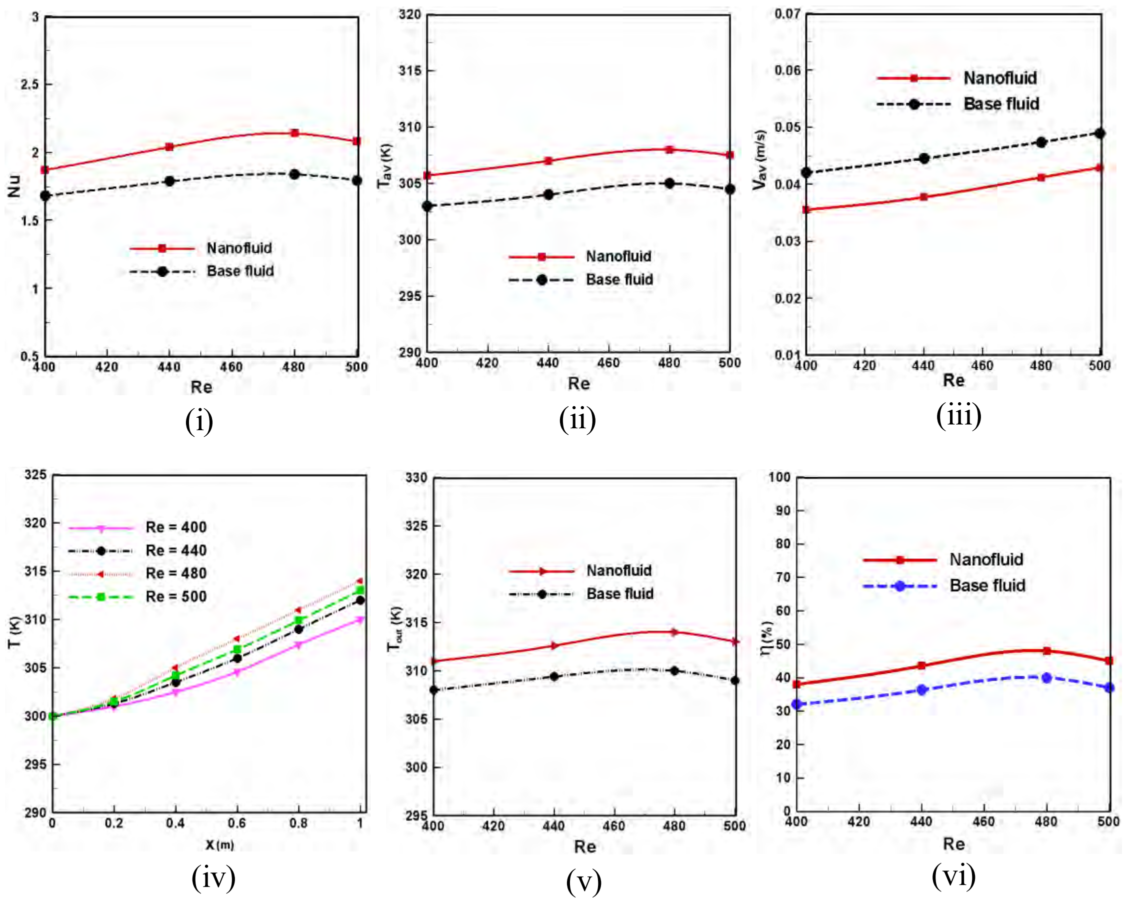

Figure 3.9: Effect of *Re* on (i) mean Nusselt number, (ii) mean bulk temperature, (iii) mean velocity, (iv) mid-height temperature, (v) mean output temperature and (vi) collector efficiency

Consequently, mean output temperature of both types of fluids increases with growing Reynolds number from 400 to 480. But at *Re* = 500 mean output temperature slightly decreases. T_{out} of water-copper nanofluid becomes 311K, 312K, 314K and 313K and of water becomes 308K, 309K, 310K, 309K for *Re* = 400, 440, 480 and 500 respectively.

Use of higher Reynolds number upto 480 can improve the thermal efficiency of FPSC. When *Re* = 500, the thermal efficiency (η) of devalues moderately. In other words, the heat extracted from riser pipe by the fluids cannot be increased for *Re* = 500. Thermal efficiency enhances from 38%-48% for water-copper nanofluid and 32%-40% for water with the variation of Reynolds number from 400 to 480.

3.4.3 Effect of Prandtl number

Figure 3.10(i)-(iii) represents the streamlines pattern, boundary plot and arrow plot of 2% concentrated water-Cu nanofluid at I = 215 W/m^2, *Re* = 480 and *Pr* = 5.8. The values of nanofluid velocity in m/s unit and temperature in Kelvin unit are also shown in right and left bars respectively.

The streamlines occupying the whole riser pipe is found at the Prandtl number (*Pr* = 5.8). Color of streamlines at the solid surfaces of riser pipe is deep blue and at the middle is red. This is due to the fact that no-slip condition is maintained at the solid surfaces of riser pipe. Thus maximum velocity is obtained at the middle of the pipe.

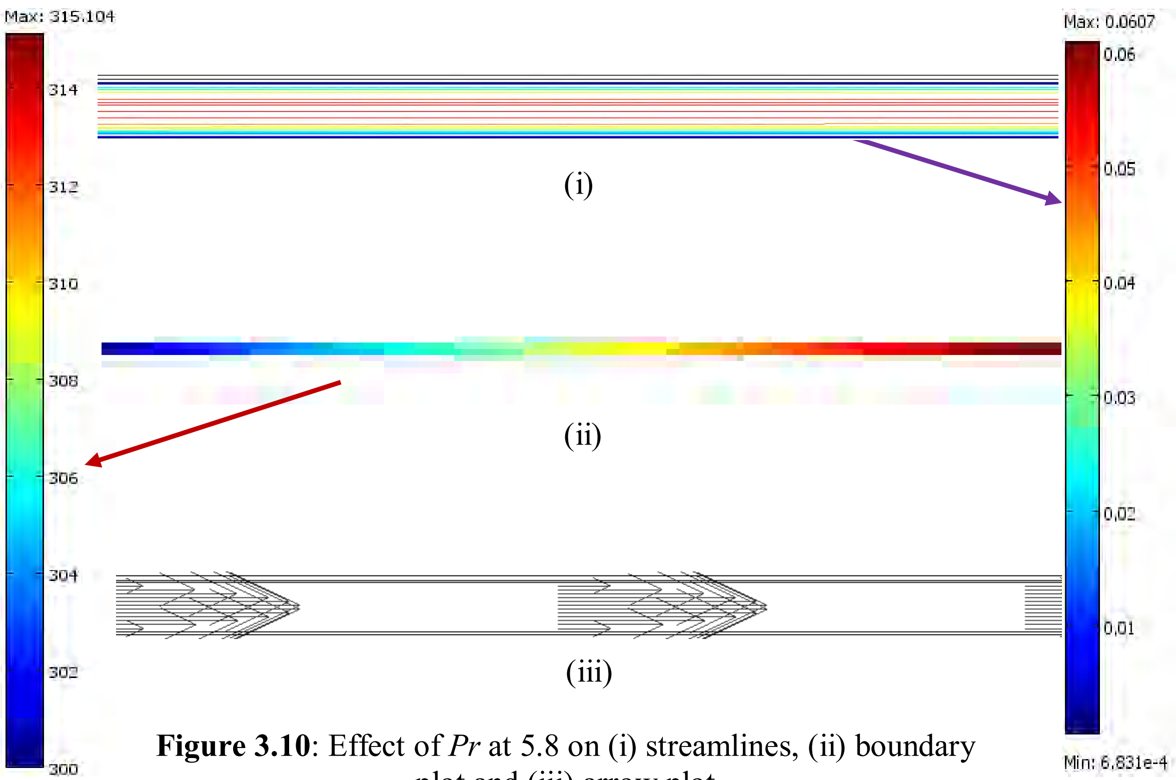

Figure 3.10: Effect of *Pr* at 5.8 on (i) streamlines, (ii) boundary plot and (iii) arrow plot

Also the boundary plot represents that fluid passes through the pipe and takes heat from top surface of riser pipe. That‟s why boundary temperature becomes low near the inlet and gradually becomes high near the exit boundary. The temperature of top surface of riser pipe is higher than the bottom surface.

Arrow plot indicates direction of fluid flow. From figure 3.10(iii) it is observed that nanofluid flow enters at the left inlet opening and exits from the right outlet opening.

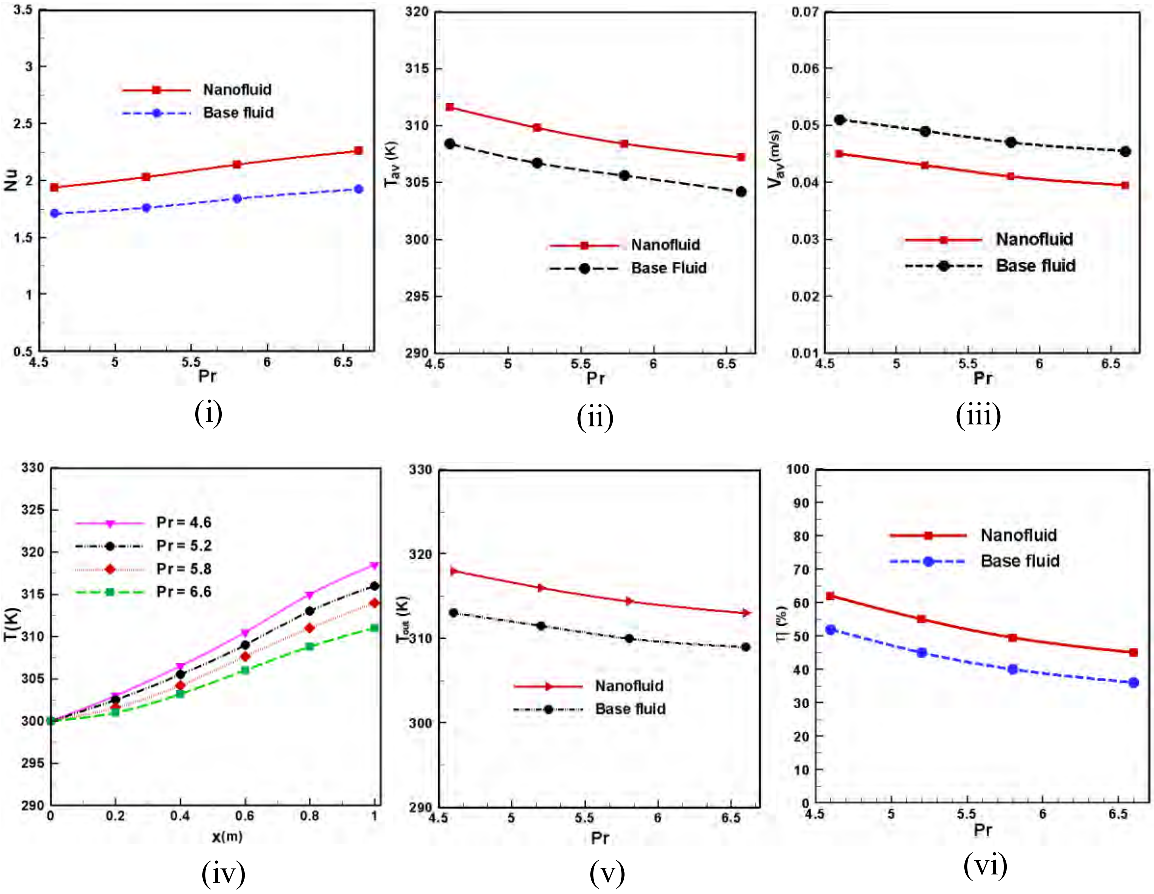

Figure 3.11: Effect of *Pr* on (i) mean Nusselt number, (ii) mean bulk temperature, (iii) mean velocity, (iv) mid-height temperature, (v) mean output temperature and (vi) collector efficiency

The effect of Prandtl number (*Pr*) on average Nusselt number (*Nu*) at the top of riser pipe, average temperature (T_{av}), magnitude of average velocity (V_{av}), mid-height temperature (*T*) of water-copper nanofluid, mean outlet temperature (T_{out}) and percentage of collector efficiency with $Re = 480$, $I = 215\text{W/m}^2$, $\phi = 2\%$ are shown in figure 3.11(i)-(vi). The values of *Pr* are chosen as 4.6, 5.2, 5.8 and 6.6. All these values of Prandtl number represent water at different temperatures. From the figure

3.11(i) it is clearly observed that as *Pr* increases, heat transfer rate enhances for both fluids. *Nu* increases by 16% and 12% with the variation of *Pr* from 4.6 to 6.6 for water-copper nanofluid and clear water respectively.

As *Pr* increases average bulk temperature (T_{av}) of the fluids decreases gradually for both fluids. It is well known that increasing Prandtl number devalues fluid temperature. Nanofluid has higher temperature than base fluid.

Mean velocity (V_{av}) devalues for higher Prandtl number because fluid with higher viscosity can‟t move freely like lower viscous fluid. Water-copper nanofluid has lower mean velocity than clear water.

Temperature (T) of water-Cu nanofluid at the middle of riser pipe is seen in figure 3.11(iv). Nanofluid temperature increases when it passes through the riser pipe. But temperature of nanofluid diminishes with growing *Pr*.

Figure 3.11(v) shows that mean outlet temperature (T_{out}) decreases with increasing Prandtl number. This describes in this way that increasing Prandtl number decreases fluid temperature. As a result lower tempered fluid can‟t become so hot at outlet exit like higher tempered fluid. Average outlet temperature becomes 318K, 316K, 314K, 313K for nanofluid and 313K, 312K, 310K, 309K for water respectively with the variation of Pr = 4.6, 5.2, 5.8 and 6.6.

Using higher values of Prandtl number the collector efficiency decreases. In this scheme water/copper nanofluid (ϕ = 2%) performs better than clear water (ϕ = 0%). Thermal efficiency devalues from 66%-45% for nanofluid and 52%-36% for water due to the variation of Prandtl number *Pr* from 4.6 to 6.6.

3.4.4 Effect of solid volume fraction

The performance of water based copper nanoparticles i.e. water-Cu nanofluid on the surface temperature plot for various solid volume fraction (ϕ) is presented in the figure 3.12 while Re = 480, Pr = 5.8 and I = 215 W/m^2. The concentrations of nanoparticles are chosen as 1%, 2% and 3% where for clear water this concentration is 0%. The values of different surface temperatures of FPSC are also given with different colours. From figure 3.12 it is observed that the surface temperature of water/copper nanofluid with 1% volume fraction is higher than base fluid. Then this surface temperature tends to be high for 2% concentrated Cu-water nanofluid. This indicates that the heat flow is conduction dominant due to more thermal conductive heat flux. Major amount of heat flux or transport occurs for $\phi = 2\%$ of water-copper nanofluid. At this stage the highest surface temperature is 314.947K. After that there is no significant change in surface temperature for further increment of solid volume fraction upto 3%. So adding more amount nanoparticles not always beneficial.

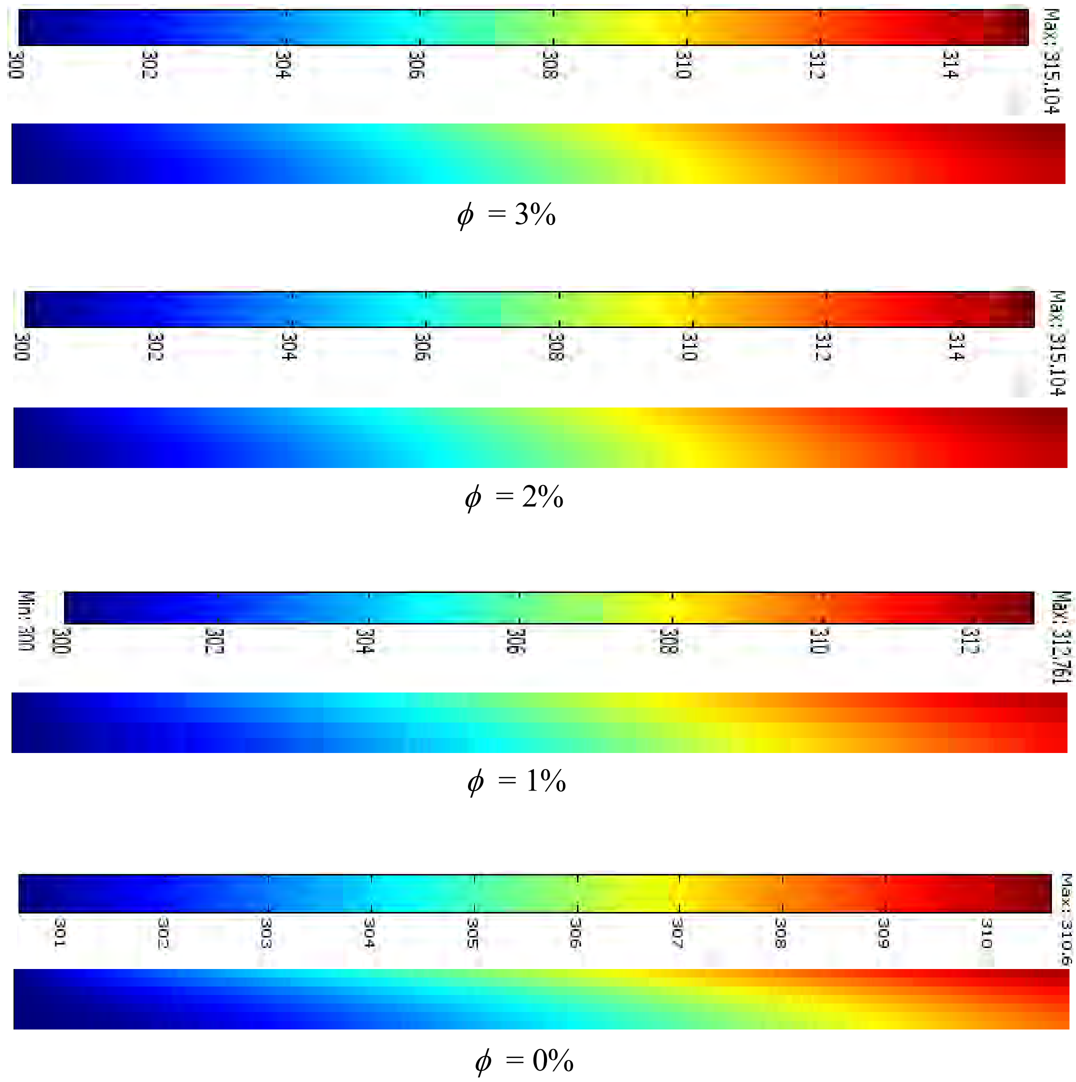

Figure 3.12: Effect of ϕ on surface temperature

The plots of Nu, T_{av}, V_{av}, T, T_{out} and η (%) profiles for nanofluid as well as base fluid are depicted in Fig. 3.13 (i)-(vi). From the plot of the average Nusselt number (Nu)-solid volume fraction (ϕ) it is observed that rate of heat transfer rises monotonically upto 2% of solid volume fraction. Here rate of heat transfer remains constant for clear water ($\phi = 0\%$) with the variation of ϕ. Heat transfer rate increases by 15% with the variation of ϕ from 0% to 2% of water-copper nanofluid. And then there is almost no change in Nu-ϕ profile for extra variation of ϕ from 2% to 3%.

Mean bulk temperature (T_{av}) along with the solid volume fraction grows sequentially for ϕ 2%. It is well known that higher concentration of solid particle enhances thermal conductivity as well as temperature of the working Cu-water nanofluid.

Growing ϕ devalues mean velocity of the nanofluid through the riser pipe of the flat plate solar collector.

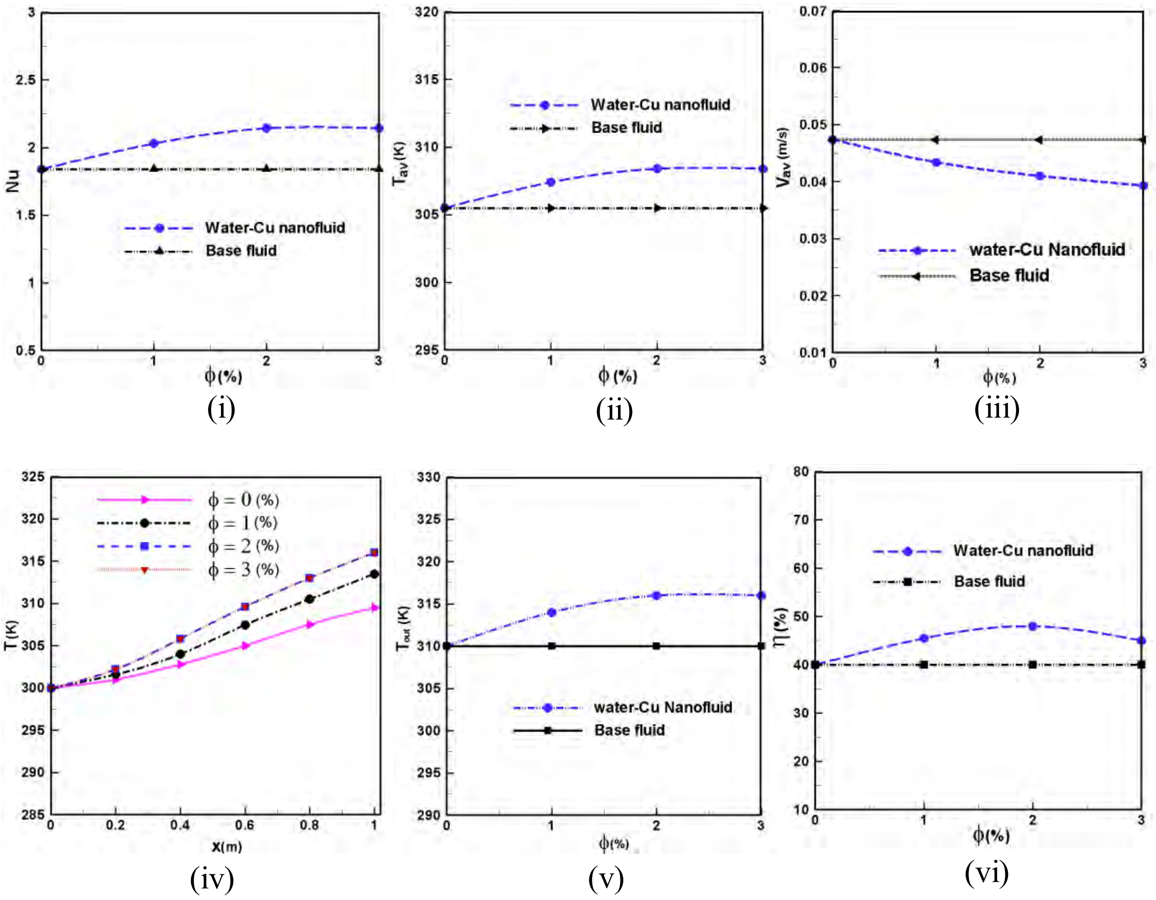

Figure 3.13: Effect of ϕ on (i) mean Nusselt number, (ii) mean temperature, (iii) mean velocity, (iv) mid-height temperature, (v) mean output temperature and (vi) collector efficiency

The temperature of water-copper nanofluid at the middle height of the riser pipe increase with the increasing solid volume fraction upto 2%. The inlet temperature of fluid is maintained at 300K and then it increases gradually with the contact of top heated solid boundary of the riser pipe attached with the absorber plate of copper material. Considerable change doesn‟t occur for 3% concentrated water-Cu nanofluid.

From figure 3.13 (v) it is found that mean output temperature (T_{out}) of nanofluid rises with the variation of solid volume fraction of Cu nanoparticles from 0% to 2%. The output temperature of nanofluid becomes 310K, 312K, 314K and 314K for ϕ = 0%, 1%, 2% and 3% respectively. T_{out} remains unchanged for ϕ = 3%.

It is observed from figure 3.13(vi) that by introducing solid particles (ϕ = 1%-2%) with water the thermal efficiency of FPSC increases. Then it decreases slightly with additional variation of ϕ. So, more solid concentration is not able to augment heat transfer system through the riser pipe. Collector efficiency rises from 40% to 48% for the variation of ϕ from 0%-2%.

3.5 Observation

The computational domain of 3D and 2D is shown in figure 3.14. Actual fact for a FPSC is that sunlight passes through the glazing (transparent glass) and strikes the absorber plate, which heats up, changing solar energy into heat energy. Some amount of heat is gone outside the collector by radiation. Then rest of the heat is transferred from absorber to riser pipe be conduction procedure. The whole riser pipe becomes hot. After that heat is transferred to liquid by convection process which passes through pipes attached to the absorber plate. The FPSC must be properly insulated.

Some problems arise in 2D numerical analysis of FPSC which are given below:

Firstly, 2D numerical analysis of FPSC doesn‟t represent accurate and practical phenomena of heat transfer system as the transverse cross section of 3D view is not possible to consider for 2D numerical analysis.

Secondly, from figure 3.14(ii) it is very clear that 2D computation (longitudinal cross-section of 3D view) only the top boundary of riser pipe becomes hot by conductive heat transfer process with absorber plate. There is no way to transfer heat by conduction from absorber to bottom boundary of riser pipe. Thus bottom boundary of riser pipe doesn‟t become hot. Then cold fluids enter the riser pipe, collect heat from top solid boundary of pipe and become hot. But at the same time cold bottom boundary of riser pipe tries to collect heat from hot fluids because at the solid –fluid interface heat continuity condition is allocated. Thus finally less heated output fluids are obtained at the exit boundary of the riser pipe.

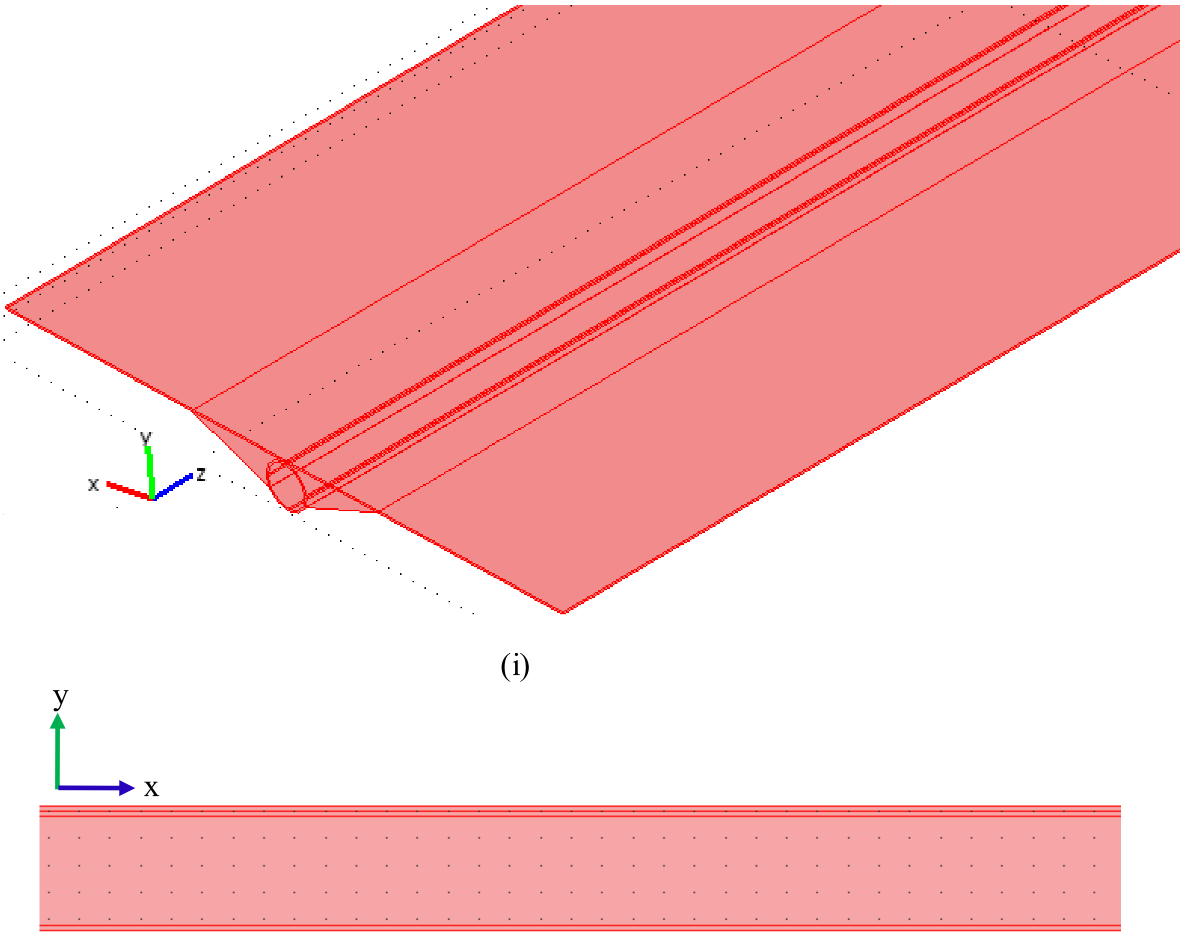

(i)

(ii)

Figure 3.14: FPSC (i) 3D domain and (ii) 2D domain

But in 3D computational domain (figure 3.14(i)) the whole riser pipe becomes hot by conductive heat transfer process with absorber. Then cold fluids enter the riser pipe, collect heat from whole solid pipe surface, become hot and finally more heated output fluids are obtained from the outlet exit of the riser pipe. Consequently thermal efficiency also enhances by this technique.

That‟s why 3D numerical analysis is needed to represent actual heat transfer system of FPSC though a good number of researchers have conducted 2D analysis of FPSC. Some of them considered only riser pipe section, some considered air space domain under the glass cover etc. But none has investigated the whole domain of FPSC in 2D still now.

3.6 Conclusions

A finite element method is used to make the present investigation for steady-state, incompressible, laminar and forced convective flow through a flat plate solar collector. 2D numerical analysis is performed in this chapter. The major conclusions have been drawn as follows:

- The elevation in solar irradiance to the FPSC causes thicker thermal boundary layer. Temperature of nanofluid at mid-height of the riser pipe escalates while passing the pipe for all values of solar irradiation. Rate of heat transfer and percentage of collector efficiency become higher for higher values of the solar irradiation. Performance of water copper nanofluid is better than that of clear water.

- The forced convection parameter *Re* has a significant effect on the temperature field. Thermal layer near the heated surface becomes thick. Mean temperature and velocity is increased at a certain level of *Re*. Heat transfer rate and thermal efficiency rise for the variation of *Re* from 400 to 480.

- The influence of Prandtl number *Pr* on streamline is remarkable. The average temperature and velocity lessen with elevating *Pr*. Due to rising *Pr* heat transfer rate increases but collector efficiency devalues. Velocity of water-copper nanofluid is lower than that of base fluid.

- The solid volume fraction ϕ of copper nanoparticle has considerable effect on temperature of surface plot. Perturbation is observed in the conductive and convective heat flux distribution nearby the hot wall with the variation of ϕ. Increasing ϕ upto 2% causes greater rate heat transfer and thermal efficiency. So adding more nanoparticles is not always helpful for heat transfer system through FPSC. This is the most important result of the present study.

Chapter 4: Three Dimensional Analysis

4.1. Introduction

Energy is the prime agent in the generation of wealth and a significant factor in economic development. Limited availability of fossil resources and environmental problems associated with them has emphasized the need for new sustainable energy supply options that use renewable energies. Solar energy is one of the best sources of renewable energy with minimal environmental impact. As the primary energy sources are depleting continuously, solar energy draws attention of researchers throughout the world. Everyday sun radiates enormous amount of energy known as solar energy. The hourly solar flux incident on the earth's surface is greater than all of human consumption of energy in a year. So, the problem lies in efficiently collecting and converting this energy into something useful form. The conversion of solar thermal energy into more usable form is done by solar collectors.

The sun is an excellent source of radiant energy, and is the world‟s most abundant source of energy. It emits electromagnetic radiation with an average irradiance of 1353 W/m^2 on the earth‟s surface. To put this into perspective, if the energy produced by 25 acres of the surface of the sun were harvested, there would be enough energy to supply the current energy demand of the world.

In this chapter, the 3D numerical study addresses the heat transfer by water/copper nanofluid as well as base fluid through the riser pipe of a FPSC. 3D numerical code validation is shown. Numerical solutions are obtained over a wide range of solar irradiation (I), Reynolds number (Re), Prandtl number (Pr), solid volume fraction (ϕ) and mass flow rate (m). The numerical results are presented graphically in terms of iso-surface plot, slice plot, streamline plot, contour temperature plot. Finally the average Nusselt number (Nu) at the inner surface of the riser pipe, mean bulk temperature (T_{av}), mean velocity (V_{av}), mid-height temperature of nanofluid, average output temperature (T_{out}) and percentage of collector efficiency (η) in a FPSC are calculated. Also effect of solid volume fraction on temperature distribution is displayed for water based nanofluid having double nanoparticles. Rate of heat transfer and thermal efficiency are compared for FPSC using different nanofluids.

Correlations are derived among the present obtained results. Comparison is shown in different ways between results obtained from 2D and 3D simulations. In addition comparison of present results is shown with the survey and project report available in the literature.

4.2 Three Dimensional Modeling

The 3D view of the computational domain is shown in figure 2.12(i).

The 3D governing partial differential equations are obtained by including another axis in equations (3.1-3.5) and can be written as follows

Continuity equation:

$$\frac{\partial u}{\partial x}+\frac{\partial v}{\partial y}+\frac{\partial w}{\partial z}=0 \tag{4.1}$$

x-momentum equation:

$$\left\{(1-\phi)+\phi\frac{\rho_s}{\rho_f}\right\}\left(u\frac{\partial u}{\partial x}+v\frac{\partial u}{\partial y}+w\frac{\partial u}{\partial z}\right)=-\frac{1}{\rho_f}\frac{\partial p}{\partial x}+\frac{1}{(1-\phi)^{2.5}}\frac{1}{Re}w_{in}D\left(\frac{\partial^2 u}{\partial x^2}+\frac{\partial^2 u}{\partial y^2}+\frac{\partial^2 u}{\partial z^2}\right) \tag{4.2}$$

y-momentum equation:

$$\left\{(1-\phi)+\phi\frac{\rho_s}{\rho_f}\right\}\left(u\frac{\partial v}{\partial x}+v\frac{\partial v}{\partial y}+w\frac{\partial v}{\partial z}\right)=-\frac{1}{\rho_f}\frac{\partial p}{\partial y}+\frac{1}{(1-\phi)^{2.5}}\frac{1}{Re}w_{in}D\left(\frac{\partial^2 v}{\partial x^2}+\frac{\partial^2 v}{\partial y^2}+\frac{\partial^2 v}{\partial z^2}\right) \tag{4.3}$$

z-momentum equation:

$$\left\{(1-\phi)+\phi\frac{\rho_s}{\rho_f}\right\}\left(u\frac{\partial w}{\partial x}+v\frac{\partial w}{\partial y}+w\frac{\partial w}{\partial z}\right)=-\frac{1}{\rho_f}\frac{\partial p}{\partial z}+\frac{1}{(1-\phi)^{2.5}}\frac{1}{Re}w_{in}D\left(\frac{\partial^2 w}{\partial x^2}+\frac{\partial^2 w}{\partial y^2}+\frac{\partial^2 w}{\partial z^2}\right) \tag{4.4}$$

Energy equation for nanofluid:

$$\left(u\frac{\partial T}{\partial x}+v\frac{\partial T}{\partial y}+w\frac{\partial T}{\partial z}\right)=\frac{\alpha_{nf}}{\alpha_f}\frac{1}{Re\,Pr}w_{in}D\left(\frac{\partial^2 T}{\partial x^2}+\frac{\partial^2 T}{\partial y^2}+\frac{\partial^2 T}{\partial z^2}\right) \tag{4.5}$$

Energy equation for absorber:

$$\left(\frac{\partial^2 T_a}{\partial x^2}+\frac{\partial^2 T_a}{\partial y^2}+\frac{\partial^2 T_a}{\partial z^2}\right)=0 \tag{4.6}$$

The effective properties of nanofluid in equations (3.6-3.10) of section 3.2, chapter 3 remain unchanged for this analysis.

The boundary conditions of the computation domain are:

1. at all solid boundaries of the riser pipe: $u = v = w = 0$
2. at the solid-fluid interface: $k_f\left(\dfrac{\partial T}{\partial n}\right)_{fluid} = k_{solid}\left(\dfrac{\partial T}{\partial n}\right)_{solid}$
3. at the inlet boundary of the riser pipe: $T = T_{in}$, $w = w_{in}$
4. at the outlet boundary: convective boundary condition $p = 0$
5. at the top surface of the absorber: heat flux $-k_a\dfrac{\partial T_a}{\partial z} = q = I\tau\kappa - U_L\left(T_{in} - T_{amb}\right)$
6. at the other surfaces of absorber plate: $\dfrac{\partial T_a}{\partial n} = 0$
7. at the outer boundary of riser pipe: $\dfrac{\partial T_a}{\partial n} = 0$
8. at the outer boundary of bonding conductance: $\dfrac{\partial T_a}{\partial n} = 0$

where n be the distances either along x or y or z directions acting normal to the surface respectively.

4.2.1 Mean Nusselt number

The non-dimensional form of local heat transfer at the riser pipe solid surface is

$$\overline{Nu} = -\frac{k_{nf}}{k_f}\frac{\partial \theta}{\partial n} = -\frac{k_{nf}}{k_f}\sqrt{\left(\frac{\partial \theta}{\partial X}\right)^2 + \left(\frac{\partial \theta}{\partial Y}\right)^2 + \left(\frac{\partial \theta}{\partial Z}\right)^2}$$

The above equations are non-dimensionalized by using the following dimensionless quantities $X = \dfrac{x}{D}$, $Y = \dfrac{y}{D}$, $Z = \dfrac{z}{D}$, $\theta = \dfrac{(T - T_{in})k_f}{qD}$

By integrating the local Nusselt number over the riser pipe, the average heat transfer rate of the collector can be written as

$$Nu = \frac{\iint_S \overline{Nu}\, ds}{\iint_s dS} = -\frac{1}{\pi DL}\frac{k_{nf}}{k_f}\iint_S \sqrt{\frac{\partial^2 \theta}{\partial X^2} + \frac{\partial^2 \theta}{\partial Y^2} + \frac{\partial^2 \theta}{\partial Z^2}}\, ds \tag{4.7}$$

where $\frac{\partial\theta}{\partial n}=\sqrt{\left(\frac{\partial\theta}{\partial X}\right)^2+\left(\frac{\partial\theta}{\partial Y}\right)^2+\left(\frac{\partial\theta}{\partial Z}\right)^2}$, L is the height of absorber tube.

4.2.2 Mean bulk temperature and velocity

The mean bulk temperature and magnitude of sub domain mean velocity of the fluid inside the collector may be written as

$$T_{av}=\frac{\iiint_{\bar{V}} T d\bar{V}}{\iiint_{\bar{V}} d\bar{V}}=\frac{4}{\pi D^2 L}\iiint_{\bar{V}} T d\bar{V}\text{, and } V_{av}=\frac{\iiint_{\bar{V}} V d\bar{V}}{\iiint_{\bar{V}} d\bar{V}}=\frac{4}{\pi D^2 L}\iiint_{\bar{V}} V d\bar{V} \tag{4.8}$$

Area of output circular boundary of riser pipe (πr^2) is 7.848056e-5 m^2. Volume of riser pipe domain ($\pi D^2 L$) is 7.60131e-5 m^3. Perimeter of circular boundary of riser pipe ($2\pi r$) is 0.031416m and area of inner surface of riser pipe (πDL) is 0.031364 m^2.

4.2.3 Mesh generation

Figure 4.1 displays the 3D finite element mesh of the present physical domain. Finer mesh size is chosen for this geometry. The mesh is composed of tetrahedral element type with ten nodes in subdomain and triangular element size with six nodes in boundaries.

4.2.4 Grid test

The three dimensional computational domain is modeled using finite element mesh as shown in the figure 4.1. The complete domain consists of 14,20,465 elements. The influence of further refinement does not complete simulation and computer shows out of memory when LU factorization. This is shown in Table 4.1.

Table 4.1: Grid sensitivity check at Pr = 5.8, Re = 480, I = 215W/m^2, ϕ =2%

Elements	4,51,098	7,26,222	**14,20,465**	27,04,288
***Nu* (Nanofluid)**	1.92154	2.28451	**2.46642**	Out of memory
***Nu* (Base fluid)**	1.79124	1.90312	**2.10124**	Out of memory
Time (s)	1469.587	3846.507	**78381.181**	---------

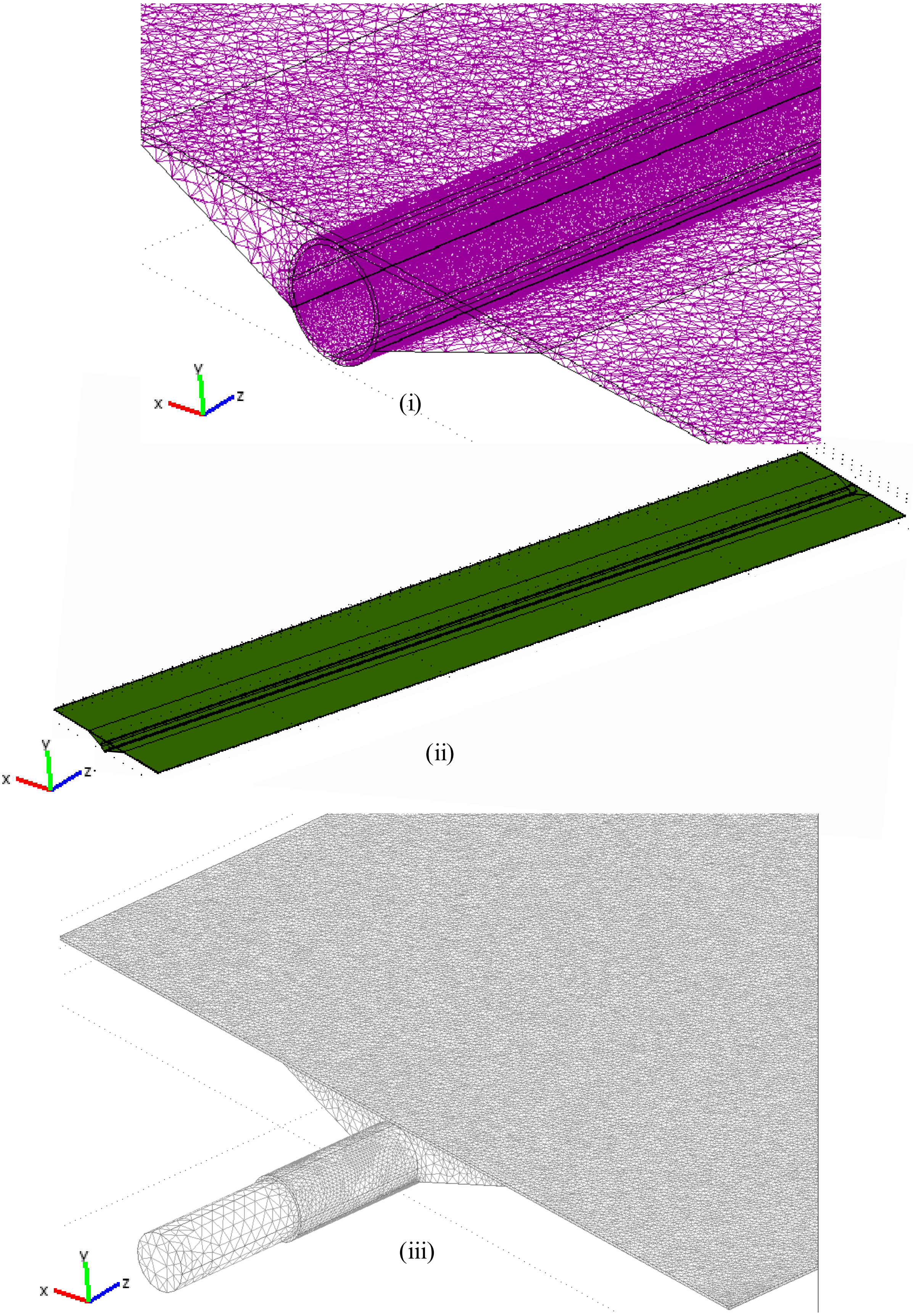

Figure 4.1: Mesh generation of the collector (i) partial view, (ii) full view and (iii) close view of riser pipe

4.2.5 Numerical results validation

The result obtained from present numerical technique is verified against the existing result available in the literature:

A comparison of temperature contour plot of absorber plate is shown in the figure 4.2 between the result using present code and Kranath *et al.* (2011). They studied numerical simulation of a solar flat plate collector using discrete transfer radiation model (DTRM) – a CFD approach.

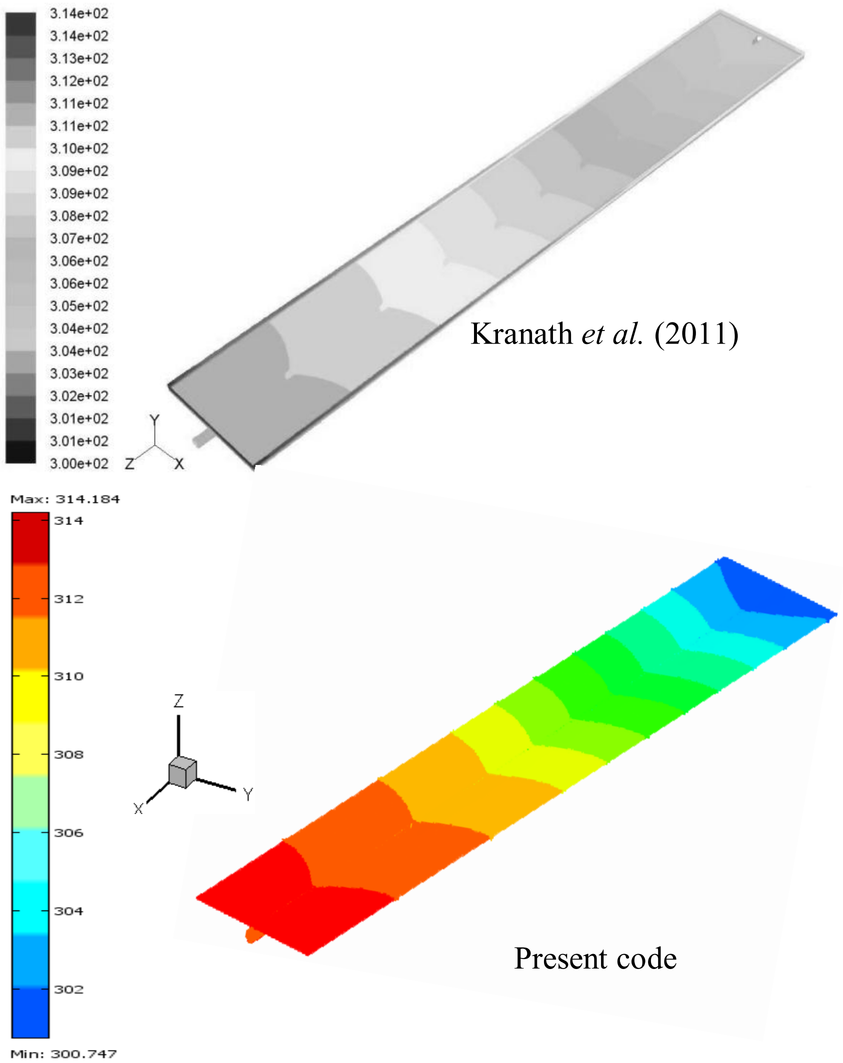

Figure 4.2: Result validation of temperature contour of absorber plate

The absorber tube has a diameter of 0.01m and 0.001m thickness. The absorber plate has length, width and thickness of 1m, 0.15m and 0.002m respectively. The numerical study is performed at solar irradiation = 800 w/m^2, inlet fluid velocity = 0.005 m/s, refractive index (glass) = 1.47, specific heat (glass) = 750 J/kgK, density (copper) = 8900 Kg/m^3, specific heat (copper) = 385 J/kgK, viscosity (water) = 0.000959 Kg/ms, specific heat (water) = 4179 J/kgK, thermal conductivity (glass) = 1.14 W/mK, thermal conductivity (copper) = 387 W/mK and thermal conductivity (water) = 0.6 W/mK. Heat transfer medium is water. A good agreement is observed from figure 4.2.

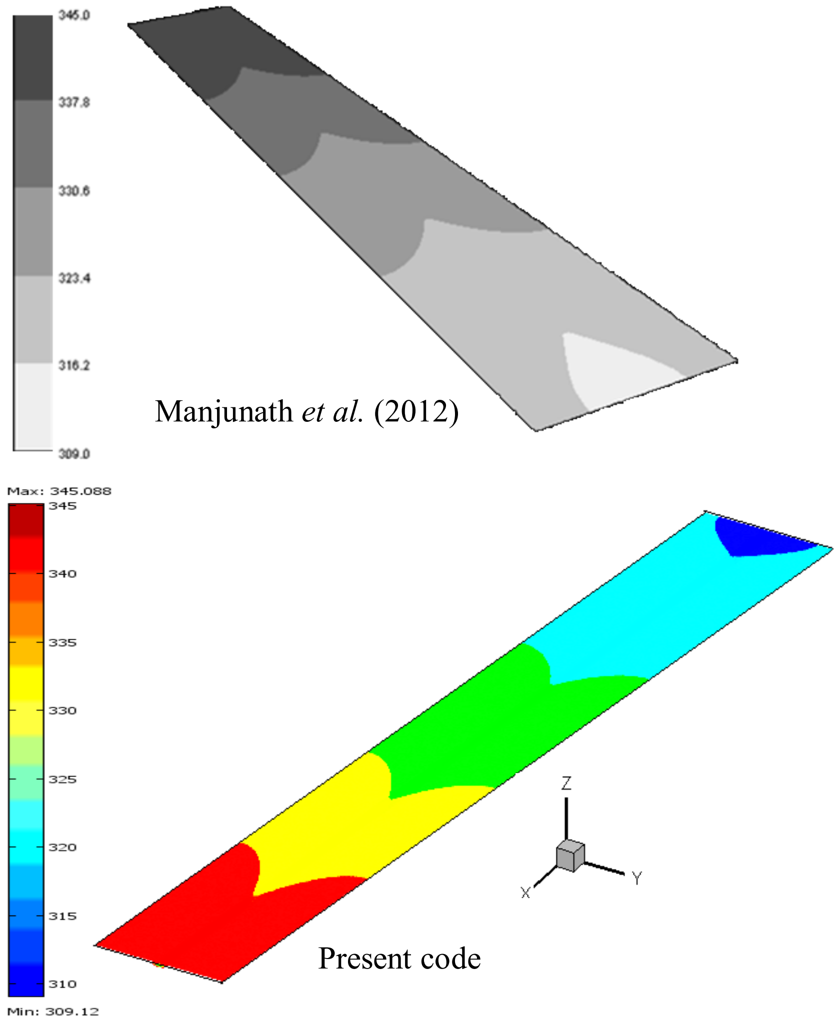

Figure 4.3: Result validation of temperature contour of absorber plate for unglazed FPSC

Also the present numerical solution is validated for unglazed FPSC by comparing the current results for temperature contour plot of absorber plate using water as heat transfer medium with the graphical representation of Manjunath *et al.* (2012). They studied a comparative CFD study on solar dimple plate collector with flat plate collector to augment the thermal performance. Water is considered as fluid passing through the FPSC. The absorber tube has a diameter of 0.01m and 0.001m thickness. The absorber plate has length, width and thickness of 1m, 0.12m and 0.002m respectively. For the computation solar irradiation = 1000 W/m^2, mass flow rate = 0.001 Kg/s, density (copper) = 8978 Kg/m^3, specific heat (copper) = 381 J/kgK, viscosity (water) = 0.001003 Kg/ms, specific heat (water) = 4182 J/kgK, thermal conductivity (copper) = 387.6 W/mK and thermal conductivity (water) = 0.6 W/mK are considered. The code validation is shown in figure 4.3. As shown in figure 4.3, the numerical solutions of present code and Manjunath *et al.* (2012) are in good agreement.

Also fluid (water) temperature along the axial line of the riser pipe obtained using present numerical code and results of Manjunath *et al.* (2012) is shown graphically in the figure 4.4. It is easily seen that there is augmented heating up of water in the absorber tube of the FPSC along the axial line of the absorber tube. Very good agreement is depicted by this figure.

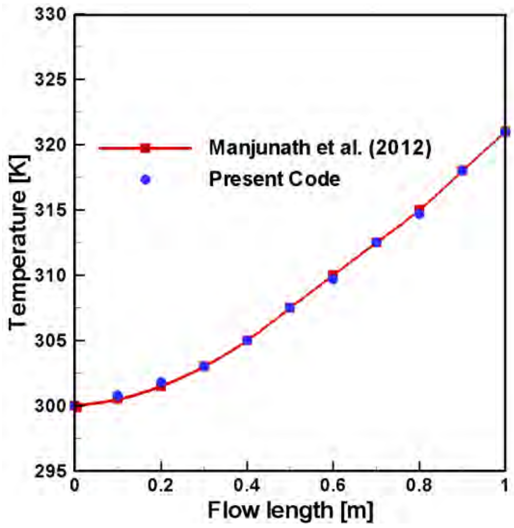

Figure 4.4: Result validation of fluid temperature along axial line of riser pipe

In addition present numerical result is validated for the outlet fluid temperature of the existing result of Ingle *et al.* (2013). The code validation is given in Table 4.2. The overall dimension for solar collector is 2000*1000*130 mm^3 with 4 mm thick glass plate which is placed at around 126 mm from the top side of the collector. The absorber plate has 2000 mm length, 1000 mm wide and 2 mm in thickness. Inlet of solar collector is of circular cross section with diameter of 70 mm. Using present numerical technique for producing result of Ingle *et al.* (2013) heat transfer medium is taken as air with mass flow rate 0.0105 Kg/sec, density 1.165 Kg/m^3, thermal conductivity 100 W/m k, specific heat at constant pressure 1005 J Kg/k. From the Table 4.2 it is seen that a fine concurrence exists between the results obtained using present code and that of Ingle et al. (2013).

Table 4.2: Result validation of outlet air temperature

Solar Irradiance (I) (W/m^2)	**Ambient Temperature (T_{amb}) (^{0}C)**	**Outlet fluid temperature obtained by Ingle *et al.* (2013) (^{0}C)**	**Present code (^{0}C)**
621.7	32.5	60.87	61.134
750.5	34.7	73.75	73.657
879.5	37	85.34	85.255
909	38.9	93.38	93.284
948	38.5	96.10	95.941
909.5	41.1	93.40	93.372
790	40	84.84	85.018
597.5	35	68.14	68.781
357	33	43.06	44.103

4.3 Result and Discussions

Finite element simulation is applied to perform the 3D numerical analysis of laminar forced convective temperature and fluid flow through a FPSC filled with water/copper nanofluid as well as base fluid. The mass flow rate per unit area (m) is chosen as 0.0248 Kg/s. Effects of the solar irradiation (I), Reynolds number (Re), Prandtl number (Pr) and solid volume fraction on heat transfer and collector efficiency have been studied. The outcomes for the different cases are presented in the following sections. Results are submitted in the International Journal of Energy.

4.3.1 Effect of solar radiation

Bangladesh gets an average sunlight around 200 W/m^2 - 240 W/m^2. The effect of I on the temperature interms of slice plot is presented in figure 4.5 for 2% concentrated water-Cu nanofluid. The considered values of solar irradiation are I (= 200W/m^2, 215W/m^2, 230W/m^2 and 240W/m^2). Different colours of slices indicate different temperatures as shown in the figure. Initially at I = 200W/m^2, irradiation is low, temperature of nanofluid at the outlet edge is low. Colour indicates the probable value of nanofluid temperature. The strength of the thermal current activities is much more activated with escalating I. Slices illustrate that solar irradiation dominant effect plays a critical role on larger heat flow from absorber walls to the passing fluid through the riser pipe. In the temperature distribution of slice plot for different values of solar irradiation shows that absorber temperature as well as nanofluid outlet temperature increases with rising values of I. The values of temperature in slice plots are given in Kelvin unit.

Figure 4.6(i)-(vi) expresses the Nu-I, T_{av}-I, V_{av}-I, mid-height temperature of nanofluid, T_{out}-I and η-I profiles of fluids through a FPSC. The average Nusselt number increases with mounting solar irradiation (I). The rate of radiative heat transfer performance enhances 14% and 10% using water-alumina nanofluid and water respectively for rising solar irradiation from 200W/m^2 to 240W/m^2.

It is seen from the figure 4.6(ii) that T_{av} rises sequentially for growing I. It is well known that higher values of solar irradiation (I) produce higher temperature of fluids. Due to escalating values of I the absorber as well as the riser pipe becomes more heated. As a result fluids can take more heat from hot walls and become hotter. Here base fluid has lower mean bulk temperature than the water-Cu nanofluid.

Magnitude of average subdomain velocity (V_{av}) has noteworthy changes with different values of solar irradiation (I). It rises consecutively for growing I. Clear water has higher velocity than water-copper nanofluid with 2% solid volume fraction.

The temperature of water-Cu nanofluid at the middle of the riser pipe is depicted in figure 4.6(iv). The fluid enters from the left inlet and takes heat form solid surfaces of the riser pipe and finally exits from the right outlet of a FPSC. The temperature of fluid increases with the effect of growing solar irradiation I.

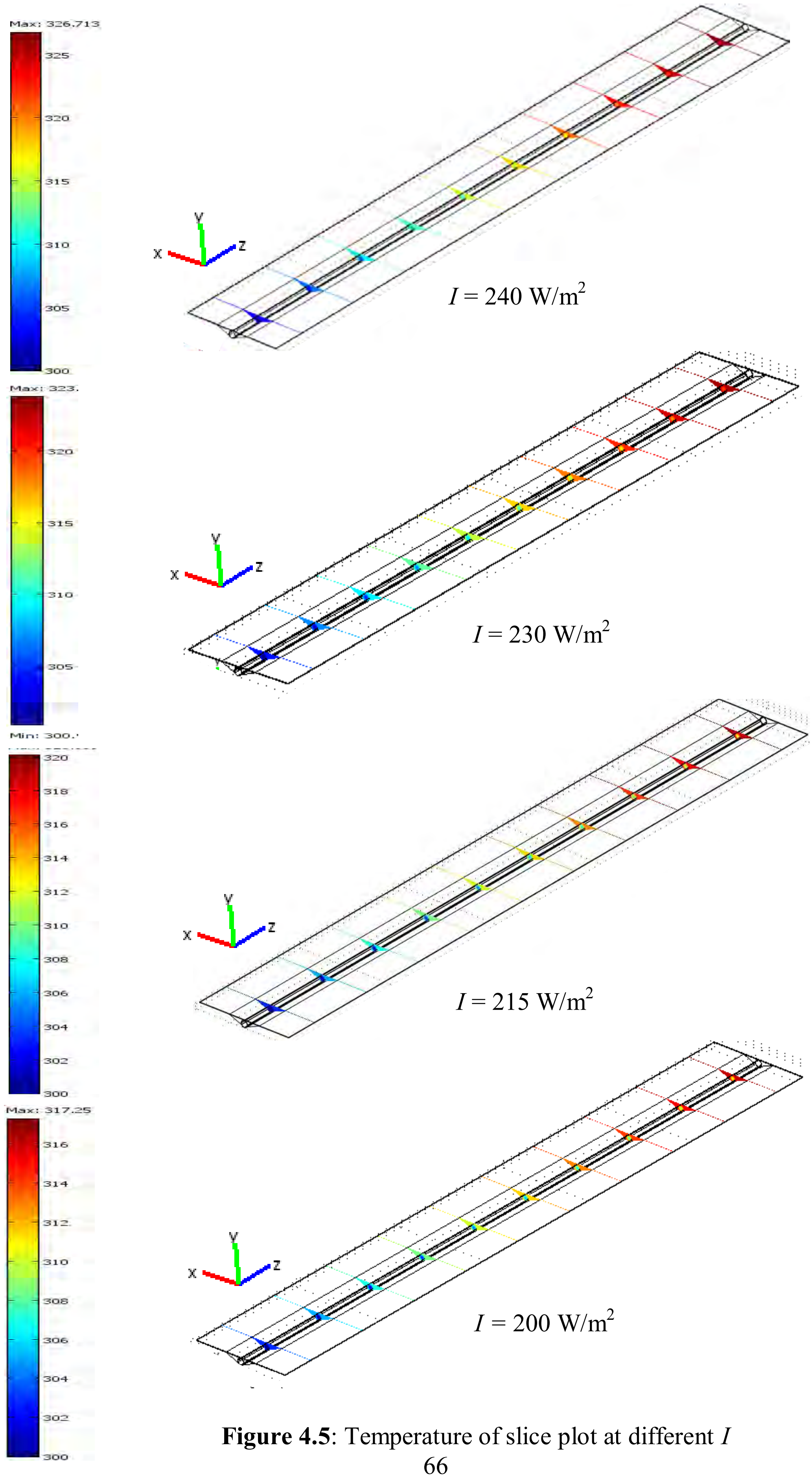

Figure 4.5: Temperature of slice plot at different I

From the figure 4.6(v) it is observed that the inlet temperature of fluid is maintained at 300K and then it increases gradually with the contact of heated solid boundaries of the riser pipe. And finally the mean output temperature of nanofluid becomes 314K, 316K, 317K, 318K and water becomes 311K, 312K, 313K, 314K for I = 200 W/m^2, 215 W/m^2, 230 W/m^2 and 240 W/m^2 respectively.

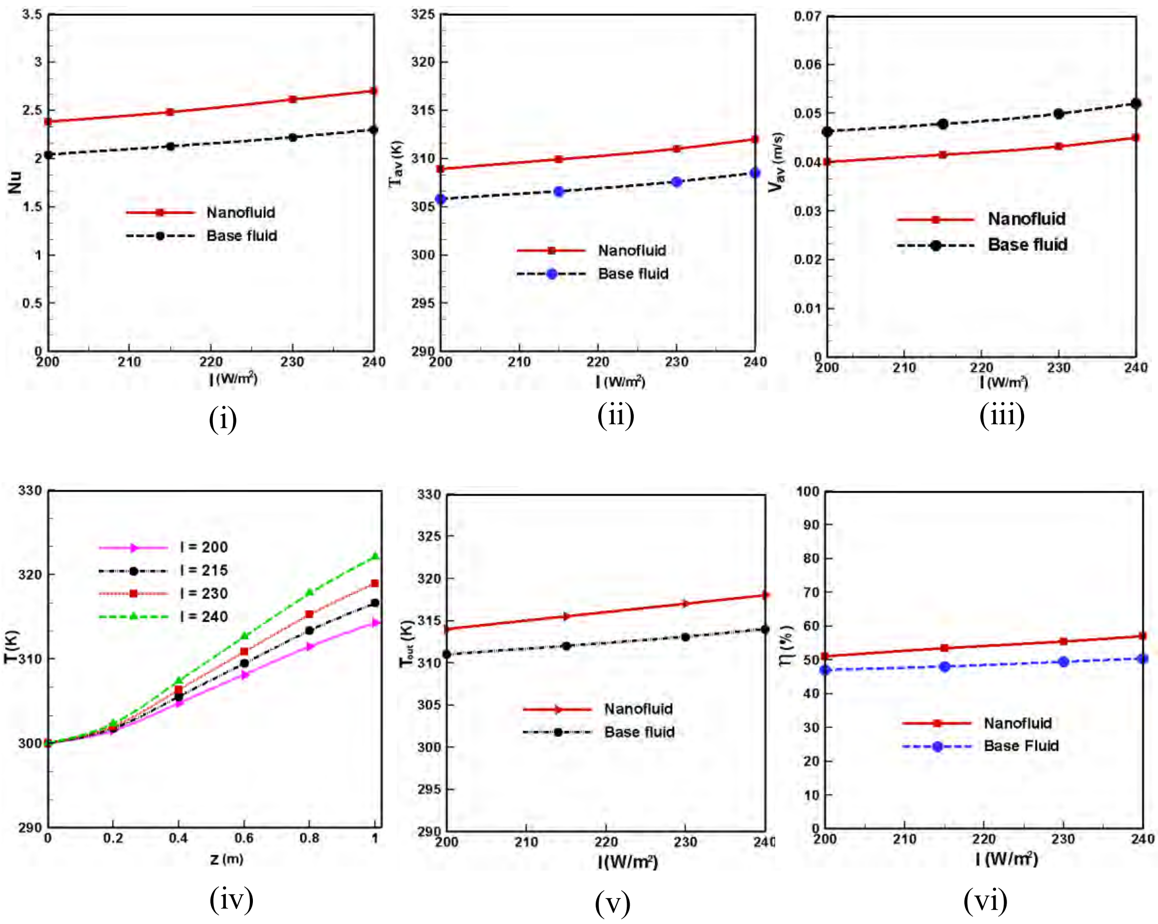

Figure 4.6: Effect of I on (i) mean Nusselt number, (ii) mean bulk temperature, (iii) mean velocity, (iv) mid-height temperature, (v) mean output temperature and (vi) collector efficiency

Using greater solar irradiation (I) the collector efficiency increases. More solar irradiance is able to augment heat transfer system through the riser pipe of a FPSC. In this scheme water/copper nanofluid (ϕ = 2%) performs better than clear water (ϕ = 0%). Thermal efficiency enhances from 51%-57% for nanofluid and 47%-50% for water.

4.3.2 Effect of Reynolds number

The effect of Re on the temperature of 2% concentrated water/Cu nanofluid interms of iso-surface plot is presented in the figure 4.7 while Pr = 5.8 and I = 215 W/m^2. The considered values of Reynolds number (Re) are Re (= 400, 440, 480 and 500). From the expression of Reynolds number different values indicate different velocity of the nanofluid. The corresponding velocities are 0.0343m/s, 0.0377m/s, 0.0412m/s and 0.0429 m/s respectively. Since inner diameter of riser pipe D is 0.01m, estimated Re ($Re = \frac{w_{in} D}{\nu_f}$) is 478, which is within the range obtained from the simulation.

Different colours of iso-surfaces indicate different temperatures as shown in the figure 4.7. Initially at Re = 400, inertia force is low, iso-surfaces appear in a long length formation. The strength of the thermal current activities is much more activated with escalating Re. Iso-surfaces illustrate that inertia force dominant effect plays a critical role on larger heat flow from riser pipe surfaces to the fluid passing through the riser pipe. In the temperature distribution of iso-surfaces for different values of Reynolds number shows that at the value of Re (= 480), the iso-surfaces of the nanofluid becomes in a short length. There is a clear difference in the heat flow trajectory for the influence of inertia force. But further increasing Reynolds number upto 500, decrement of temperature of water/Cu nonofluid is happened; as a result the iso-surfaces are more lengthen due to higher velocity.

The Nu-Re, T_{av}-Re, V_{av}-Re, mid-height temperature of nanofluid, T_{out}-Re and η-Re profiles for fluids are depicted in the figure 4.8(i)-(vi). It is seen from figure 4.8(i) that average Nusselt number forms parabolic shape with mounting Reynolds number. The rate of forced convective heat transfer enhances 15% and 11% using nanofluid and water respectively for rising inertia force from 400 to 480.

Further increasing Reynolds number increases inertia force. Consequently fluid velocity increases. That‟s why fluid passes through the riser pipe quickly and can‟t gather more heat from riser pipe. Thus rate of heat transfer falls slightly at Re = 500.

From figure 4.8(ii) it is seen that mean bulk temperature (T_{av}) of both fluids increases sequentially for growing Re from 400 to 480. At Re = 500 average temperature falls a little. Here base fluid has lower mean temperature than the water-copper nanofluid.

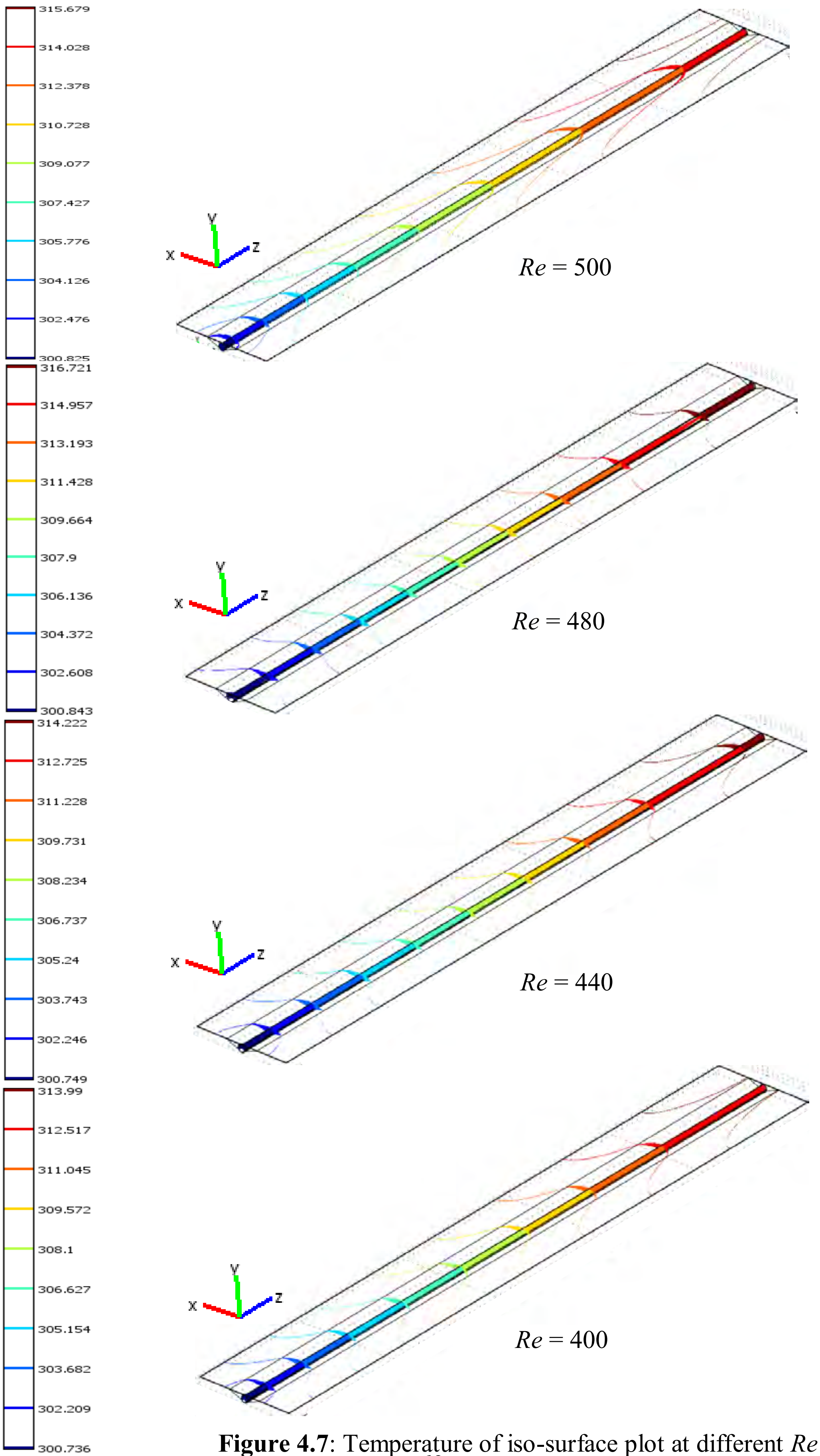

Figure 4.7: Temperature of iso-surface plot at different *Re*

Growing inertia force enhances the magnitude of mean sub-domain velocity of the fluids through the riser pipe of the flat plate solar collector as shown in figure 4.8(iii). Water has higher velocity than water-Cu nanofluid. Clear water moves freely than solid concentrated nanofluid.

The temperature of water-copper nanofluid at the middle of the riser pipe with the influences of Reynolds number is displayed in figure 4.8(iv). It is shown that the inlet temperature of fluid is maintained at 300K and then it increases gradually for all values of Reynolds number with the contact of heated solid circular surface of the riser pipe. Higher temperature is obtained at $Re = 480$.

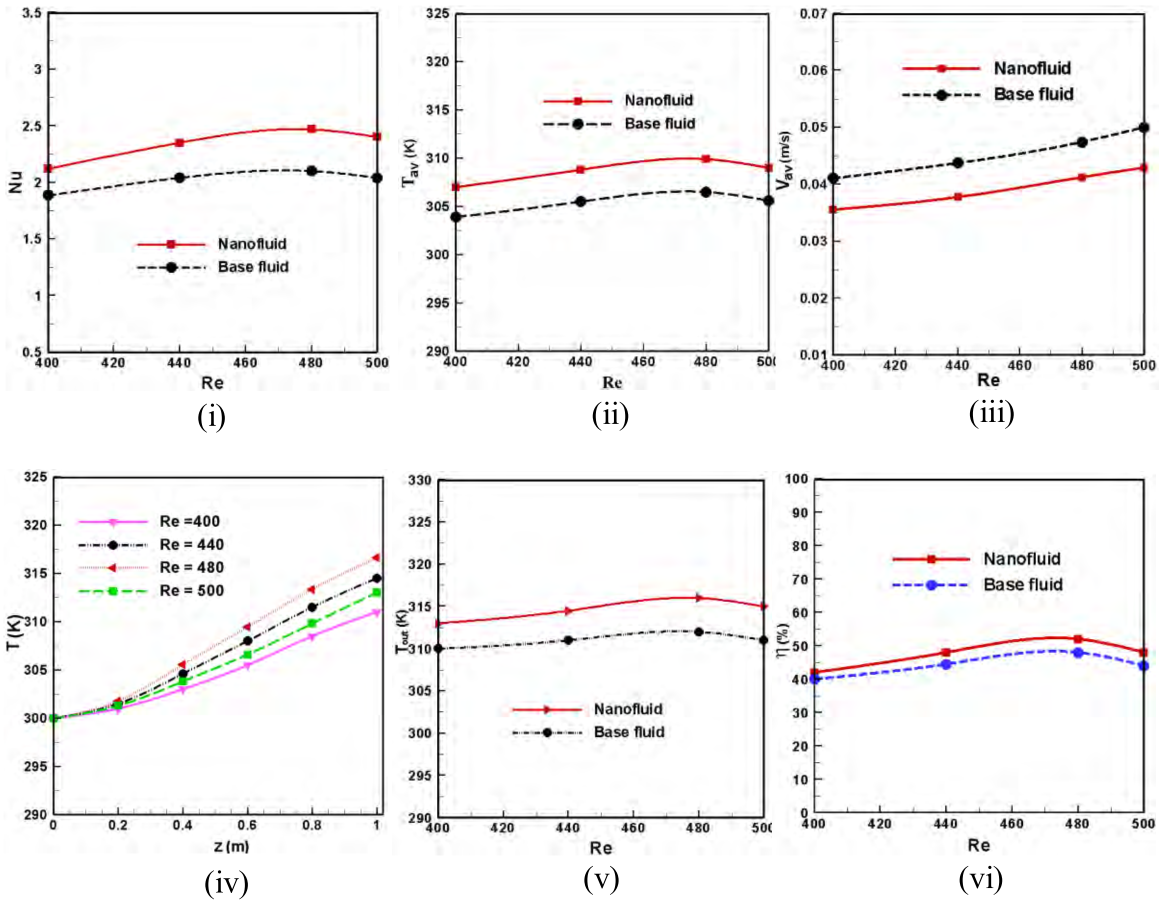

Figure 4.8: Effect of *Re* on (i) mean Nusselt number, (ii) mean bulk temperature, (iii) mean velocity, (iv) mid-height temperature, (v) mean output temperature and (vi) collector efficiency

The average output temperature (T_{out}) of both fluids is found from figure 4.8(v). T_{out} becomes 313K, 314K, 316K, 315K for nanofluid and 310K, 311K, 312K, 311K for water with the variation of Reynolds number Re = 400, 440, 480 and 500 respectively.

The variation of percentage of collector efficiency as a function of the Reynolds number is exposed in the figure 4.8(vi). It is observed that by introducing greater inertia force from 400 to 480 the collector efficiency increases using both types of fluids as heat transfer medium. More inertia force is able to augment heat transfer system through the riser pipe. After that when Re = 500, thermal efficiency tends to decrease. In this scheme water copper nanofluid performs better than clear water. Thermal efficiency of FPSC enhances from 42% to 52% for nanofluid and from 40% to 48% for water with the variation of Re from 400 to 480.

4.3.3 Effect of Prandtl number

Figure 4.9(i)-(ii) represents the streamlines pattern of water-Cu nanofluid at Re = 480, Pr = 5.8, ϕ = 2%, and I = 215W/m^2. The values of velocity in m/s unit and temperature in Kelvin unit are also shown. The different colours indicate different magnitudes of velocity and temperature of nanofluid. 3D formation of streamlines are shown interms of front view, cross-sectional view and back view. In all views of streamline plot it is observed that the flow is laminar and the streamlines are parallel to each other. The streamlines occupy the whole riser pipe of the flat plate solar collector.

Streamline plot with color expression for temperature is expressed in figure 4.9(i). It is well known that streamlines near the solid circular surface of heated riser pipe have higher temperature. Similarly at the middle of the riser pipe streamlines have lower temperature. This behavior of fluid is exposed in the figure 4.9(i). For more visualization streamlines are shown in tube format with a fixed radius.

Figure 4.9(ii).depicts the streamline plot with color expression for velocity field for water-copper nanofluid. No-slip condition is given at the solid circular surface of riser pipe. That‟s why streamline at the solid surface has the lowest velocity and streamline at the middle of the riser pipe has the higher velocity. So, actual practical phenomenon is reflected by this 3D numerical analysis.

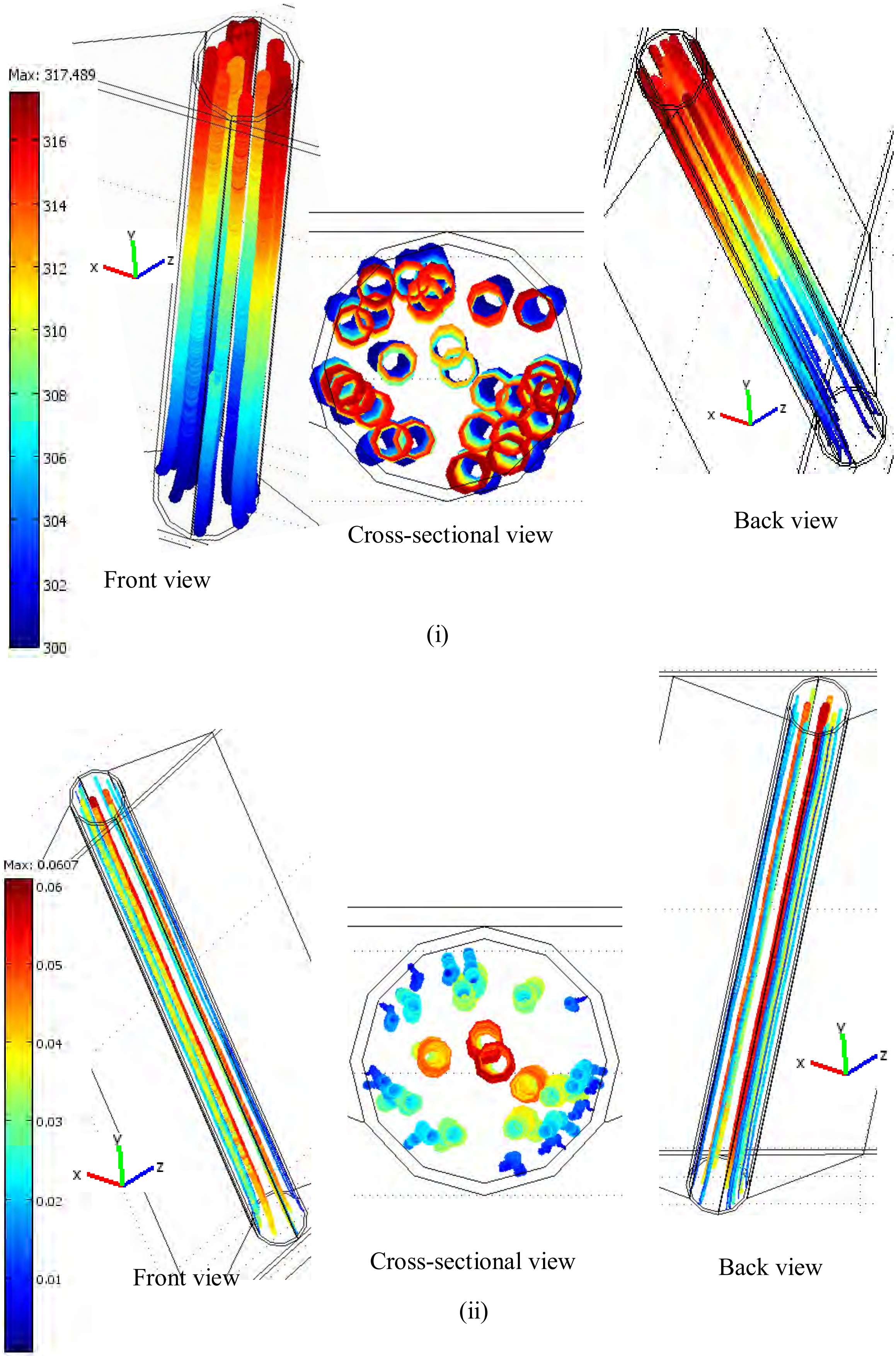

Figure 4.9: Effect of *Pr* at 5.8 on streamlines with color expression for (i) temperature and (ii) velocity

The effect of Prandtl number on average Nusselt number, mean bulk temperature, average sub-domain velocity, mid-height temperature of the copper/water nanofluid, mean output temperature and percentage of collector efficiency is expressed in the figure 4.10(i)-(vi). The range of Prandtl number is considered as (4.6-6.6). All values chosen for the Prandtl number represent water at different temperature. These values of *Pr* are 4.6 (at 310K), 5.2 (at 305K), 5.8 (at 300K) and 6.6 (at 295K). These temperatures of water represent the normal temperature of whole year that is from hot summer season to winter season in Bangladesh.

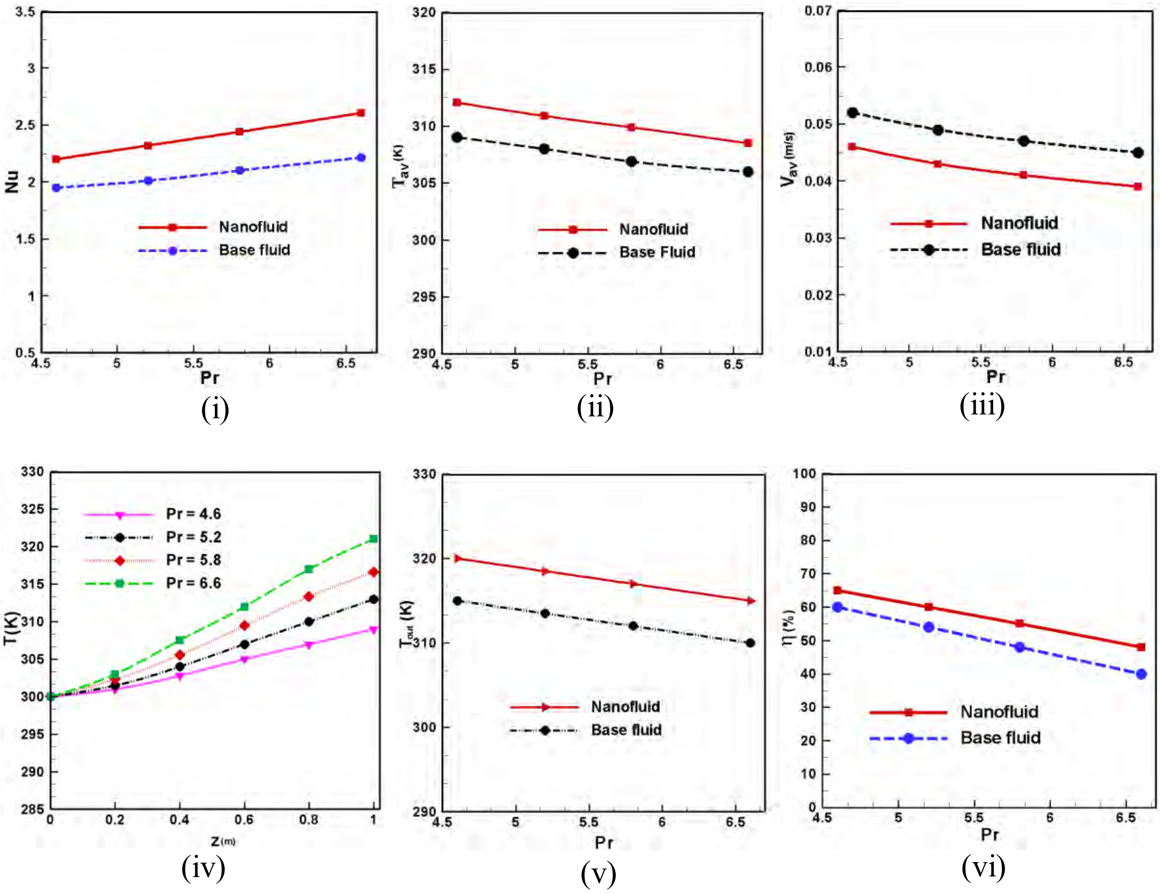

Figure 4.10: Effect of *Pr* on (i) mean Nusselt number, (ii) mean temperature, (iii) mean velocity, (iv) mid-height temperature, (v) mean output temperature and (vi) collector efficiency

Figure 4.10(i) shows that *Nu* enhances gradually with growing *Pr*. The rate of heat transfer for water-copper nanofluid is found to be more effective than the clear water due to higher thermal conductivity of solid nanoparticles. Increasing Prandtl number decreases fluid temperature inside the collector. Consequently increases heat transfer rate at the solid inner circular surface of riser pipe. Heat transfer rate rises by 18% and 13% for nanofluid and base fluid respectively.

Consequently, mean bulk temperature (T_{av}) along with the Prandtl number for both types of fluids falls sequentially. It is well known that higher values of Pr indicate lower temperature of fluids. Here base fluid has lower mean temperature than the water-Cu nanofluid.

Magnitude of mean velocity (V_{av}) has notable changes with different values of viscous forces. Falling viscous force enhance the mean velocity of the fluids through the riser pipe of the flat plate solar collector. It is established that velocity of higher viscous fluid is less than that of lower viscous fluid. Clear water moves freely than solid concentrated nanofluid.

Temperature (T) of water-copper nanofluid with 2% concentration decreases with growing Pr. From the figure 4.10(iv) it is observed that temperature of nanofluid increases when it passes through the riser pipe of FPSC.

The mean output temperature (T_{out}) of both fluids is displayed in figure 4.10(v). Average output temperature of water-Cu nanofluid becomes 320K, 318K, 316K, 314K for nanofluid and 315K, 314K, 312K, 310K for water for Pr = 4.6, 5.2, 5.8 and 6.6 respectively.

From figure 4.10(vi) it is observed that rising Pr devalues the percentage of collector efficiency (η) because greater Pr represents water of low temperature. Normal water at lower temperature is found in winter season. So temperature of output water can‟t so high as in summer season. Thermal efficiency devalues from 65%-48% for nanofluid and 60%-40% for water with the rising values of Prandtl number from 4.6 to 6.6 respectively.

4.3.4 Effect of solid volume fraction

Figure 4.11 represents the temperature of contour plot for different values of solid volume fraction (ϕ = 0%, 1%, 2%, 3%) of Cu nanoparticles at I = 215 W/m^2, Re = 480 and Pr = 5.8. Also the temperature bars in Kelvin unit are given in this figure. Initially at ϕ = 0% i.e. water is working fluid then the temperature contour of absorber plate is not high. Mixing nanoparticles with base fluid from 0% to 2% the

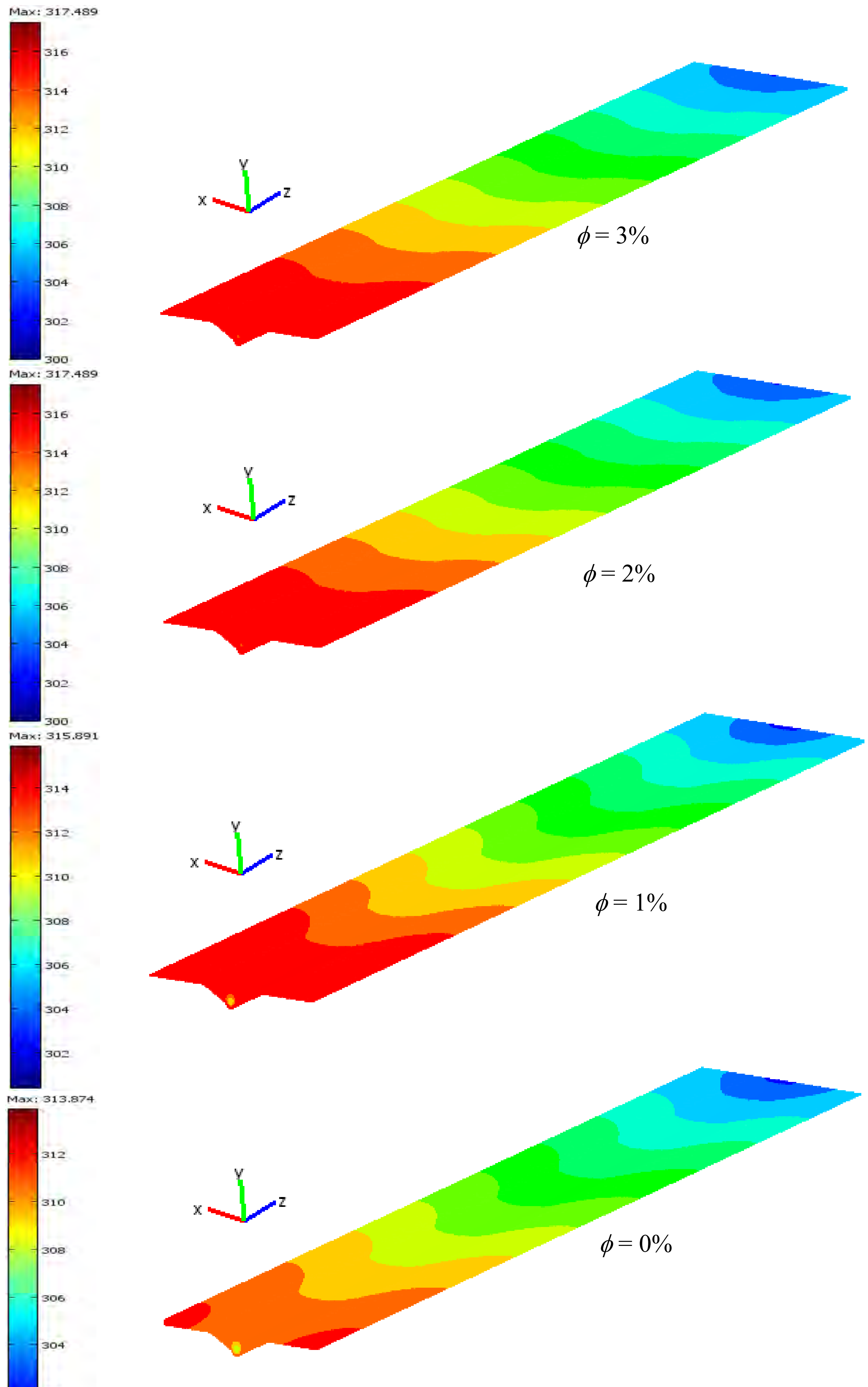

Figure 4.11: Temperature of contour plot at different ϕ

temperature of absorber plate as well as output nanofluid become high. But after that for 3% solid concentrated nanofluid does not have higher temperature. This phenomenon can be explained as increasing nanoparticles concentration increases nanofluid absorption coefficient and consequently increases the collector optical absorption. Using a certain concentration causes complete absorption of the incoming solar radiation, but beyond this maximum value, any further increase of the nanofluid absorption coefficient results in a shorter length for the radiation attenuation inside the fluid. This higher concentration of absorbed energy causes an increase of the surface temperature and, therefore, the heat losses to the environment increase as well.

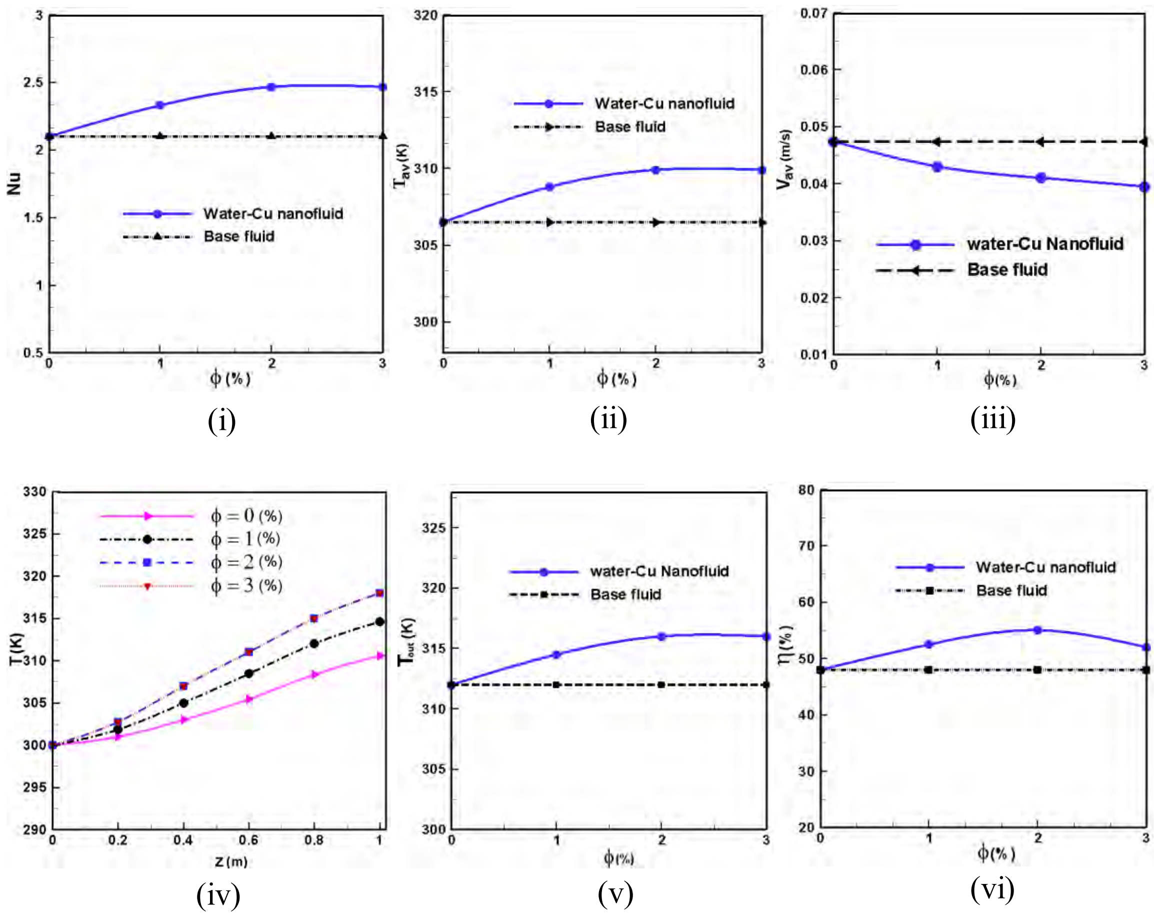

Figure 4.12: Effect of ϕ on (i) mean Nusselt number, (ii) mean bulk temperature, (iii) mean velocity, (iv) mid-height temperature, (v) mean output temperature and (vi) collector efficiency

The plots of Nu, T_{av}, V_{av}, mid-height temperature, T_{out} and η (%) profiles for water-copper nanofluid with the effect of solid volume fraction are displayed in the figure.

4.12(i)-(vi). From the plot of the average Nusselt number (Nu)-solid volume fraction (ϕ) it is observed that rate of heat transfer rises monotonically up to 2% of solid volume fraction. The rate of heat transfer for water-copper nanofluid is found to be more effective than that for clear water due to higher thermal conductivity of solid nanoparticles. For growing solid concentration of Cu nanoparticle from 0% to 2% rate of heat transfer rises 17%. For additional mixing solid concentration doesn"t increase heat transfer rate. So increasing solid concentration after a certain level is not advantageous.

Mean bulk temperature (T_{av}) along with the solid volume fraction grows sequentially for ϕ upto 2%. It is well known that higher concentration of solid particle enhances thermal conductivity as well as temperature of the working Cu-water nanofluid. Further adding solid volume fraction doesn"t show any considerable change in mean bulk temperature of nanofluid.

Magnitude of sub-domain average velocity of water-copper fluid enhances due to increasing solar irradiation. It is well known that density of nanofluid is higher than water. That"s why velocity of clear water is higher than water-Cu nanofluid. Average velocity of nanofluid devalues gradually along with the increasing solid volume fraction.

The temperature of water-copper nanofluid at the middle of the riser pipe increase with the increasing solid volume fraction upto 2%. The inlet temperature of fluid is maintained at 300K and then it increases gradually with the contact of heated solid circular surfaces of the riser pipe attached with the absorber plate of copper material. At $\phi = 3\%$ no significant change is observed at the mid-height temperature profile.

From figure 4.12(v) it is seen that mean output temperature (T_{out}) increases with growing values of solid volume fraction (ϕ) from 0% to 2%. After that no augmentation is found in outlet temperature of water-copper nanofluid for ϕ =3%. And finally the T_{out} of nanofluid becomes 312K, 314K, 316K and 316K for $\phi = 0\%$, 1%, 2% and 3% respectively.

The variation of percentage of collector efficiency as a function of the solid volume fraction varies from 0%-3% is exposed in the figure 4.12(vi). It is noticed from this figure that by introducing solid nanoparticles (ϕ = 0%-2%) with water the thermal efficiency increases. Then it decreases slightly with additional variation of ϕ. So, more solid concentration is not able to augment heat transfer system through the riser pipe of FPSC. Collector efficiency rises from 48% to 56% for the deviation of ϕ from 0% to2%.

4.3.5 Effect of mass flow rate

Non-dimensional temperature (T_a (z) / T_{ai}) of the absorber plate versus plate length for various m and thermal efficiency versus mass flow rate are expressed in the Fig. 4.13(i)-(ii). T_a (z) is the temperature of absorber along z direction and T_{ai} is the temperature of absorber at the starting length of absorber that is at z = 0 It is observed that there is a decrement in the plate temperature with a consequent increase in the mass flow rate for the condition of a simulated constant solar heat flux. This is because, as the mass flow rate increases, the heat is carried away from the plate due to convection at a faster rate within the tube. It is corroborated by the temperature gradient for the water passing through the absorber tube (riser pipe).

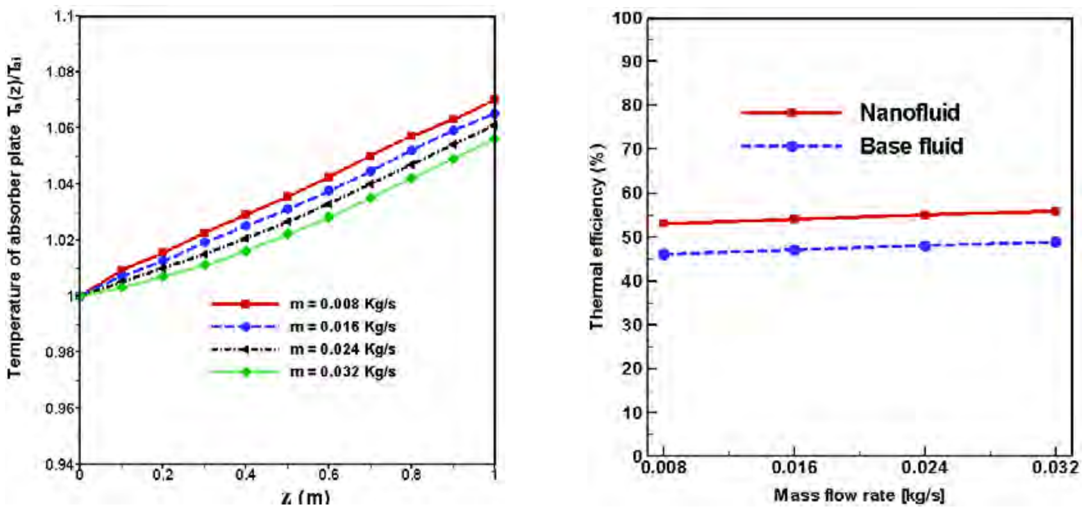

(i) (ii)

Figure 4.13: Effect of mass flow rate on (i) absorber temperature and (ii) collector efficiency

There is a gradual increase in the temperature of both types of fluids along the length of the tube. As explained earlier, the temperature of fluids increase due to the heat transfer at the absorber plate all along its length due to conjugate heat transfer. But it is observed that with increase in mass flow rate, there is a relative decrease in the temperature rise of water. This can be explained by the fact that as the velocity is increased due to increase in the mass flow rate, the fluids go forward at a faster rate thereby a perceptible lower temperature rise is observed for the considered fluids.

Non-dimensional temperature of absorber plate devalues gradually with the increment of mass flow rate per unit area. In the foregoing analysis, three different mass flow rates are employed to bring out the effect clearly. As seen from the figure 4.13 (i)-(ii), the trend lines match the physical explanation given above. On the other hand, collector efficiency increases for water/copper nanofluid as well as clear water and it is shown from the figure 4.13(ii). But using nanofluid gives higher thermal efficiency than base fluid. Thermal efficiency rises by 53%-56% for nanofluid and 46%-49% for water with the variation of mass flow rate per unit area from 0.008 Kg/s to 0.032 Kg/s.

4.3.6 Correlation

From the current 3D numerical study the calculated average Nusselt number (*Nu*) and percentage of collector efficiency (η) are correlated with solar irradiance (*I*), Reynolds number (*Re*), Prandtl number *Pr* and solid volume fraction (ϕ) with $4.6 \leq Pr \leq 6.6$, $200 \leq I \leq 240$, $400 \leq Re \leq 480$ and $0\% \leq \phi \leq 2\%$ through the FPSC. These correlations can be written as

$$Nu = (-0.0847 + 6.67\text{e-}5*I + 0.0142*Pr + 0.1*\phi)\,(Re)^{0.84} \qquad (4.9)$$

where the confidence coefficient is $r^2 = 97.3\%$.

$$\text{and } \eta = 0.2363 + 0.00114*I - 0.083*Pr + 3.5*\phi + 0.001*Re \qquad (4.10)$$

where the confidence coefficient is $r^2 = 98.7\%$.

4.3.7 Comparison

The present results are verified against the existing results available in the literature:

The current numerical result is compared for collector efficiency - temperature difference [T_i - T_a] profile of water with the graphical representation of Kalogirou (2004) of flat plate solar thermal collector. T_i and T_a are temperatures of input fluid and ambient air respectively. The computation is done taking heat transfer medium as water with irradiation level 1000 W/m^2 and the mass flow rate per unit area 0.015 kg/s. A survey report on various types of solar thermal collectors and applications was presented by Kalogirou (2004). He presented that generally the collector efficiency linearly depended on temperature difference for a FPSC. Figure 4.14(i) demonstrates the above stated comparison.

The present numerical solution may be treated as a particular case of general concept of Kalogirou (2004).Another comparison of thermal efficiency between the present work and Fabio (2008) has been shown in the figure 4.14(ii). Strukmann (2008) presented a project report on analysis of a flat plate solar collector. The collector efficiency is plotted against $(T_{in} - T_{amb})/I$. Water is considered as heat transfer medium and ambient temperature (T_{amb}) is 25^{0}C. From the figure 4.14(ii) it is seen that good agreement exists between the present work and that of Strukmann (2008).

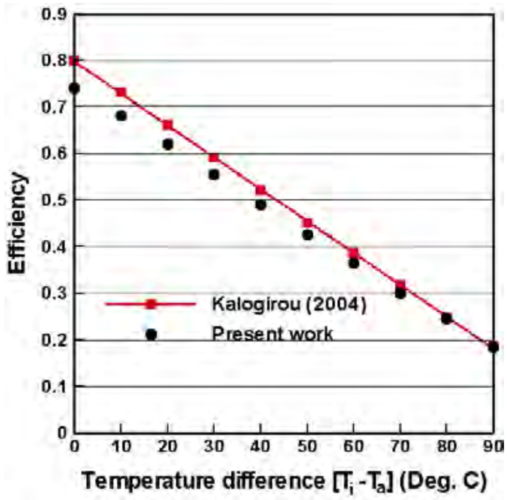

(i)

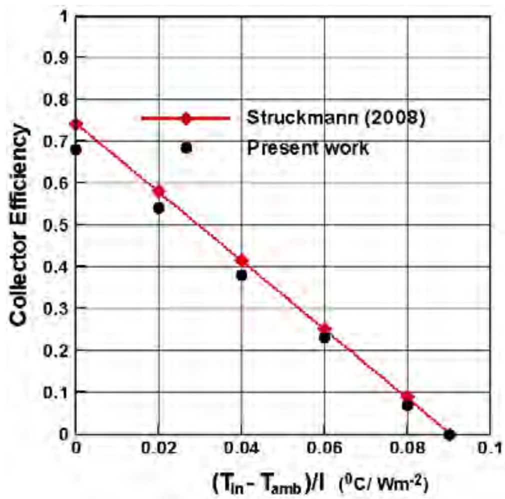

(ii)

Figure 4.14: Comparison of thermal efficiency between present work and (i) Kalogirou (2004) and (ii) Strukmann (2008).

4.4 Nanofluid with double nanoparticles

In order to analyze the comparison of heat transfer performance of a water based nanofluid having single and double nanoparticles the governing equations (4.1-4.6) with appropriate boundary conditions are solved numerically. For the case of water based nanofluid having double nanoparticles these effective properties of nanofluid must be modified. Now the modified form of the effective properties of nanofluid that is equations (3.7-3.10) are as follows:

effective density $\rho_{nf} = (1-\phi_1-\phi_2)\rho_f + \phi_1\rho_{s1} + \phi_2\rho_{s2}$ (4.11)

the effective heat capacitance

$$(\rho C_p)_{nf} = (1-\phi_1-\phi_2)(\rho C_p)_f + \phi_1(\rho C_p)_{s1} + \phi_2(\rho C_p)_{s2} \tag{4.12}$$

the effective dynamic viscosity (modified form) of Brinkman model (1952)

$$\mu_{nf} = \mu_f(1-\phi_1-\phi_2)^{-2.5} \tag{4.13}$$

and the effective thermal conductivity (modified form) of Maxwell Garnett (MG) model (1904) $k_{nf} = k_f \dfrac{(k_{s1}+k_{s2})+2k_f-2\phi_1(k_f-k_{s1})-2\phi_2(k_f-k_{s2})}{(k_{s1}+k_{s2})+2k_f+\phi_1(k_f-k_{s1})+\phi_2(k_f-k_{s2})}$ (4.14)

where suffixes 1 and 2 represent two types of nanoparticles such as Cu and Ag respectively. If solid volume fraction of Ag nanoparticle ϕ_2 = 0 then these expressions (4.11-4.14) are transferred to the expressions (3.7-3.10). This idea of modification is first explored by **Nasrin** and Alim (2013b).

4.4.1 Effect of double nanoparticles

The effect of ϕ (= ϕ_1 + ϕ_2) of water based nanofluid having copper and silver nanoparticles on the subdomain thermal field is presented in figure 4.15 while Re = 480, Pr = 5.8, I = 215W/m^2. The strength of the thermal current activities is more activated with escalating volume fraction of water/Cu/Ag nanofluid. Here ϕ varies from 0% to 3%. The temperature bars are given with each plot of subdomain temperature. ϕ (solid volume fraction of copper and silver nanoparticles) is distributed equally in water for Cu and Ag nanoparticles. That means $\phi = \phi_1 + \phi_2$ = 0.05% + 0.05% = 1%. The subdomain temperature of with the rising values of ϕ from 0% to 2%, the temperature distributions become distorted resulting in an increase in the overall heat transfer. This result can be attributed to the dominance of the solid concentration. This is because the thermal conductivity of the solid particles is very high.

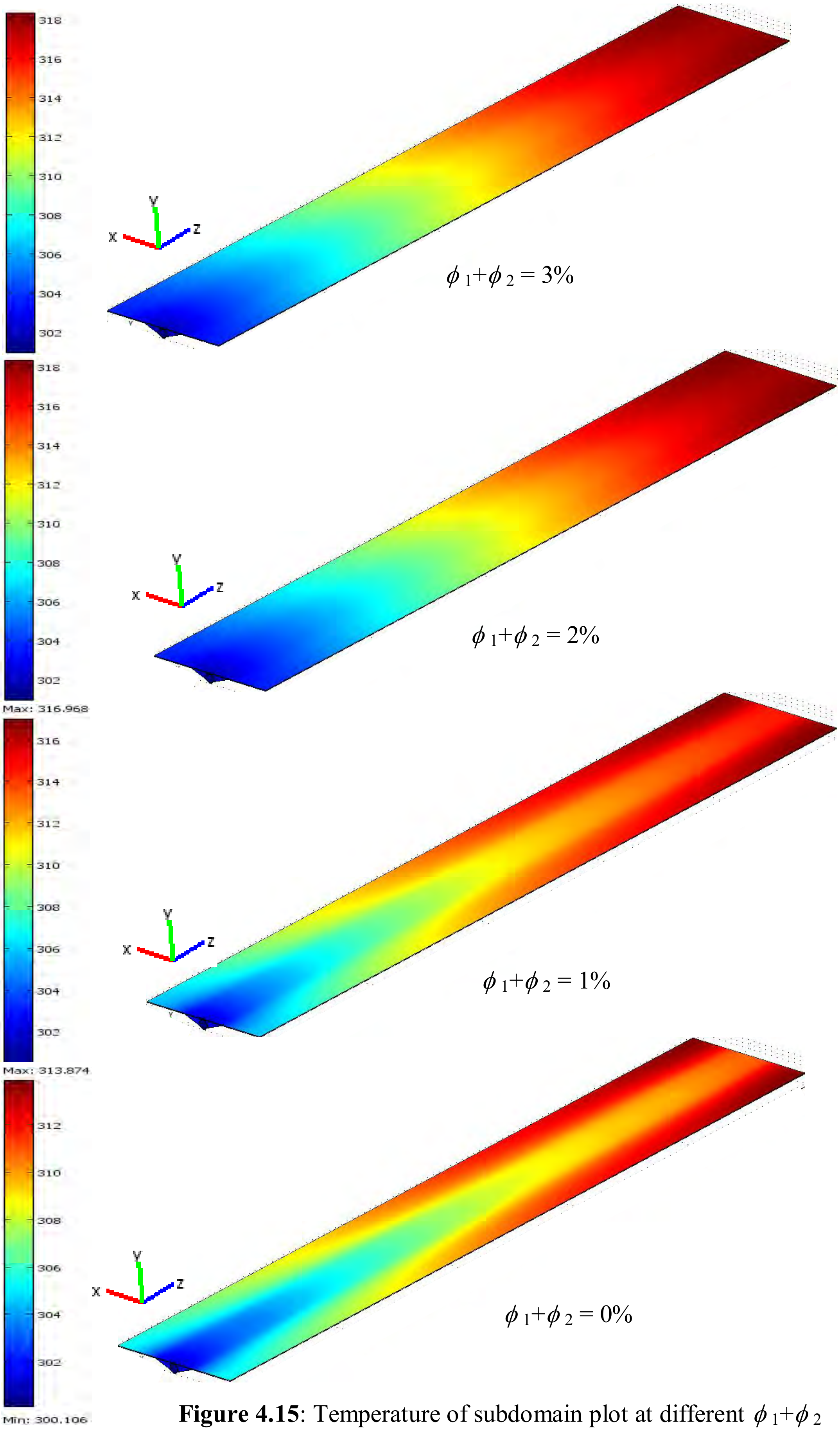

Figure 4.15: Temperature of subdomain plot at different $\phi_1+\phi_2$

This means that higher heat transfer rate is predicted by the nanofluid having two nanoparticles namely Cu and Ag. It is worth noting that as the solid volume fraction of Cu and Ag nanoparticles increases, the thermal boundary layer near output surface of the riser pipe becomes thick which indicates a steep temperature gradients and hence, an increase in the overall heat transfer from the absorber plate containing pipe to the outlet edge. But further increasing ϕ to 3% (=1.5% + 1.5%) there is no perturbation observed in the temperature profile at all.

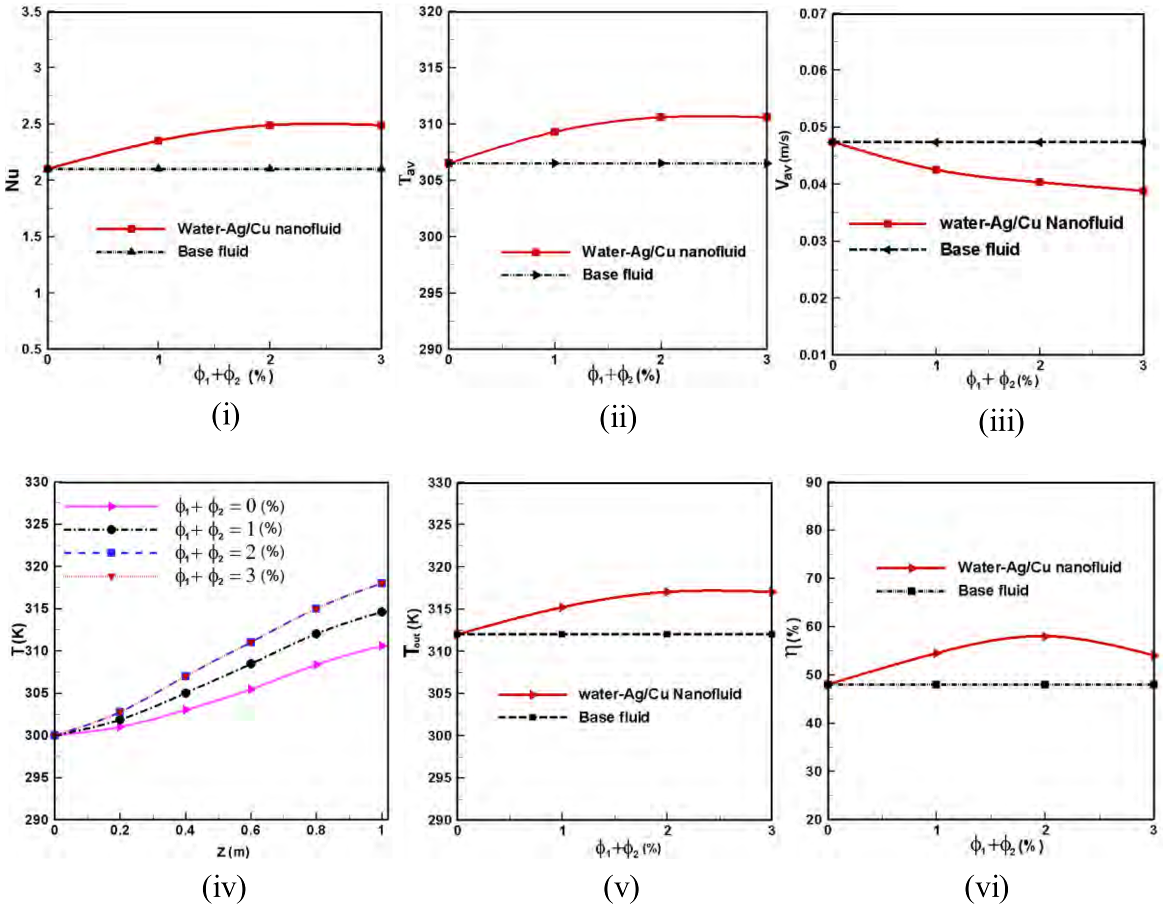

Figure 4.16: Effect of $\phi_1+\phi_2$ on (i) mean Nusselt number, (ii) mean bulk temperature, (iii) mean velocity, (iv) mid-height temperature, (v) mean output temperature and (vi) collector efficiency

In Figure 4.16 (i)-(vi) displays average Nusselt number at the hot riser pipe surface, mean temperature, mean subdomain velocity, mid-height temperature, mean output temperature and collector efficiency with various solid volume fraction are accounted for nanofluid having double nanoparticles as well as clear water. *Nu* enhances with growing ϕ upto 2% and then remains unchanged for advance mixture of solid volume faction for water based nanofluid having double nanoparticles. Rate of heat transfer enhances by 18% with the variation of ϕ from 0% to 2% for water-Cu/Ag nanofluid. Thus addition of more solid volume fraction is not advantageous.

Mean bulk temperature (T_{av}) grows sequentially for the variation ofϕ. Higher thermal conductivity is capable to carry more heat. It is observed from the 4.16(ii) that average bulk temperature of water-Cu-Ag nanofluid increases There is no change of water ($\phi = 0\%$) due to the deviation of nanoparticles volume fraction.

The magnitude of average sub-domain velocity field is shown in the figure 4.16(iii). Mean velocity falls down with rising values of solid volume fraction of water/Cu/Ag nanofluid. This is because density of water/Cu/Ag nanofluid is high.

The temperature of water/copper/silver nanofluid at the middle of the riser pipe increases gradually for increasingϕ from 0% to 2%. At ϕ = 3% there is almost no change is observed in the temperature profile.

Mean output temperature is shown in the figure 4.16(v). Inlet temperature of water, water based nanofluid having single and double nanoparticles are 300K. And finally the output temperature of water/alumina/copper nanofluid becomes 312K, 315K, 317K, 317K for water/Cu/Ag nanofluid for $\phi = 0\%$, 1%, 2% and 3% respectively.

From the figure 4.16(vi) it is shown that adding low quantities of nanoparticles leads to the remarkable enhancement of the efficiency until a volume fraction of approximately 2%. After a volume fraction of 2%, the efficiency begins to level off with increasing volume fraction. The authors attribute this unchanging to the high increase of the fluid absorption at high particle loadings. The main difference in the steady-state efficiency occurs in water based nanofluid having copper and silver nanoparticles. Thermal efficiency enhances from 48%-59% for water/Ag/Cu nanofluid.

4.4.2 Comparison among nanofluids

Table 4.3 describes the comparison on the rate of heat transfer and percentage of collector efficiency among water based nanofluid having single (either copper or silver) and double nanoparticles (both copper and silver). From this table the readers can easily understand that water-silver nanofluid has better performance than water/copper nanofluid as well as water/Cu/Ag nanofluid on the mechanism of heat transfer from riser pipe surface to the nanofluid and thermal efficiency of FPSC. This is explained in this way that Ag nanoparticle has higher thermal conductivity (429 W/mK) than double nanoparticles (mean value of 400 W/mK and 429 W/mK) as well as Cu nanoparticle (400 W/mK) for each effect of solid volume fraction. It is well known that silver nanoparticle is more costly than copper nanoparticle. Though Ag-water nanofluid has higher thermal performance than Cu/water nanofluid it is economically friendly to use water/Cu nanofluid as heat transfer medium in FPSC.

Table 4.3: Rate of heat transfer and thermal efficiency for variation of ϕ from 0% to 2% while Re = 480, I = 215W/m^2 and Pr = 5.8

Rate	Water/Cu nanofluid	Water/Ag nanofluid	Water/Cu/Ag nanofluid
Nu	17%	19%	18%
η	48%-56%	48%-61%	48%-59%

In addition, figure 4.17 (i)-(ii) expresses the comparison of mean output temperature and magnitude of mean subdomain velocity between water based nanofluid having double and single nanoparticles. Initial temperature of water/copper/silver nanofluid and water-Cu nanofluid is maintained at 300K and then it increases gradually when passes through the solid circular heated riser pipe. At last the mean output temperature of water-alumina/copper nanofluid becomes 312K, 316K, 318K, 318K for water-Ag nanofluid, 312K, 315K, 317K, 317K for water-Cu/Ag nanofluid and 312K, 314K, 316K, 316K for water-Cu nanofluid for ϕ = 0%, 1%, 2% and 3% respectively. Higher thermal conductivity is capable to carry more heat. Thus average outlet temperature of water/Cu/Ag is found higher in the figure 4.17(i).

Mean subdomain velocity (V_{av}) decreases sequentially for the variation of ϕ. It is well known that density of silver nanoparticle (10500 Kg/m^3) is higher than copper/silver nanoparticles (mean value of 8933 kg/m^3 and 10500 Kg/m^3) as well as copper nanoparticle (8933 Kg/m^3). That‟s why water-Ag nanofluid has lower mean velocity than that of other nanofluids considered in this investigation.

To use water based nanofluid having double nanoparticles is better than nanofluid having single nanoparticle as heat transfer medium through a FPSC provided that the total thermal conductivity of double nanoparticles is higher than single nanoparticle. It is established that Ag nanoparticle is more costly than Cu nanoparticle. So to minimize cost and to get standard performance in heat transfer and collector efficiency phenomena one can use water-Cu nanofluid as heat transfer medium for a FPSC.

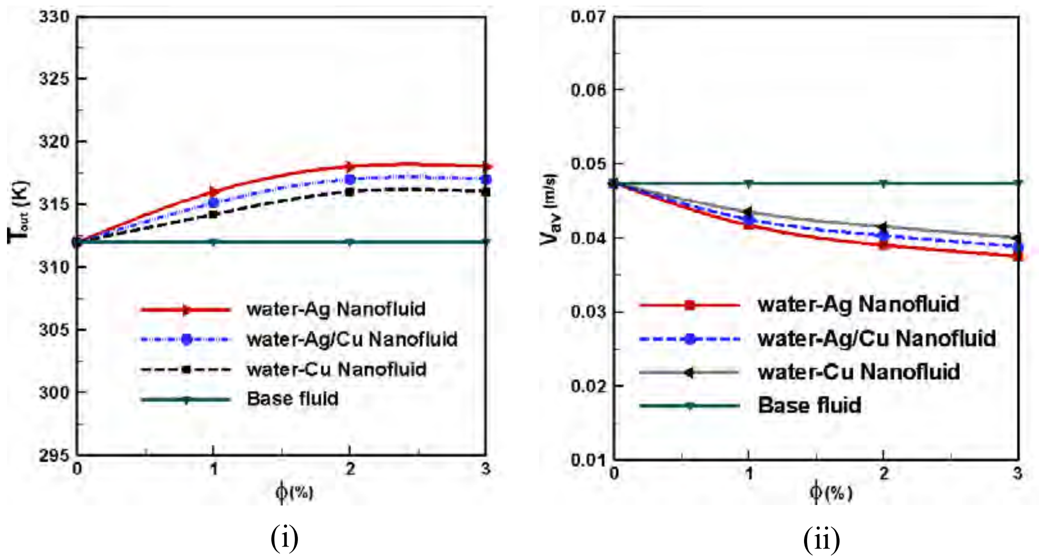

Figure 4.17: Comparison for (i) mean output temperature and (ii) mean velocity

4.5 Comparison between 2D and 3D results

Various comparisons between the results found by 2D and 3D numerical analyses are shown below:

4.5.1 Temperature distribution

A comparison is made between the results obtained from 2D and 3D numerical analyses of a considered FPSC at Re = 480, Pr = 5.8, I = 215 W/m^2, ϕ = 2% and L = 0.65m. This comparison is shown in figure 4.18. Temperature distribution from top of the absorber plate to the bottom of the riser pipe at the position 0.65m of FPSC is shown taking water/Cu nanofluid as heat transfer medium. In the region from top of absorber plate upto centre of fluid, higher temperature is found for 3D analysis than that of 2D analysis. Again in the fluid region, the temperature distribution of 2D analysis doesn‟t reflect actual concept of FPSC at all. That‟s why 3D numerical analysis represents accurate heat transfer phenomena of FPSC.

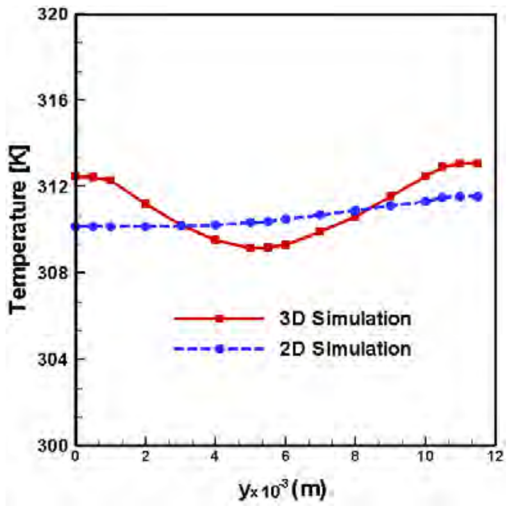

Figure 4.18: Temperature distribution from top to bottom at L = 0.65m

Temperature distribution of 2% concentrated water/copper nanofluid along top length, middle length and bottom length of the FPSC obtained from the results of 3D and 2D simulations is presented in the figure 4.19 (i-iii). From this figure it is observed that temperatures along the top and the bottom surface of FPSC are higher in 3D simulation than 2D simulation. At the middle of the riser pipe the fluid temperature is lower in 3D simulation than in 2D simulation. This is shown in the figure 4.19(ii). The cause is described for the figure 4.18. Figure 4.19(iii) shows that there is a big difference between results of 3D and 2D modeling. This difference is not expected. The reason is described in section 3.5, chapter 3.

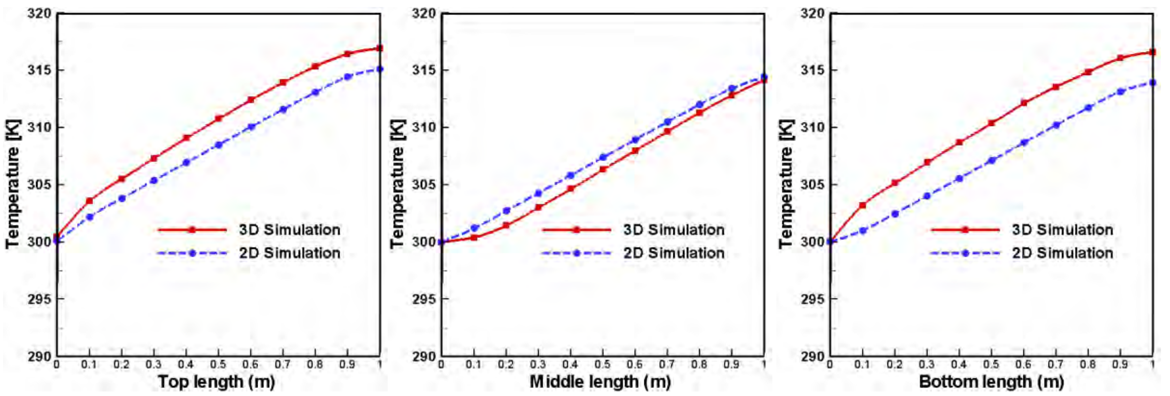

(i) (ii) (iii)

Figure 4.19: Temperature distribution along length at (i) top, (ii) middle and (iii) bottom

4.5.2 Output temperature and thermal efficiency

Figure 4.20 (i)-(ii) shows comparison between the results found from 2D and 3D numerical analyses. Considering heat transfer medium as water figure 4.20(i) displays data for mean output temperature against solar irradiation obtained by 2D and 3D numerical computation. Again taking water/Cu nanofluid as heat transfer medium for FPSC figure 4.20(ii) represents results for thermal efficiency against solid volume fraction found by 2D and 3D analyses. From figure 4.20 (i)-(ii) it is observed that 3D numerical computation gives better result than that of 2D analysis. Thus this comparison gives the information that for getting more accurate results three dimensional numerical analysis is useful.

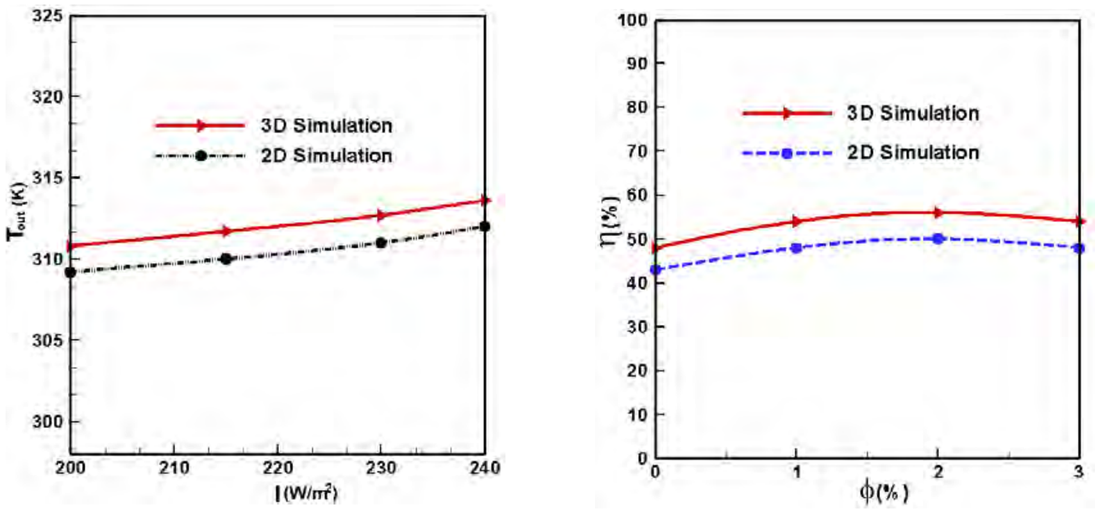

(i) (ii)

Figure 4.20: Comparison for (i) mean output temperature of water and (ii) thermal efficiency using nanofluid

4.5.3 Heat transfer rate and mean bulk temperature

Figure 4.21 shows comparison between the results found from 2D and 3D numerical analyses. Considering heat transfer medium as 2% concentrated water/Cu nanofluid figure 4.21(i) displays data for rate of heat transfer (mean Nusselt number) at the riser pipe surface. Computation is completed with the variation of Prandtl number from 4.6 to 6.6 with I = 215 W/m^2, Re = 480. From the figure 4.21(ii) it is observed that value of Nu is higher in 3D simulation than that of 2D simulation.

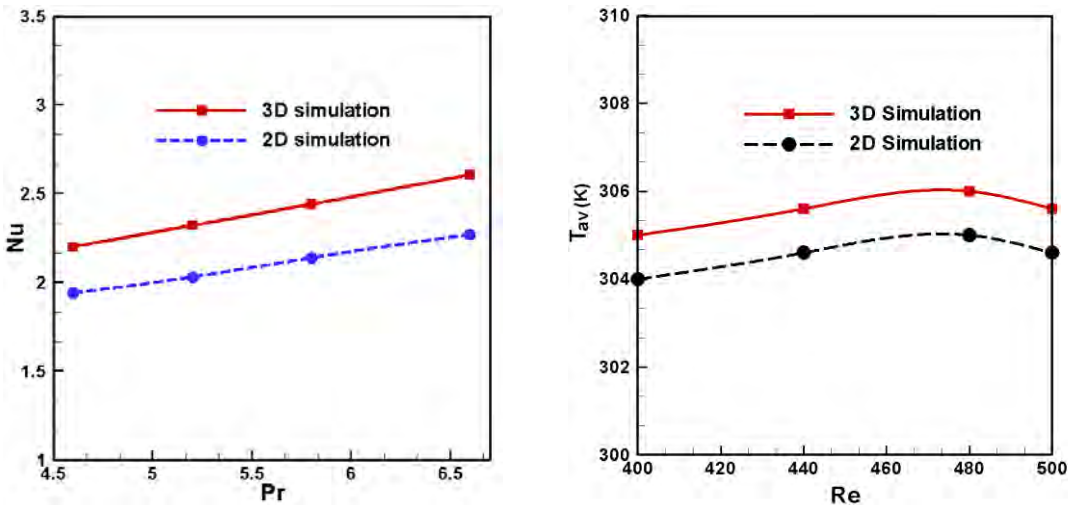

(i) (ii)

Figure 4.21: Comparison of (i) mean Nusselt number against *Pr* and (ii) mean subdomain temperature against *Re*

4.5.4 Transverse model

Figure 4.22(i)-(iii) depicts the temperature distribution from absorber plate to the riser pipe at the length L = 0.65m of 3D slice plot (full view and close view) and 2D transverse cross section. Computational domain of 2D transverse cross section is given in figure 2.12(ii), chapter 2. Numerical computation is shown for 2% concentrated water/Cu nanofluid at Re = 480, I = 215W/m^2, Pr = 5.8. Figure 4.22(iii) shows surface temperature of 2D transverse cross-sectional model. The mean temperature of fluid is calculated from 3D simulation and then imposed as boundary condition in 2D simulation. The temperature distribution is symmetric from the centre line of riser pipe to both sides of the absorber plate.

Also figure 4.23 shows the data taken from figure 4.22(ii)-(iii). This figure represents temperature distribution from top of the absorber plate to the inner diameter of the riser pipe. The data sets are equal. There is no variation between the temperature distributions in 3D and 2D transverse cross sectional models.

Figure 4.24(i)-(ii) depicts the temperature distribution from absorber plate to the bottom of riser pipe at the length L = 0.35m of 3D slice plot (close view) and 2D transverse cross section surface plot. As there is no fluid flow passage in figure 4.24(ii) so values of Reynolds number, Prandtl number, inlet fluid velocity etc are not imposed. Nanofluid properties that is thermal conductivity, density, viscosity, specific heat at constant pressure and no-slip condition is imposed. It is clear from figure 4.24 (ii) that there is no change in data of temperature in the fluid region. Fluid contains constant initial temperature which is assigned as boundary condition.

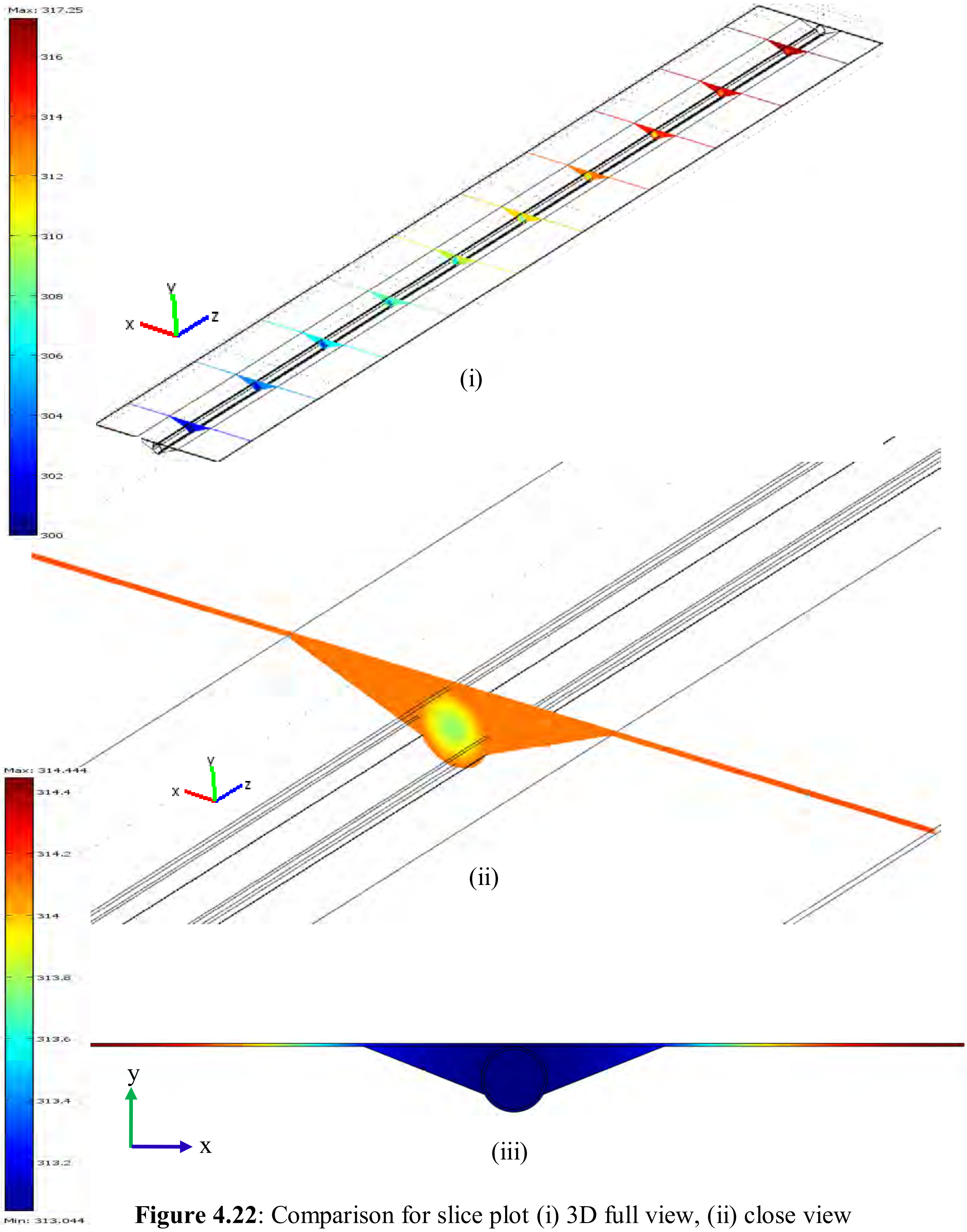

Figure 4.22: Comparison for slice plot (i) 3D full view, (ii) close view at L = 0.65m and (ii) 2D transverse view

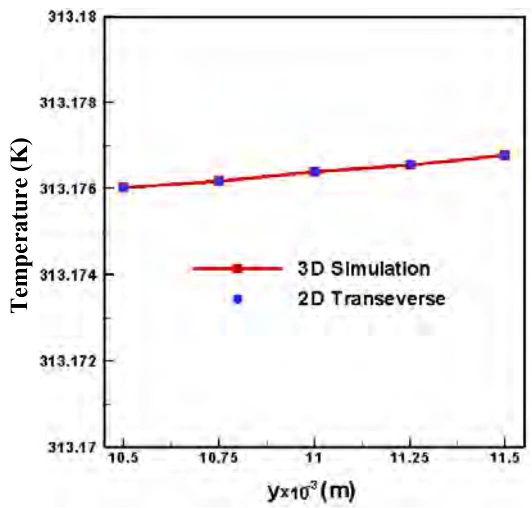

Figure 4.23: Temperature distribution from absorber to riser pipe at L = 0.65m

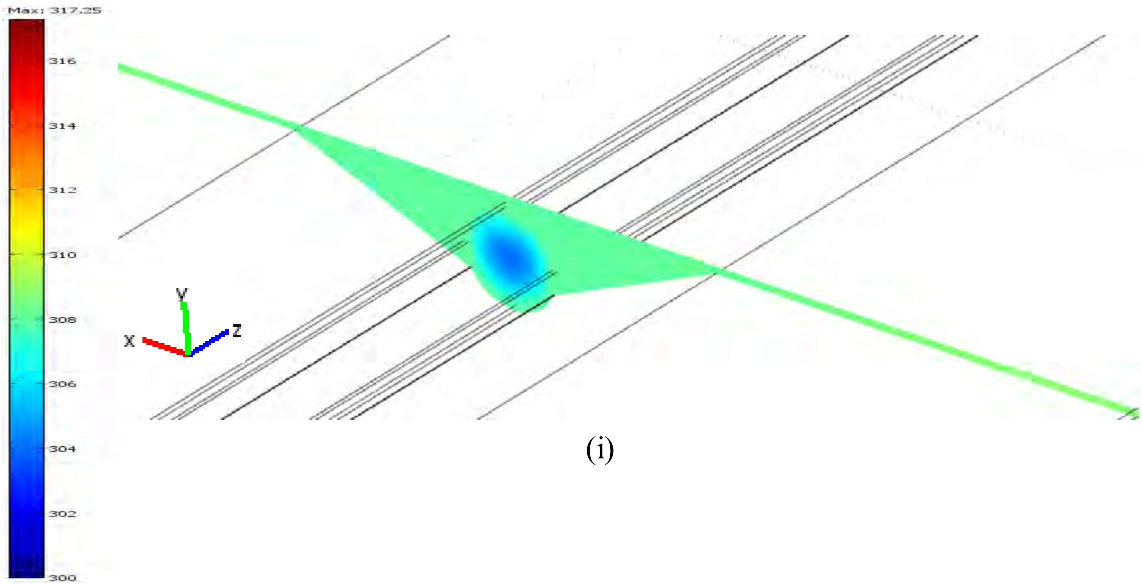

(i)

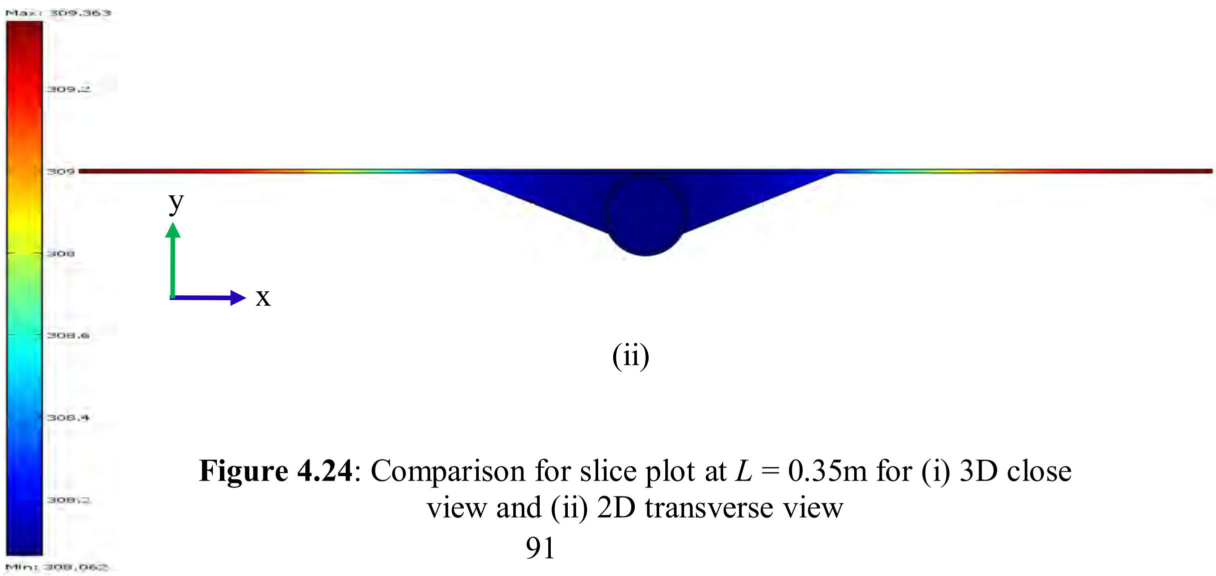

(ii)

Figure 4.24: Comparison for slice plot at L = 0.35m for (i) 3D close view and (ii) 2D transverse view

That means the fluid region does not have any importance in 2D transverse simulation because there is no fluid flow passage. Also 2D transverse simulation cannot be possible without knowing fluid initial temperature at any length from 3D simulation. The purpose for which FPSC made is not served by this model of 2D transverse cross section. That‟s why all researchers who are interested in 2D numerical simulation on FPSC consider 2D longitudinal cross section for getting results.

The data file is shown graphically in the figure 4.25. At the region from 0.0115m to 0.0105m that is from top of the absorber to the inner diameter of the riser pipe temperature is observed and there is no change in the temperature distribution obtained from the simulations of 3D and 2D transverse. Inside the fluid region in 2D transverse simulation no temperature change is observed in this figure 4.25. This is due to the boundary condition.

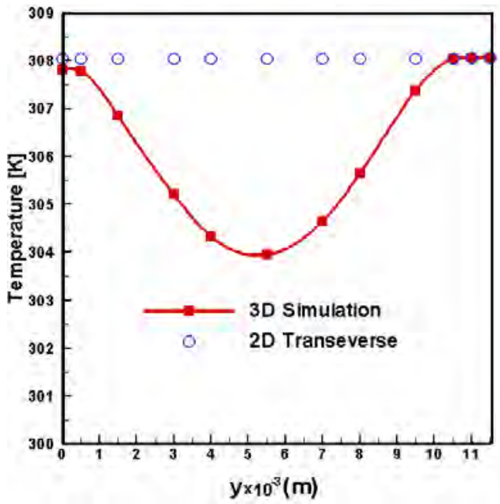

Figure 4.25: Temperature distribution from top of absorber to bottom of riser pipe at $L = 0.35$m

4.6. Quadratic form of thermal efficiency

The instantaneous thermal efficiency of the collector is described in chapter 3, sub-section 3.7.3 and is given below

$$\eta = \frac{Q_{\text{usfl}}}{AI} = \frac{F_R A\left[I(\tau\kappa) - U_L\left(T_{in} - T_{amb}\right)\right]}{AI} = F_R(\tau\kappa) - F_R U_L \frac{\left(T_{in} - T_{amb}\right)}{I}$$

It linearly depends on (T_{in} - T_{amb}) if all other terms are constant for a specific collector. Actually U_l is not constant. It is a function of collector inlet and ambient temperatures thus it is chosen that

$$F_R U_L = b + c\left(T_{in} - T_{amb}\right)$$

Then maximum useful energy can be rewritten as

$$Q_{usfl} = F_R AI\left(\lambda\kappa\right) - bA\left(T_{in} - T_{amb}\right) - cA\left(T_{in} - T_{amb}\right)^2$$

Thus the derived quadratic form of thermal efficiency is

$$\begin{aligned}\eta = \frac{Q_{usfl}}{AI} &= \frac{F_R AI\left(\lambda\kappa\right) - bA\left(T_{in} - T_{amb}\right) - cA\left(T_{in} - T_{amb}\right)^2}{AI} \\ &= F_R\lambda\kappa - b\frac{\left(T_{in} - T_{amb}\right)}{I} - c\frac{\left(T_{in} - T_{amb}\right)^2}{I} = a - bt - cIt^2\end{aligned} \tag{4.15}$$

where $a = F_R \lambda \kappa$, $t = (T_{in} - T_{amb})/I$

4.6.1 Effect of temperature difference

The effect of temperature difference (T_{in} - T_{amb}) on the temperature of contour plot is presented in figure 4.26 while Re = 480, Pr = 5.8, I = 215W/m^2, T_{amb} = 300K, A = 1.24 m^2, mass flow per unit area m = 0.0248 Kg/s. The heat transfer medium is chosen as water.

The temperature difference between input temperature and ambient temperature of fluid varies from 0K to 25K. The ambient temperature is kept fixed and only variation is shown for input temperature of water. The chosen values of input temperature of water are 300K, 310K, 320K and 325K. Temperature bar is also given with each contour plot of absorber. Actually when temperature difference becomes higher then heat loss from the absorber surface to the ambient air becomes also higher. As a result mean output temperature of water becomes lower. So value of collector efficiency becomes lower.

From the present numerical study using water as heat transfer medium at I = 215 W/m^2, Pr = 5.8, T_{amb} = 300K, A = 1.24 m^2, mass flow per unit area m = 0.0248 Kg/s, the computed value of thermal efficiency and temperature differences (T_{in} - T_{amb}) are displayed in Table 4.4.

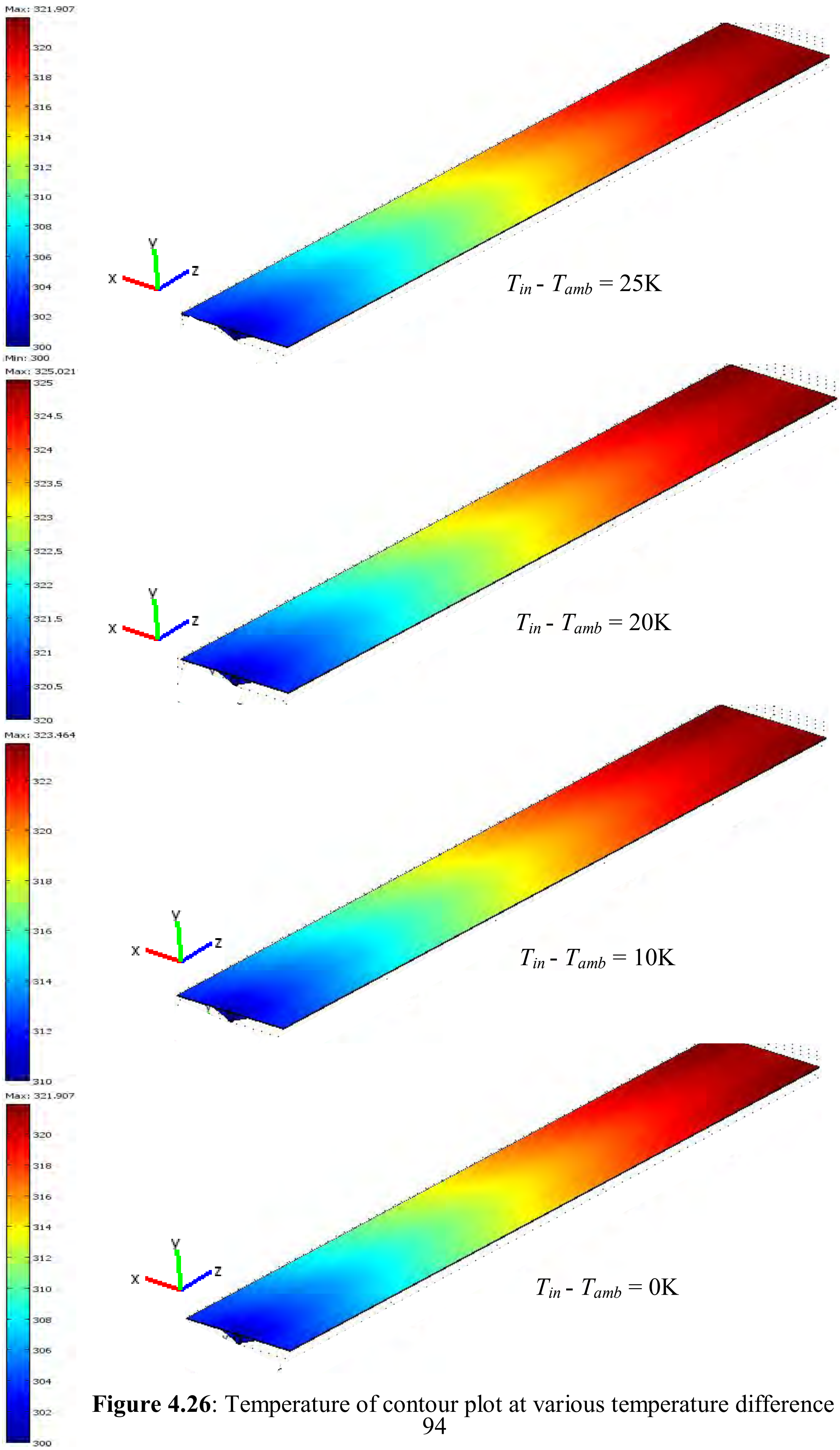

Figure 4.26: Temperature of contour plot at various temperature difference

Table 4.4: Thermal efficiency and temperature differences for water

$(T_i - T_a)$	0 K	5 K	10 K	15 K	20 K	25 K
η (%)	76%	61%	46%	32%	17%	3%

From the values represented in Table 4.4 a quadratic form of collector efficiency is derived as $\eta = 0.76 - 6.9\frac{(T_{in} - T_{amb})}{I} - 0.01\frac{(T_{in} - T_{amb})^2}{I}$ with correlation coefficient is $r^2 = 0.998$.

In the survey report "Solar thermal collectors and applications" of Kalogirou (2004) the thermal efficiency of a good FPSC was given as

$$\eta = 0.792 - 6.65\frac{(T_{in} - T_{amb})}{I} - 0.06\frac{(T_{in} - T_{amb})^2}{I}$$

4.6.2. Comparison

A comparison of quadratic form of collector efficiency between present numerical study and Kalogirou (2004) is shown in figure 4.27. In this figure values of thermal efficiency (η) are plotted against temperature differences (T_{in} - T_{amb}). A very good agreement is observed from this figure.

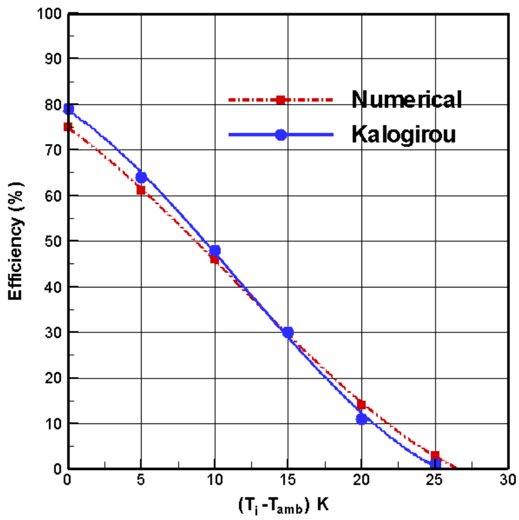

Figure 4.27: Comparison between numerical result and Kalogirou (2004)

4.7 Conclusions

The 3D numerical study addresses the heat transfer through a FPSC. Comparisons are shown for heat transfer and collector efficiency mechanism among 2D and 3D analyses. Another comparison is exposed between nanofluid having single and double nanoparticles considered as heat transfer medium. The conclusions have been drawn as follows:

- Solar irradiation has considerable effect on the flow and temperature field. Stronger solar radiation grows up the heat transfer rate as well as the thermal efficiency of the FPSC. The mid height temperature of nanofluids increase steadily while passing through the riser pipe for all values of solar radiation.
- There is a significant effect of Reynolds number on the pattern of iso-surfaces in the FPSC. A remarkable effect of Re on the average value of Nusselt number is observed which indicate enhanced rate of heat transfer upto $Re = 480$.
- Fluids with a low Prandtl number having less viscous and higher inertia effect is responsible for greater output temperature of fluids as well as thermal efficiency of FPSC. High viscous fluid has lower velocity.
- Rate of heat transfer, mean outlet temperature and percentage of collector efficiency is obtained maximum for 2% solid volume fraction of water-copper nanofluid. Average velocity is lower for nanofluid than base fluid. Using more than 2% solid volume fraction of nanoparticle is not beneficial.
- Temperature distribution from top of the absorber plate to the bottom of the riser pipe at any position (length) of FPSC is obtained higher for 3D analysis than 2D analysis. Higher output temperature and thermal efficiency are found for 3D numerical analysis than that of 2D analysis.
- The structure of the temperature interms of subdomain plot through the solar collector is found to appreciably depend upon solid volume fraction ϕ $(= \phi_1+\phi_2)$ of water/copper/silver nanofluid. Adding double nanoparticles with base fluid is more effective in enhancing performance of heat transfer rate and percentage of thermal efficiency than that of single nanoparticle. Mean subdomain velocity is lower for nanofluid with double nanoparticles than nanofluid with single nanoparticle.
- Water-silver nanofluid is better than water-copper nanofluid to enhance heat transfer through FPSC.

Chapter 5: Numerical Modeling of an Experimental Study

5.1 Introduction

Flat plate solar collector is a practical geometry. In order to continue research based on this geometry experiment is needed. In Bangladesh researchers do not have enough scope to conduct experimental research. Thus many of them continue their research depending on numerical or analytical studies. In this chapter 3D numerical modeling of a published experimental study of FPSC is conducted. Then the numerical result is compared with experimental result and percentage of error is also calculated. A correlation is derived from this numerical result.

5.2 Numerical Modeling

Martín *et al.* (2011) performed experimental heat transfer research in enhanced flat-plate solar collector in Cartagena, Spain in the month of May 2011. Cartagenan has Latitude +37.61 (37°36'36"N), Longitude -0.98 (0°58'48"W). To test the enhanced solar collector and compare with a standard one, an experimental side-by-side solar collector test bed was designed and constructed in their study. A numerical modeling is conducted using all information given by Martin *et al.* (2011) to analyze heat transfer system. Figure 5.1 shows 3D view of the geometry.

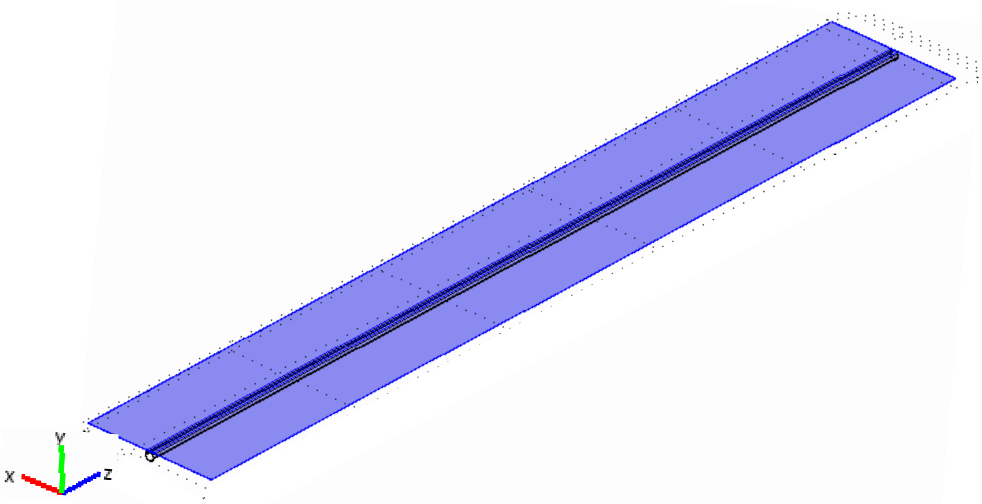

Figure 5.1: 3D numerical formation of FPSC (measurement taken from experimental study)

The working fluid is water. The governing equations and boundary conditions are similar to the equations described in chapter 4, section 4.2. and solved by Galerkin‟s Finite Element method. That‟s why the governing equations and boundary conditions are not repeated in this chapter. Figure 5.2 (i)-(ii) displays 3D and cross-sectional views of finite element mesh. Finer type meshing is used with elements 10,32,306 and time needed for solving is 1815.78 s. The tetrahedral element type with 10 nodes is used for finite element meshing in the subdomain and triangular element with 6 nodes is used in the boundary. Here vertical bonding is used to connect the absorber and the riser pipe.

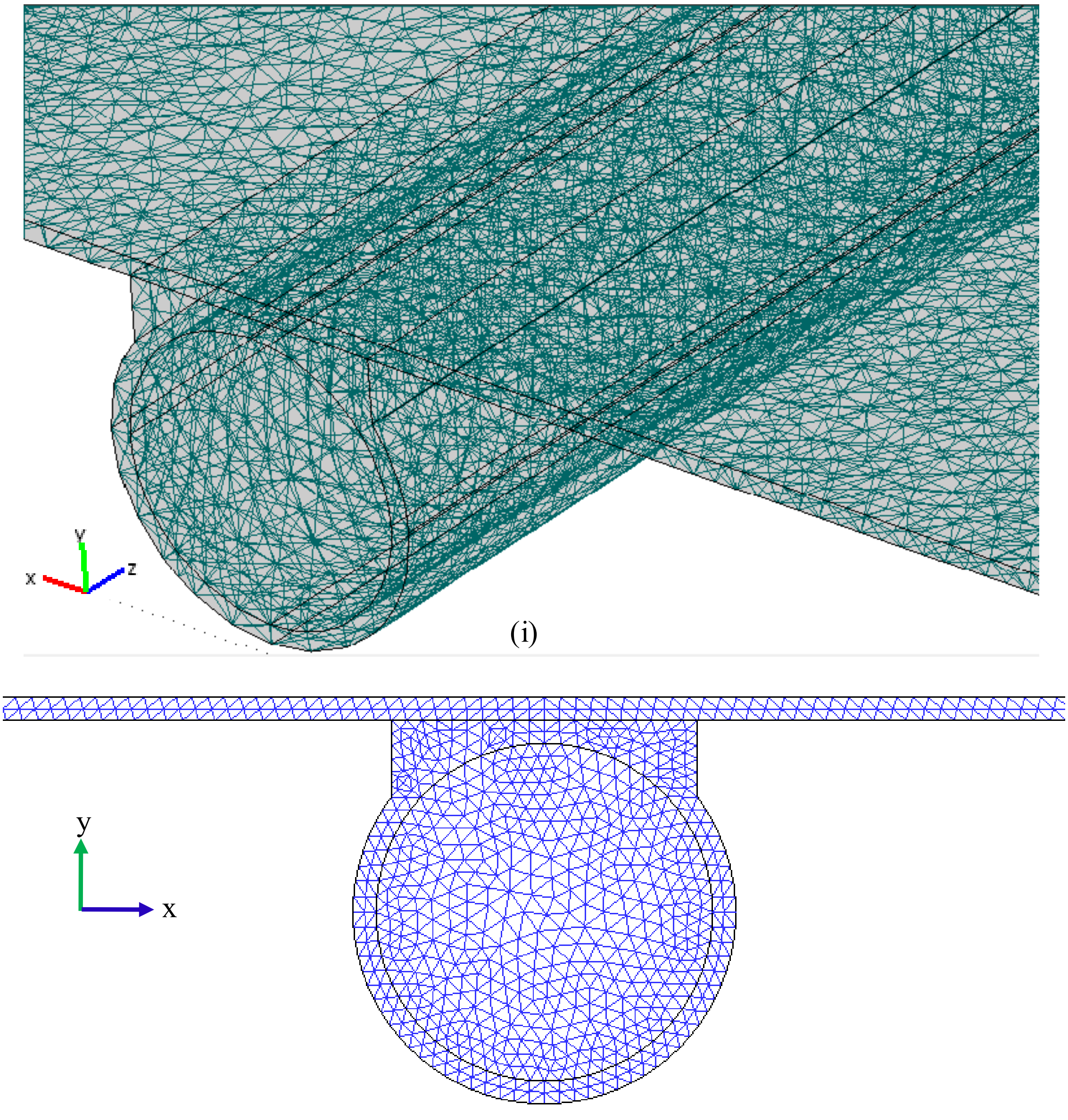

(ii)

Figure 5.2: Finite element meshing of (i) 3D view and (ii) 2D view

5.2.1 Measurement of FPSC

For the drawing of 3D geometry data written in Table 5.1 is collected from their study. For experiment fluid velocity w_{in} = 1 m/s, ambient temperature T_{amb} = 18.06^{0}C = 291.06K, thermal conductivity k = 0.6 W/mK, specific heat at constant pressure C_p = 4179 J/kgK, density ρ = 997.1 kg/m^3, mass flow rate m = 0.04 Kg/s were chosen.

Temperature difference was considered by Martín *et al.* (2011) as

$T^* = (T_m - T_{amb})/I$, where $T_m = T_{in} + (T_{in} - T_{amb})/2$

Value of solar irradiation was not given in the paper of Martín *et al.* (2011). Mean value of solar irradiation in Cartagena, Spain in the month of May, 2011 at the tilt angle 45^0 is obtained from internet facility [17]. The value of solar irradiation is I = 5.89 kWh/m²/day = 245 W/m². In the experiment the FPSC with 9 tubes was considered. For numerical analysis absorber plate with single tube is considered. For numerical computation amount of mass flow rate and total heat flux are obtained from their experimental value divided by number of risers.

Table 5.1: Measurement of FPSC used in experimental study

Components of FPSC	Size and property
Gross surface area	2.022 m²
Edge area	0.2348 m²
Solar collector	length 1.83m, width 0.1227m
Glass cover	highly transparent, anti-reflection, single glass, transmission 93%,emmittance 88%
Absorber (aluminium)	thermal conductivity 209.3W/mK, absorption 95%; emmision 5%; thickness 0.0005 m,
Inner diameter of pipe	0.007m
Riser pipe (copper)	thickness 0.0005m, thermal conductivity 372.1W/mK
Insulation	thickness 0.025m, thermal conductivity 0.05W/mK

5.3 Result

Temperature of computational domain interms of contour plot for various T^* is displayed in figure 5.3(i)-(iii). T_{amb} = 291.06K is fixed. Only variation of input temperature is performed and the results are shown. For each part of this figure 5.3(i)-(iii) the temperature bars are given side by side.

For the figure 5.3(i) mean input temperature of water T_{in} = 291.55K is considered. From the temperature bar it is seen that mean output temperature (T_{out}) is obtained 293.58K. Then temperature difference is found

$$T^* = (T_m - T_{amb})/I = 0.0035.$$

Similarly for the figure 5.3(ii) mean input temperature of water T_{in} = 295K is considered. Average output temperature (T_{out}) is found as 296.78K. Then temperature difference is

$$T^* = (T_m - T_{amb})/I = 0.0235.$$

Again for the figure 5.3(iii) mean input temperature of water T_{in} = 302.9K is considered. Obtained mean output temperature (T_{out}) is 303.95K. Then calcualted temperature difference is

$$T^* = (T_m - T_{amb})/I = 0.0723.$$

Actually numerical simulation is performed for six different values of T^*. Contour plot is shown for only three values of T^* in the figure 5.3(i)-(iii).

Then at each temperature difference (T^*) the thermal efficiency is obtained numerically. Thermal efficiency is calculated using the following formula stated in their experimental work:

$$\eta = \frac{\text{useful gain}}{\text{available energy}} = \frac{Q_{\text{usfl}}}{AI} = \frac{mC_p\left(T_{out} - T_{in}\right)}{AI}$$

Percentage of error between numerical and experimental results is calculated using very well known formula:

$$\text{Percentage of error} = \frac{|\text{experimental data - numerical data}|}{\text{experimental data}} \times 100.$$

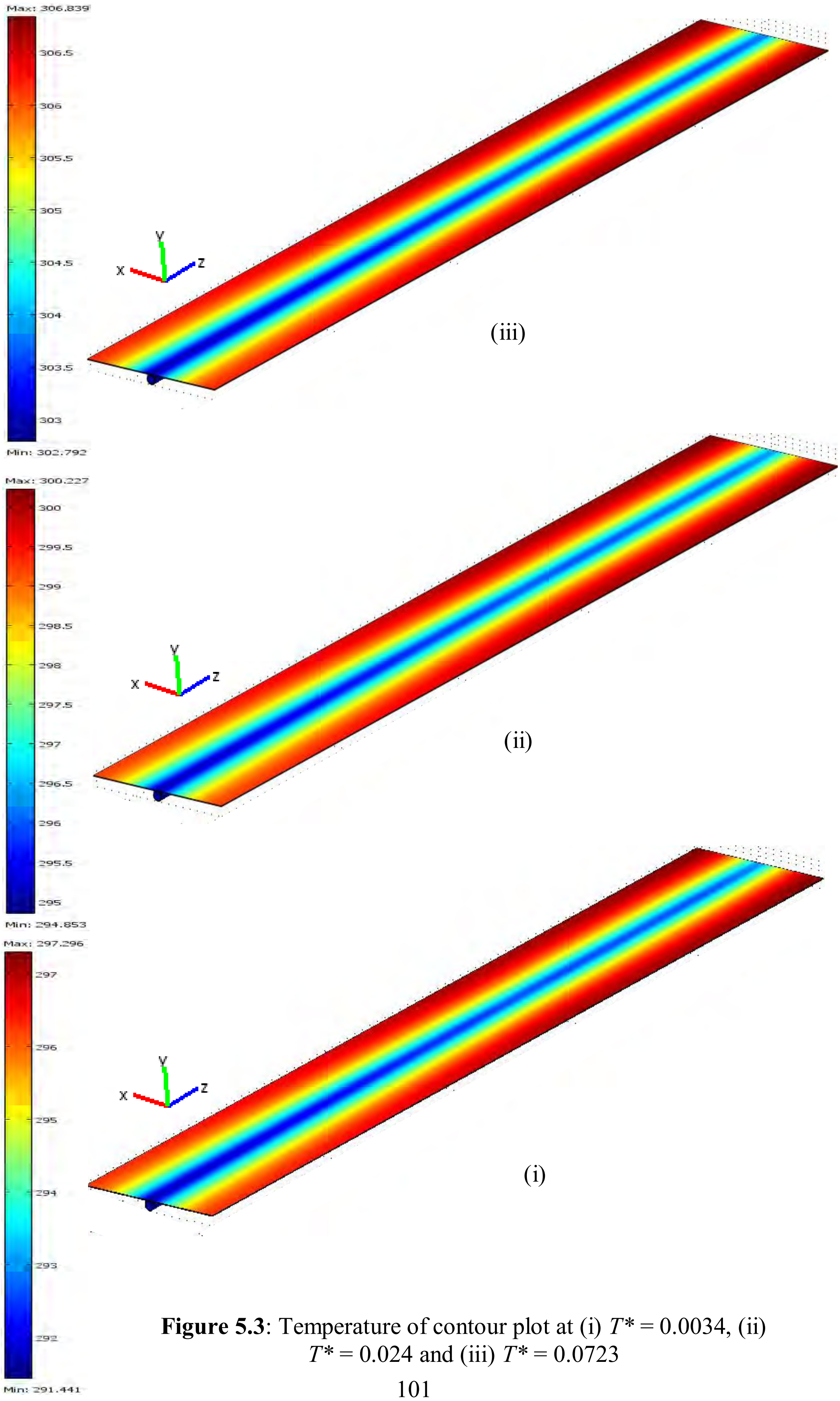

Figure 5.3: Temperature of contour plot at (i) T^* = 0.0034, (ii) T^* = 0.024 and (iii) T^* = 0.0723

These numerical values, experimental values and percentage of error between numerical and experimental results are shown in Table 5.2. Percentage of error lies in the range of (2% - 4.9%) between numerical and experimental data sets.

Table 5.2: Thermal efficiency for different values of temperature difference

$T^* = (T_m - T_{amb})/I$	η (%) obtained from numerical study	η (%) obtained from experimental study (Martin *et al.* (2011)	Percentage of error
0.0035 K	67.83 %	66.49%	2%
0.0096 K	66.01%	63.03%	4.7%
0.0235 K	57.20%	54.66%	4.6%
0.0447 K	45.01 %	43.14%	4.3%
0.0489 K	43.78 %	41.9 %	4.5%
0.0723 K	26.44 %	25.20%	4.9%

5.3.1 Comparison

The present numerical result of Table 5.2 for a flat plate solar collector is compared with the experimental result of Martin *et al.* (2011). The comparison is shown in the figure 5.4.

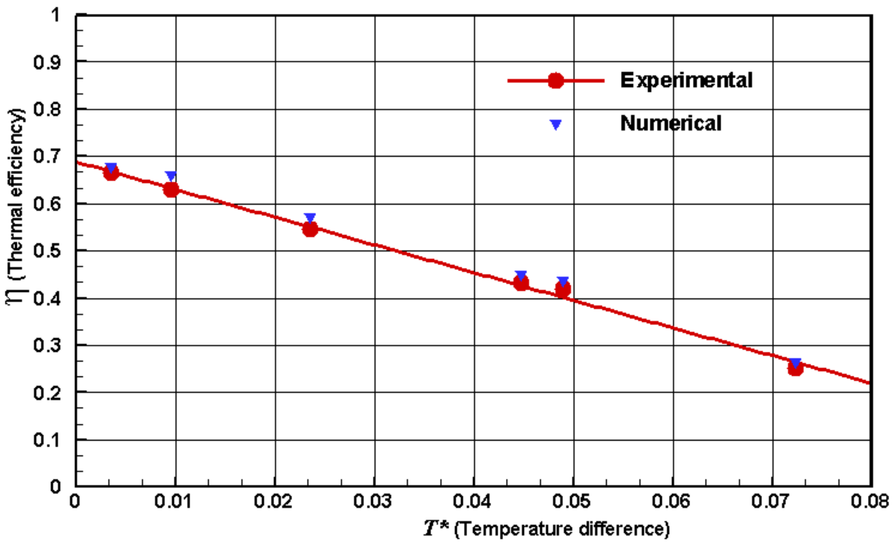

Figure 5.4: Comparison between numerical and experimental results

A difference is observed in results between numerical and published experimental studies (given in figure 5.4). The probable causes are:

- Mean solar radiation of Cartagena, Spain in the month of May, 2011 is used in numerical study. Actual value of irradiation was not mentioned in the paper of Martin *et al.* (2011).
- Wind velocity is not considered in numerical study.
- Solar irradiation varies at different time of a particular day.
- Difference may be occurred due to convergency level.
- Error may be occurred due to numerical iteration.

5.3.2 Correlation

Linear correlation between T^* (temperature difference divided by solar irradiance) and collector efficiency η(%) is developed from the 3D numerical result with $291.55\text{K} \le T_{in} \le 302.9\text{K}$, $T_{amb} = 291.06\text{K}$, $I = 245\ \text{W/m}^2$. The correlation is

$$\eta = 0.7122 - 5.5833T^*, \text{ where } T^* = (T_m - T_{amb})/I$$

The correlation coefficient is $r^2 = 0.989$. This is shown in figure 5.5. In experimental work of Martin *et al.* (2011) linear correlation coefficient was $r^2 = 0.9874$.

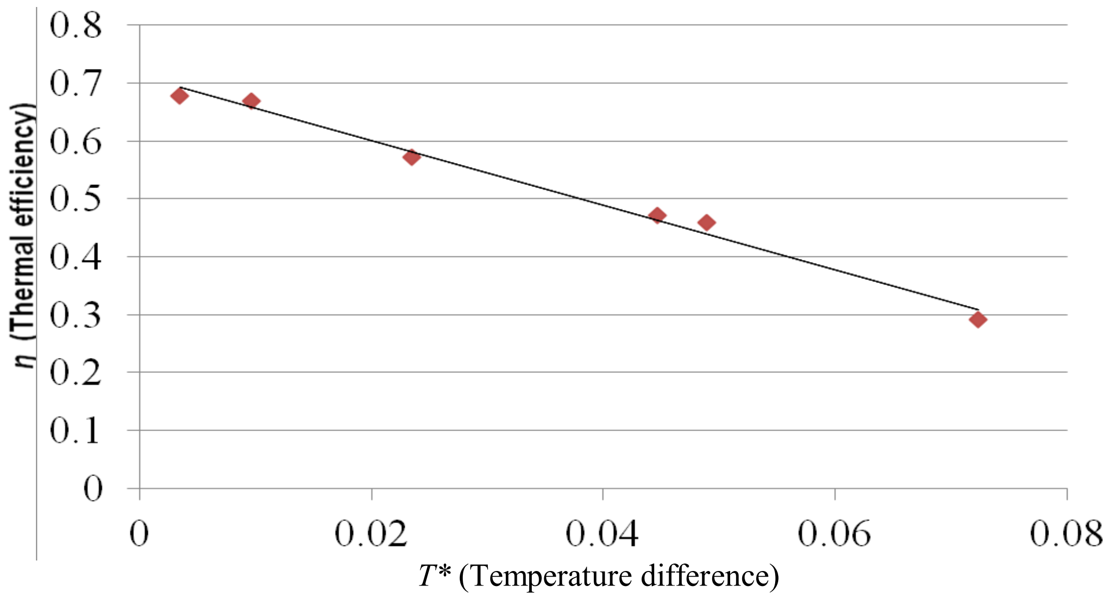

Figure 5.5: Correlation between T^* and collector efficiency η

5.4 Conclusions

Based on the results and discussions as furnished in chapter 5 of 3D numerical modeling of a published experimental study for FPSC the following conclusions are drawn:

- To optimize collector efficiency of a FPSC input and ambient temperatures of fluid should be same.
- A good correlation coefficient is found for the correlation of the thermal efficiency and temperature difference.

An experimental study is always preferable for doing research in such type of practical geometry. For the lack of facility of experimental research numerical modeling should be performed based on experimental data available in the literature.

Chapter 6: Conclusions and Recommendations

Numerical study of thermofluid characteristics of a flat plate solar collector using nanofluid has been performed by solving steady state two-dimensional as well as three-dimensional Navier-Stokes equations, energy equations and continuity equation. The work reported in this thesis is dependent on thermofluid characteristics in forced convective heat transfer and thermal efficiency phenomena through FPSC. Also an experimental study is formulated numerically. Based on the outcome of the numerical investigation, attention has to be paid on some factors, specific conclusions and recommendations for future work have been presented in this section.

6.1 Important Factors

Maximum heat transfer rate and collector efficiency is expected by making choice of combination of different relevant properties of material and fluid. The theoretical prediction in this thesis may be a useful source for researchers as well as for engineers to design the FPSC. Any interested person can calculate this 3D analysis by considering half of the domain along width of the absorber plate. This is due to the fact that from the centre of the riser pipe to the both side walls of the absorber plate along width direction heat transfer mechanism is symmetric. Then less time is needed for each simulation. To find better thermal performance of a FPSC, attention should be given on the following important factors:

- Dimension ($H \times L \times W$) of solar collector and number of riser pipes
- Location and tilt angle
- Heat transfer medium
- Solid volume fraction of nanoparticle
- Input and ambient temperature
- Solar irradiation
- Fluid velocity and mass flow rate and fluid properties
- Absorber and riser pipe material
- Glass cover properties
- Maintaining proper insulation at all sides except top surface

- ❖ Thickness of glass cover, air gap, absorber plate and riser pipe etc
- ❖ Wind velocity and proper insulation

6.2 Conclusions

Considering heat transfer medium as water based nanofluid improves the thermal performance of a FPSC. This is due to the fact that nanoparticle is more costly than water. Cost is also involved to use nanofluid as heat transfer medium. Also people can‟t use output nanofluid directly. Heat exchanger is needed to collect heat from output nanofluid and to use this heat for various purposes. This technique is costly. Recently a very few experimental study have been conducted taking nanofluid filled FPSC. Hopefully companies will be interested to make FPSC based on nanofluid as heat transfer medium. Though none may be interested to use nanofluid filled FPSC on his own house roof at present. But in future it may be necessary to improve thermal performance of FPSC for any country or organization who won‟t worry about cost. So, present 3D numerical study of nanofluid filled FPSC has great applications. The overall conclusions can be written as follows:

- 2D numerical analysis of FPSC doesn‟t represent accurate and practical phenomena of heat transfer system.
- 3D numerical analysis is necessary to represent actual heat transfer system of FPSC.
- Mean subdomain velocity decreases by 18% using nanofluid than water in 3D simulation.
- Water/Cu nanofluid enhances thermal efficiency about 8% in 3D simulation.
- 17% heat transfer rate is obtained for increasing ϕ from 0% to 2% in 3D simulation.
- More heat transfer rate of about 3% is obtained in 3D simulation than 2D.
- In 3D simulation mean outlet temperature of water increases about 1.6K than 2D.
- Collector efficiency increases about 5% in 3D simulation than 2D.

6.3 Recommendations

There is a lot of scope for research in this area in future. Since study of nanofluids is under initial stages so there is a lot of scope in development of nanofluids. The size, shape, material and volume fraction of nanoparticles play a very important role in the absorption of solar energy by nanofluids. If a country or a company has large availability of nanofluids the size of the collector can be increased. Due to high absorption characteristics of the nanofluids large amount of heat can be absorbed and this heat can be used for desired purposes. So, if a country is able to produce large quantities of nanofluids this problem can be overtaken. In consideration of the present investigation of 3D numerical study of thermofluid characteristics of a flat plate solar collector using nanofluid, the following recommendation for future works have been provided:

- In future, the study can be extended by incorporating different physics like unsteady state flow condition, slip symmetry condition, capillary effects etc.
- The absorber, riser pipe and bonding conductance are taken in copper metal in this research. Use of various metals may be another extension of the current work.
- Trapezium shaped bonding conductance is assumed for the present study. So this deliberation may be extended by considering other formations of bonding conductance analyses to investigate the thermal performance of FPSC.
- The FPSC may be structured at different measurements of absorber and riser pipe for checking which one is better.
- The geometry can be modeled considering double glass layer.
- The problems can be analyzed through including the temperature dependent properties of thermal conductivity, viscosity or density of fluid.
- Thermal efficiency calculated form quadratic form may be the subject of future analysis.
- Water/Cu, Water/Ag and water/Ag/Cu nanofluids with single phase flow are considered as heat transfer medium in this thesis work. It can be investigated for different nanofluids as well as for multiphase flow also.

References

Al-Ajlan, S.A., Al-Faris, H., and Khonkar, H.A., “Simulation modeling for optimization of flat plate collector design in Riyadh, Saudi Arabia”, Renewable Energy, Vol. 28, pp. 1325-1339, 2003.

Álvarez, A., Muñiz, M.C., Varela, L.M., Cabeza, O., “Finite element modelling of a solar collector”, International Conference on Renewable Energies and Power Quality, Granada, Spain, 2010.

Amrutkar, S.K., Ghodke, S., Patil, Dr. K.N., “Solar flat plate collector analysis”, IOSR J. of Engineering, Vol. 2, No. 2, pp. 207-213, 2012.

Azad, E., “Interconnected heat pipe solar collector”, IJE Transactions A: Basic, Vol. 22, No. 3, pp. 233-242, 2009.

Basavanna, S. and Shashishekar, K.S., “CFD analysis of triangular absorber tube of a solar flat plate collector”, International Journal Mechanical Engineering & Robotics Research, Vol. 2, No. 1, pp. 19-24, 2013.

Brinkman, H.C., “The viscosity of concentrated suspensions and solution”, Journal of Chemical Physics, Vol. 20, pp. 571–581, 1952.

Chabane, F., Moummi, N., Benramache, S., Bensahal, D., Belahssen, O., Lemmadi, F.Z., “Thermal performance optimization of a flat plate solar air heater”, International Journal of Energy & Technology, Vol. 5, No. 8, pp. 1–6, 2013.

Choi, S.U.S, “Nanofluid technology: current status and future research”, Energy Technology Division, Argonne National Laboratory, Sep 28, 1998.

Dara, J.E., Ikebudu, K.O., Ubani, N.O., Chinwuko, C.E., Ubachukwu, O.A., "Evaluation of a passive flat-plate solar collector”, International Journal of Advancements in Research & Technology, Vol. 2, No. 1, 6 pages, 2013.

Das, K.S, Choi, S.U.S, YU, W., Pradeep, T., “Nanofluids science and technology”, John Wiley & Sons, Hoboken, NJ, USA, 2008.

Dechaumphai, P., “Finite Element Method in Engineering”, 2nd edition, Chulalongkorn University Press, Bangkok, 1999.

Duffie, J.A. and Beckman, W.A., "Solar Engineering of Thermal Processes", Toronto, John Wiley, 1991.

Ekramian, E., Etemad, S.Gh., Haghshenasfard, M., Numerical analysis of heat transfer performance of flat plate solar collectors, Journal of Fluid Flow Heat and Mass Transfer, Vol. 1, pp. 38-42, 2014.

Gao W, "Analysis and performance of a solar air heater with cross corrugated absorber and back-plate", MS thesis, Yunnan Normal University, Kunming, 1996.

Gao, W., Lin, W., Lu, E., "Numerical study on natural convection inside the channel between the flat-plate cover and sine-wave absorber of a cross-corrugated solar air heater", Energy Conversion & Management, Vol. 41, pp. 145-151, 2000.

Ho C.D., Chen T.C., "The recycle effect on the collector efficiency improvement of double-pass sheet-and-tube solar water heaters with external recycle‟, Renewable Energy, Vol. 31, No. 7, pp. 953–97, 2006.

Hussain, A., "The performance of a cylindrical solar water heater", Renewable Energy, Vol. 31, No. 11, pp.1751–1763, 2006.

Ingle, P.W., Pawar, A.A., Deshmukh, B.D., Bhosale, K.C., "CFD analysis of solar flat plate collector", International Journal of Emerging Technology and Advanced Engineering., Vol. 3, No. 4, pp. 337-342, 2013.

Iordanou, G., „Flat-plate solar collectors for water heating with improved heat transfer for application in climatic conditions of the mediterranean region", Doctoral thesis, Durham University, 2009.

Joudi, K.A., Hussein, I.A., Farhan, A.A., "Computational model for a prism shaped storage solar collector with a right triangular cross section", Energy Conversion and Management, Vol. 45, pp. 391–409, 2004.

Kalogirou, S.A., "Solar thermal collectors and applications", Progress in Energy and Combustion Science, Vol. 30, pp. 231–295, 2004.

Karanth, K.V., Manjunath, M.S., Sharma, N.Y., "Numerical simulation of a solar flat plate collector using discrete transfer radiation model (DTRM) – a CFD approach", Proceeding of the World Congress on Engineering, London, U.K., III, 2011.

Karuppa, R.R.T., Pavan, P. and Rajeev, D.R., “Experimental investigation of a new solar flat plate collector”, Research Journal of Engineering Science, Vol.1, No.4, 1-8, 2012.

Kazeminejad, H., “Numerical analysis of two dimensional parallel flow flat-plate solar collector”, Renewable Energy, Vol. 26, pp. 309–323, 2002.

Klein, H.H., Karni, J., Ben-Zvi, R., Bertocchi, R., ”Heat transfer in a directly irradiated solar receiver/reactor for solid gas-reactions”, Solar Energy, Vol. 81, No. 10, pp. 1227-1239, 2007.

Kolb A., Winter E.R.F., Viskanta R., “Experimental studies on a solar air collector with metal matrix absorber”, Solar Energy, Vol. 65, No. 2, pp. 91–98, 1999.

Konttinen P., Lund P.D., Kilpi R.J., “Mechanically manufactured selective solar absorber surfaces”, Solar Energy Material & Solar Cells, Vol. 79, No. 3, pp. 273–283, 2003.

Kreith, F., Kreider, J.F., “Principles of solar engineering”, New York, McGraw-Hill, 1978.

Lambert, A.A., Cuevas, S., del Rı´o, J.A., “Enhanced heat transfer using oscillatory flows in solar collectors”, Solar Energy, Vol. 80, 1296–1302, 2006.

Lund, K.O., “General thermal analysis of parallel-flow flat-plate solar collector absorbers”, Solar Energy, Vol. 36, No.5, pp. 443-450, 1986.

Mahian, O., Kianifar, A., Kalogirou, S.A., Pop, I., Wongwises, S., “A review of the applications of nanofluids in solar energy”, International Journal of Heat and Mass Transfer, Vol. 57, pp. 582–594, 2013.

Manjunath, M.S., Karanth, K.V., Sharma, N.Y., “Three dimensional numerical analysis of conjugate heat transfer for enhancement of thermal performance using finned tubes in an economical unglazed solar flat plate collector”, Proceeding of the World Congress on Engineering, London, U.K., III, 2011.

Manjunath, M.S., Karanth, K.V., Sharma, N.Y., “A comparative CFD study on solar dimple plate collector with flat plate collector to augment the thermal performance”, World Academy of Science, Engineering and Technology, Vol. 6, pp. 10-21, 2012.

Martín, R.H., Pinar, A.G., García, J.P., "Experimental heat transfer research in enhanced flat-plate solar collectors", World Renewable Energy Congress, Solar Thermal Applications, Sweden, 2011.

Maxwell-Garnett, J.C., "Colours in metal glasses and in metallic films", Philosophy Transaction Royal Society. A, Vol. 203, pp. 385–420, 1904.

Modest M.F., "Radiative heat transfer", 2nd edition, Academic Press, 2003.

Molineaux B., Lachal B., Gusian O., "Thermal analysis of five outdoor swimming pools heated by unglazed solar collectors", Solar Energy, Vol. 53, No. 1, pp. 21–26, 1994.

Moningi, M.K., "Conduction convection radiation processes of a solar collector using FEA", Report, 4 pages, University of Massachusetts, Amherst, 2008.

Nag, A., Misra, D., De, K.E., Bhattacharya, A., Saha, S.K., "Parametric study of parallel flow flat plate solar collector using finite element method", In: Numerical Methods in Thermal Problems, Proceeding of the 6th International Conference, Swansea, UK, 1989.

Nasrin, R. and Alim, M.A. and Chamkha, A.J., "Effects of physical parameters on natural convection in a solar collector filled with nanofluid", Heat Transfer Asian Research, Vol. 42, No. 1, pp. 73-88, 2013.

Nasrin, **R**. and Alim, M.A., "Aspect ratio effect on convective flow in a solar collector with sinusoidal wavy absorber using nanofluid", Engineering e Transaction, Vol. 7, No. 2, pp. 77-85, 2012.

Nasrin, R. and Alim, M.A., "Buoyancy flow and heat transfer analysis in a prism shaped solar collector", International Journal of Energy & Technology, Vol. 5, No. 3, pp. 1-10, 2013.

Nasrin, R. and Alim, M.A., "Dufour-Soret effects on buoyant convection through a nanofluid with different nanoparticles-filled solar collector", International Journal of Heat & Technology, Vol. 31, No. 1, pp. 31-40, 2013.

Nasrin, R. and Alim, M.A., "Dufour-Soret effects on natural convection inside a solar collector utilizing water-CuO nanofluid", International Journal of Energy & Technology, Vol. 4, No.23, pp. 1-10, 2012.

Nasrin, R. and Alim, M.A., "Effect of nanoparticle volume fraction on buoyant flow in a solar collector with undulating absorber", International Journal of Energy & Technology, Vol. 4, No. 19, pp. 1-9, 2012.

Nasrin, R. and Alim, M.A., "Effect of radiation on convective flow in a tilted solar collector filled with water-alumina nanofluid", International Journal of Engineering, Science & Technology, Vol. 4, No. 4, pp. 1-12, 2012.

Nasrin, R. and Alim, M.A., "Entropy generation by nanofluid with variable thermal conductivity and viscosity in a flat plate solar collector", International Journal of Engineering, Science & Technology, Vol. 7, No. 2, PP. 80-93, 2015.

Nasrin, R. and Alim, M.A., "Finite element simulation of forced convection in a flat plate solar collector: Influence of nanofluid with double nanoparticles", Journal of Applied Fluid Mechanics, Vol. 7, No. 3, pp.543-557, 2014.

Nasrin, R. and Alim, M.A., "Free convective analysis in a solar collector using nanofluid", Engineering e Transaction, Vol. 8, No. 1, pp. 19-27, 2013.

Nasrin, R. and Alim, M.A., "Free convective flow of nanofluid having two nanoparticles inside a complicated cavity", International Journal of Heat and Mass Transfer, Vol. 63, pp. 191-198, 2013.

Nasrin, R. and Alim, M.A., "Heat transfer by nanofluid with different nanoparticles in a solar collector", Heat Transfer-Asian Research, Vol. 43, No. 1, pp.61-79, 2014.

Nasrin, R. and Alim, M.A., "Modeling of a solar water collector with water based nanofluid using nanoparticles", Heat Transfer-Asian Research, Vol. 43, No. 3, pp. 270-287, 2014.

Nasrin, R. and Alim, M.A., "Modeling of double diffusive buoyant flow in a solar collector with water-CuO nanofluid", Heat Transfer-Asian Research, Vol. 42, No. 3, pp. 212-229, 2013.

Nasrin, R. and Alim, M.A., "Performance of nanofluids on heat transfer in a wavy solar collector", International Journal of Engineering, Science & Technology, Vol. 5, No. 3, pp. 58-77, 2013.

Nasrin, R. and Alim, M.A., "Prandtl number effect on free convective flow in a solar collector utilizing nanofluid", Engineering e Transaction, Vol. 7, No. 2, pp. 62-72, 2012.

Nasrin, R. and Alim, M.A., "Semi-empirical relation for forced convective analysis through a solar collector", Solar Energy, Vol. 105, pp. 455-467, 2014.

Nasrin, R. and Alim, M.A., "Thermal performance of nanofluid filled solar flat plate collector", International Journal of Heat & Technology, Vol. 33, No. 1, pp. 17-24, 2015.

Nasrin, R., Ahmed, K.F.U. and Alim, M.A., "Semi-empirical relation for air space of a solar collector", Journal of Computer Science and Applied Mathematics, Vol. 1, No. 1, pp. 1-9, 2014.

Nasrin, R., Alim, M.A. and Ahmed, S.R., "Comparative study between 2D and 3D modeling of nanofluid filled flat plate solar collector", International Journal of Thermal Sciences, 2015 (Submitted).

Nasrin, R., Alim, M.A. and Chamkha, Ali J., "Numerical simulation of non-darcy forced convection through a channel with non-uniform heat flux in an open cavity using nanofluid", Numerical Heat Transfer, Part A-Application, Vol. 64, No. 10, pp. 820-840, 2013.

Nasrin, R., Alim, M.A. and M. Hasanuzzaman, "Assisted convective heat transfer and entropy generation inside a tilted solar collector filled nanofluid", Applied Mathematical Modelling, (Sumbitted).

Nasrin, R., Parvin, S. and Alim, M.A., "Buoyant flow of nanofluid for heat-mass transfer through a thin layer", Mechanical. Engineering Research Journal, Vol. 9, pp. 7-12, 2013.

Nasrin, R., Parvin, S. and Alim, M.A., “Effect of Prandtl number on free convection in a solar collector filled with nanofluid”, Procedia Engineering, Vol. 56, pp. 54-62, 2013.

Nasrin, R., Parvin, S. and Alim, M.A., “Entropy generation inside a narrow channel with thermal radiation”, International Journal of Energy & Technology, Vol. 6, No. 27, pp. 1-9, 2014.

Nasrin, R., Parvin, S. and Alim, M.A., “Heat transfer and collector efficiency through direct absorption solar collector with radiative heat flux effect”, Numerical Heat Transfer, Part A- Application, Vol. 68, No. 8, pp. 887-905, 2015.

Nasrin, R., Parvin, S. and Alim, M.A., “Heat Transfer by nanofluids through a flat plate solar collector, Procedia Engineering, Vol. 90, pp. 364-370, 2014.

Natarajan, E. & Sathish, R., “Role of nanofluids in solar water heater”, International Journal of Advanced Manufacturing Technology, Vol. 45, 5 pages, 2009.

Orel, Z.C., Gunde, M.K., Hutchins, M.G., “Spectrally selective solar absorbers in different non-black colours”, Proceeding. of WREC VII, Cologne on CD-ROM, 2002.

Otanicar, T., Phelan, P.E., Prasher, R.S., Rosengarten, G., Taylor, R.A., “Nanofluid based direct absorption solar collector”, Journal of Renewable and Sustainable Energy, Vol. 2, pp. 033102, 2010.

Otanicar, T., Taylor, R.A., Phelan, P.E., Prasher, R., “Impact of size and scattering mode on the optimal solar absorbing nanofluid”, San Francisco: ASME ES, pp. 90066, 2009.

Parker, B.F., Lindley, M.R., Colliver, D.G., Murphy, W.E., “Thermal performance of three solar air heaters”, Solar Energy, Vol. 51, No. 6, pp. 467-479, 1993.

Parvin, S., **Nasrin, R.** and Alim, M.A., “Heat transfer and entropy generation through nanofluid filled direct absorption solar collector”, International Journal of Heat and Mass Transfer, Vol. 71, pp. 386-395, 2014.

Piao, Y., Hauptmann, E.G., Iqbal, M., “Forced convective heat transfer in cross-corrugated solar air heaters”, ASME Journal of Solar Energy Engineering, Vol. 116, pp. 212-214, 1994.

Polvongsri, S. and Kiatsiriroat, T., “Enhancement of Flat-Plate Solar Collector Thermal Performance with Silver Nano-fluid”, The 2nd TSME International Conference on Mechenical Engineering, Krabi, 2011.

Rao, P.P, „Two-dimensional analysis of a flat plate solar collector”, Journal of Energy, Vol. 1, pp. 324, 1977.

Robert, A.T, Patrick, E.P., Todd, P.O., Ronald, A., Ravi, P., “Nanofluid optical property characterization: towards efficient direct absorption solar collectors”, Nanoscale Research Letters, Vol. 6, pp. 225, 2011.

Saleh, A.M., “Modeling of flat-plate solar collector operation in transient states”, Thesis, M. Sc. in Engineering, Purdue University, Fort Wayne, Indiana, May 2012.

Sandhu, G., “Experimental study of temperature field in flat-plate collector and heat transfer enhancement with the use of insert devices”, Thesis, M. of Engineering Science, The School of Graduate and Postdoctoral Studies, The University of Western Ontario London, Ontario, Canada, 2013.

Soltau, H., “Testing the thermal performance of uncovered solar collectors”, Solar Energy, Vol. 49, No. 4, pp. 263–272, 1992.

Strukmann, F., “Analysis of a flat-plate solar collector”, Project Report, 2008 MVK160 Heat and Mass Transport, Lund, Sweden, May 08, 2008.

Sukhatme, S.P., “Solar energy, principles of thermal collection and storage”, New Delhi, Tata McGraw-Hill, 1991.

Tagliafico, I.A., Scarpa, F., Rosa, M.D., “Dynamic thermal models and CFD analysis for flat-plate thermal solar collectors – a review”, Renewable and Sustainable Energy Review, Vol. 2, No. 30, pp. 526-537, 2014.

Taylor, C., Hood, P., “A numerical solution of the Navier-Stokes equations using finite element technique”, Computer and Fluids, Vol. 1, pp. 73–89, 1973.

Taylor, R.A., Phelan, P.E., Otanicar, T., Walker, C.A., Nguyen, M., Trimble, S., and Prasher, R., "Applicability of nanofluids in high flux solar collectors", Journal of Renewable and Sustainable Energy, Vol. 3, No. 2, 15 pages, 2011.

Tripanagnostopoulos, Y., Souliotis, M., Nousia, T., "Solar collectors with colored absorbers", Solar Energy, Vol. 68, pp. 343–356, 2000.

Tyagi, H., Phelan, P.E., Prasher, R., "Predicted efficiency of a low-temperature nanofluid-based direct absorption solar collector", Journal of Solar Energy Engineering., Vol. 131, No. 4, pp. 041004, 2009.

Varol, Y. and Oztop, H.F., "Buoyancy induced heat transfer and fluid flow inside a tilled wavy solar collector", Building Environment, Vol. 42, pp. 2062-2071, 2007.

Vestlund, J., "Gas-filled flat plate solar collector", Thesis, Ph. D., Building Services Engineering, Department of Energy and Environment, Chalmers University of Technology, Gothenburg, Sweden, 2012.

Wazwaz, J., Salmi, H., Hallak, R., "Solar thermal performance of a nickel-pigmented aluminium oxide selective absorber", Renewable Energy, Vol. 27, pp. 277–292, 2002.

Xiaowu, W., Hua, B., "Energy analysis of domestic-scale solar water heaters", Renewable and Sustain Energy Review, Vol. 9, No. 6, pp. 638–645, 2005.

Xuesheng, W., Ruzhu, W., Jingyi, W., "Experimental investigation of a new-style double-tube heat exchanger for heating crude oil using solar hot water", Applied Thermal Engineering, Vol. 25, No. 11-12, pp.1753–1763, 2005.

Zambolin, E., "Theoretical and experimental study of solar thermal collector systems and components", Scuola di Dottorato di Ricerca in Ingegneria Industriale, Indirizzo Fisica Tecnica, 2011.

Zienkiewicz, O.C. and Taylor, R.L., "The finite element method", Fourth Edition, McGraw-Hill, 1991.

1. http://apesnature.homestead.com/files/fg15_006.jpg, 2013.
2. http://www.ruralenergy.wisc.edu/images/solar_thermal/glazed-flat-solar-panel.gif, 2013.
3. http://www.alternative-energy-tutorials.com/images/stories/heating/alt47.gif, 2013.
4. http://www.apricus.com/flat-plate-solar-collectors-3/#.VTYMpCGqqko/, 2013.
5. http://www.everredtronics.com/Solar.Download.html/, 2011.
6. http://www.ledgrowlight-hydro.com/ledlights-blog/choosing-the-right-kind-led-grow-lights-is-extremely-important/, 2011.
7. http://blog.indeeco.com/calculate-heat-loss/, 2014.
8. http://thegreenhome.co.uk/wp-content/uploads/2013/08/Flat-Plate-Thrmal-Collector-Overview-2-500x266.jpg, 2013.
9. http://www.sunmaxxsolar.com/flat-plate-solar-collectors.php/, 2011.
10. http://energy.gov/energysaver/articles/sizing-new-water-heater/, 2011
11. http://buildipedia.com/knowledgebase/division-22-plumbing/22-10-00-plumbing-piping-and-pumps/22-12-00-facility-potable-water-storage-tanks/, 2012.
12. http://www.schenectady.k12.ny.us/users/pattersont/Mech%20Eng%20Website/Definitions%20Graphics/flatplatecollector.gif, 2013.
13. http://www.homepower.com/sites/default/files/articles/ajax/docs/3_Flat-Plate-detail-shadows.jpg, 2014
14. http://www.rvr.ie:900/index.php?title=Specifiers:_Solar_Thermal_Collector_Types/, 2014.
15. http://www.solarserver.com/knowledge/basic-knowledge/solar-collectors.html/, 2011.
16. http://www.volker-quaschning.de/articles/fundamentals4/index_e.php/, 2011.
17. http://www.gaisma.com/en/location/cartagena.html, 2014.

18. http://www.lged-rein.org/solar.php, 2013

19. https://mawyin.wordpress.com/2012/02/07/february-7-renewable-energy-in-bangladesh/, 2012.

20. http://www.assignmentpoint.com/science/importance-and-impact-of-solar-home-system-shs-in-bangladesh.html, 2011.

21. http://www.mpoweruk.com/solar_power.htm, 2011.

Appendix

A.1. Optimization of thermal performance of FPSC in Dhaka City

Bangladesh is a country of enormous sunshine. But the availability of an energy source does not mean much, if the necessary technology to harness it is not available. It is located between $20^{0}30^{/}$ and $26^{0}45^{/}$ north latitude and the climate is tropical, the very location makes Bangladesh good recipient of solar energy. Bangladesh has a total area of 1.49E+11 m^2 and an average of 5KWh/m^2 solar radiation falls on this land over 365 days per annum. During the last decades considerable advances in some of the solar energy technologies have been made and some have already reached the commercial stage.

A.1.1 Solar radiation in Bangladesh

Solar radiation map [18] of Bangladesh is given in figure A.1.

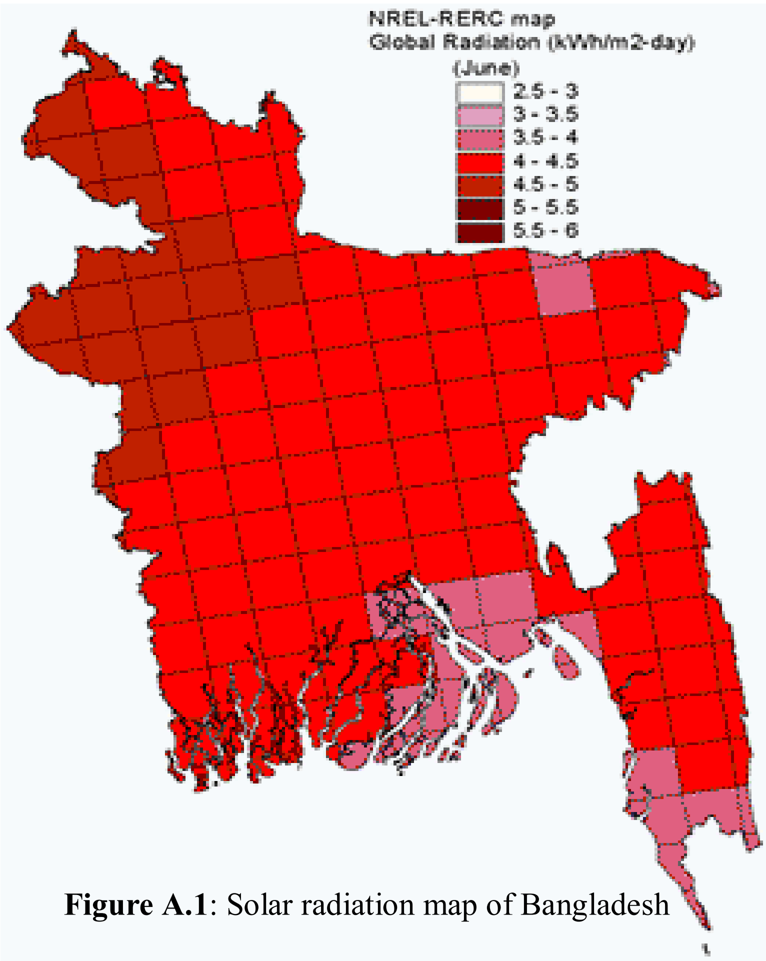

Figure A.1: Solar radiation map of Bangladesh

It was jointly prepared by Renewable Energy Research Centre (RERC), Dhaka, Bangladesh and National Renewable Energy Laboratory (NREL), USA. Bangladesh gets an average around 200 W/m^2 - 240W/m^2 of sunlight.

Monthly solar irradiation (KWh/m^2) at different locations of Bangladesh is shown in Table A.1. This data [19] was recorded by Dr. Shahida Rafique, University of Dhaka, for ten years period from 1988 to 1998. Maximum irradiation all over the country was observed in the month of May and minimum was observed in December.

Table A.1: Monthly solar irradiation (KWh/m^2) of Bangladesh

Month	Dhaka	Rajshahi	Sylhet	Bogra	Barishal	Jessore
January	4.03	3.96	4.00	4.01	4.17	4.25
February	4.78	4.47	4.63	4.69	4.81	4.85
March	5.33	5.88	5.20	5.68	5.30	4.50
April	5.71	6.24	5.24	5.87	5.94	6.23
May	5.71	6.17	5.37	6.02	5.75	6.09
June	4.80	5.25	4.53	5.26	4.39	5.12
July	4.41	4.79	4.14	4.34	4.20	4.81
August	4.82	5.16	4.56	4.84	4.42	4.93
September	4.41	4.96	4.07	4.67	4.48	4.57
October	4.61	4.88	4.61	4.65	4.71	4.68
November	4.27	4.42	4.32	4.35	4.35	4.24
December	3.92	3.82	3.85	3.87	3.95	3.97
Average	4.73	5.00	4.54	4.85	4.71	4.85

In Bangladesh daily sunlight time is recorded from 7 to 10 hours. But due to rainfall, cloud, fog, dust over the solar collector this time period is reduced by 54% (to 4.6 hours). Daily average bright sunshine (hours) at Dhaka city is given in the Table A.2. The data was recorded for twenty years period from 1961 to 1980 and source is REEIN, 2010.

Table A.2: Daily average bright sunshine (hours) at Dhaka city

Month	Daily Mean	Maximum	Minimum
January	8.7	9.9	7.5
February	9.1	10.7	7.7
March	8.8	10.1	7.5
April	8.9	10.2	7.8
May	8.2	9.7	5.7
June	4.9	7.3	3.8
July	5.1	6.7	2.6
August	5.8	7.1	4.1
September	6.0	8.5	4.8
October	7.6	9.2	6.5
November	8.6	9.9	7.0
December	8.9	10.2	7.4
Average	7.55	9.13	6.03

Location (latitude and longitude angles and altitude length) of six divisions in Bangladesh in northern hemisphere is given in Table A.3.

Table A.3: Location of six meteorological stations in Bangladesh

Station Name	Latitude (degree)	Longitude (degree)	Altitude (meter)
Dhaka	23.71	90.41	22
Chittagong	22.33	91.83	10
Barisal	22.7	90.37	8.54
Khulna	22.82	89.55	6.88
Sylhet	24.89	91.87	23.03
Rajshahi	24.37	88.6	26.38

Monthly average hourly solar radiation I (KWh/m^2) in Dhaka city of Bangladesh is shown in Table A.4. The data [20] is recorded three years time period from 2003 to 2005 and source is SWERA Project, RERC, University of Dhaka.

Table A.4: Monthly average hourly solar radiation (KWh/m^2) in Dhaka city

Hours/ months	**Jan**	**Feb**	**Mar**	**Apr**	**May**	**Jun**	**Jul**	**Aug**	**Sep**	**Oct**	**Nov**	**Dec**
5:30			1	5	17	19	11	7	3			
6:30	3	8	29	66	106	93	86	66	58	46	31	11
7:30	57	93	148	198	252	200	198	180	165	169	157	97
8:30	175	254	318	354	406	321	355	288	303	324	331	237
9:30	300	424	489	521	561	416	438	433	435	473	490	382
10:30	411	573	629	666	681	494	503	514	485	487	580	479
11:30	494	672	712	751	727	532	548	537	485	520	614	498
12:30	518	701	722	764	711	593	570	535	486	488	573	489
13:30	483	646	657	693	641	500	503	482	441	406	510	426
14:30	379	528	541	553	577	451	463	453	385	323	377	309
15:30	236	353	377	402	419	329	372	356	281	208	204	183
16:30	94	175	204	237	257	215	244	231	164	76	57	54
17:30	10	37	55	72	93	93	107	89	45	6	1	2
18:30			2	4	11	17	18	8	1			
Daily average	3.16	4.46	4.88	5.28	5.46	4.22	4.42	4.18	3.74	3.53	3.92	3.17

A.1.2 Solar azimuth, altitude and zenith angles

The sun‟s position on the celestial sphere [21] is usually specified in terms of the solar azimuth angle ψ and the solar altitude angle α. These are displayed in the figure A.2. The solar altitude angle measures the sun‟s angular distance from the horizon and the azimuth angle measures the sun‟s angular distance from the south. The solar zenith angle φ is the sun‟s angular distance from the zenith, which is the point directly overhead on the celestial sphere. Thus φ and α are complementary angles.

The tilt angle is just the angle at which the surface is inclined from horizontal and is taken positive for south facing surfaces.

The solar altitude and azimuth angles are computed for any time, date and location using the formula

$$\alpha = 90^0 - \varphi + \delta$$

where φ is the latitude taken north of the equator and δ is declination angle.

Another form of δ is

$$\delta = 23.45^0 \sin\left[\frac{360}{365}(284 + d)\right]$$

where d is the day of the year like from 1 to 365.

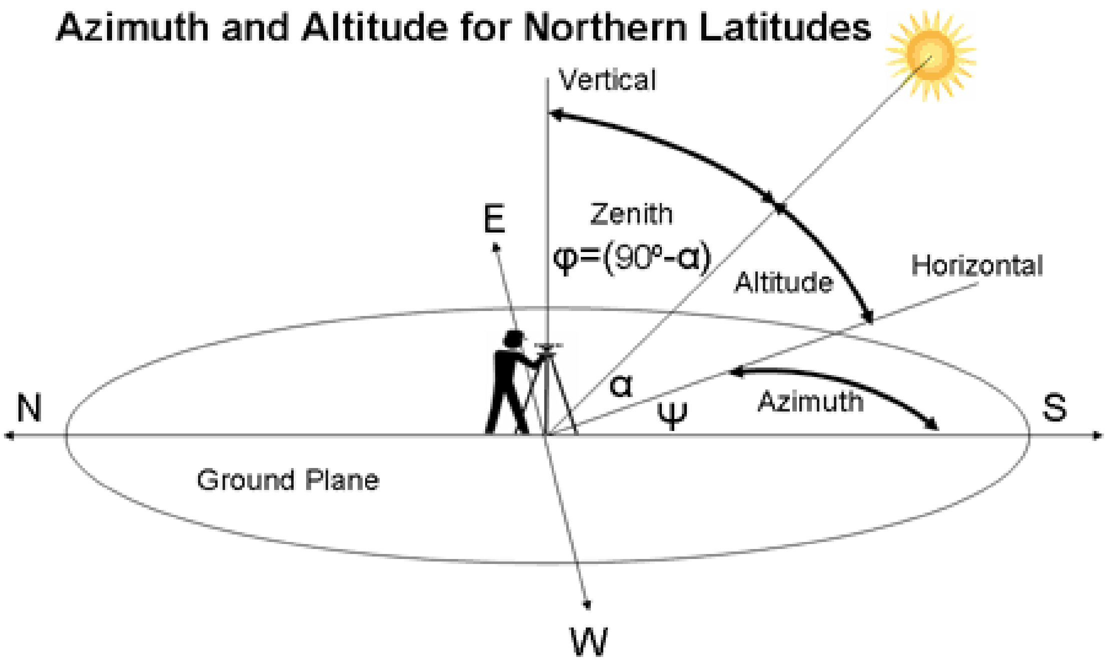

Figure A.2: Solar azimuth, altitude and zenith angles

For the incident ray to be perpendicular to the surface

$$\alpha + \beta = 90^0$$

where α is elevation angle and β is tilt angle of the solar collector measured from the horizontal surface. Then from above equation it is clear that

$\beta = \varphi - \delta$

For Dhaka city latitude and longitude are 23.7^0N and 90.41^0E. The tilt angle will be

a) For May 25, 2014 (Summer), $d = 31+28+31+30+25 = 145$.

   So, $\delta = 20.916^0$

   Now $\beta = \varphi - \delta = 23.7^0 - 20.916^0 = 2.78^0$

b) For October 3, 2014 (Autumn), $d = 276$.

   So, $\delta = -5.007^0$

   Now $\beta = \varphi - \delta = 23.7^0 - (-5.007^0) = 28.707^0$

Similarly the tilt angle of solar collector for 365 days in Dhaka city is calculated and average value is obtained as 23.8^0. As β is positive, collector will be facing south. Maximum yearly solar radiation can be achieved using a tilt angle approximately equal to a site's latitude. To optimize performance in winter, collector can be tilted 15° greater than the latitude. To optimize performance in summer, collector can be tilted 15° less than the latitude. The south facing solar collector at a fixed angle is shown in the figure A.3.

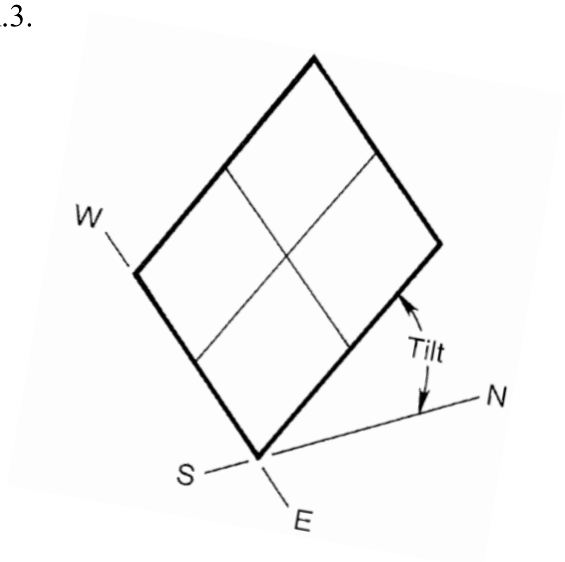

Figure A.3: South facing solar collector

A.2. Conclusions

The tilt angle has a major impact on the solar radiation incident on a surface. For a fixed tilt angle, the maximum power over the course of a year is obtained when the tilt angle is equal to the latitude of the location. However, steeper tilt angles are optimized for large winter loads, while lower title angles use a greater fraction of light in the summer. To optimize the thermal performance of a FPSC in Dhaka city, Bangladesh one should consider the following:

- Ideal locations for solar collector will be house roofs with minimum cloud cover, high solar radiation availability and exhibit high average sunlight hours throughout a year.
- Maximum yearly solar radiation can be achieved using a tilt angle approximately equal to 23.8^0.
- To optimize performance in winter, collector can be tilted at 38.8^0.
- To optimize performance in summer, collector can be tilted at 8.8^0.
- Average annual solar radiation on a 24^0 inclined surface is estimated as 5 $KWh/m^2/day$.
- Solar collector must be facing south.